Univerza v Ljubljani

Fakulteta za elektrotehniko

Tadeja Forjanič

Modeliranje biološkega odziva na elektroporacijo v elektrokemoterapiji in genski terapiji

DOKTORSKA DISERTACIJA

Mentor: prof. dr. Damijan Miklavčič

Ljubljana, 2018

University of Ljubljana

Faculty of Electrical Engineering

Tadeja Forjanič

Modeling the biological response to electroporation for electrochemotherapy and gene therapy

DOCTORAL DISSERTATION

Mentor: prof. Damijan Miklavčič, Ph. D.

Ljubljana, 2018

Univerza *v Ljubljani*
Fakulteta *za elektrotehniko*

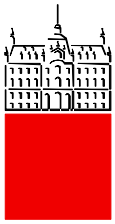

I Z J A V A

Spodaj podpisani/-a, Tadeja Forjanič, z vpisno številko 64130382 s svojim podpisom izjavljam, da sem avtor/-ica zaključnega dela z naslovom:

Modeliranje biološkega odziva na elektroporacijo v elektrokemoterapiji in genski terapiji

S svojim podpisom potrjujem:

- da je predloženo zaključno delo rezultat mojega samostojnega raziskovalnega dela in da so vsa dela in mnenja drugih avtorjev skladno s fakultetnimi navodili citirana in navedena v seznamu virov, ki je sestavni del predloženega zaključnega dela,
- da je elektronska oblika zaključnega dela identična predloženi tiskani obliki istega dela,
- da na Univerzo v Ljubljani neodplačno, neizključno, prostorsko in časovno neomejeno prenašam pravici shranitve avtorskega dela v elektronski obliki in reproduciranja ter pravico omogočanja javnega dostopa do avtorskega dela na svetovnem spletu preko Repozitorija Univerze v Ljubljani (RUL).

V Ljubljani, 17. 4. 2018 Podpis avtorja/-ice:

_____

PREDGOVOR

Doktorska disertacija je rezultat raziskovalnega dela, ki je temeljilo na modeliranju pojavov, povezanih z elektroporacijo. Raziskovalno delo je bilo opravljeno v okviru doktorskega študija na Fakulteti za elektrotehniko, Univerza v Ljubljani, Slovenija. Rezultati so predstavljeni v člankih, ki so objavljeni oziroma oddani v objavo v sledečih revijah:

Članek 1: Forjanič T, Miklavčič D. **Mathematical model of tumor volume dynamics in mice treated with electrochemotherapy.**
Med Biol Eng Comput 55/7: 1085–1096, 2017.

Članek 2: Forjanič T, Markelc B, Bellard E, Couillaud F, Golzio M, Miklavčič D. **Numerical model of the thermal stress and gene electrotransfer in the skin.**
IEEE T. Biomed. Eng., oddano v objavo

Članek 3: Forjanič T, Miklavčič D. **Numerical model of gene electrotransfer efficiency based on electroporation volume and electrophoretic movement of plasmid dna.**
Biomed. Eng. Online, oddano v objavo

ZAHVALA

Iskreno se zahvaljujem mentorju prof. dr. Damijanu Miklavčiču za vse strokovne nasvete, spodbude in pomoč v času doktorskega študija, za usmerjanje in upoštevanje želja pri določanju teme doktorske disertacije, ter za vso potrpežljivost pri postopnem nadgrajevanju numeričnih modelov.

Hvala sodelavcem Laboratorija za Biokibernetiko za prijetno delovno okolje, za vse nasvete in pomoč, ter za zanimive pogovore in druženja.

Posebna zahvala gre mojim staršem, ki so me spodbujali, me podpirali pri mojih odločitvah in mi stali ob strani vse od začetka šolanja.

Hvala tudi novim sodelavcem iz oddelka za Radiofiziko OI za vso razumevanje, ki sem ga bila deležna pri zaključevanju doktorske disertacije in za prijetno, sproščeno delovno okolje.

KAZALO

POVZETEK

Na področju biomedicine ima poleg eksperimentov pomembno vlogo pri razlagi bioloških procesov tudi modeliranje. Še posebej pomembno vlogo ima modeliranje v medicini, kjer se uporablja kot orodje za načrtovanje in optimizacijo različnih terapij, med drugim tudi terapij na osnovi elektroporacije.

Elektroporacija je prehodni pojav začasne povečane prepustnosti celične membrane ob izpostavitvi električnemu polju. Visokonapetostni električni pulzi povzročijo vrsto strukturnih sprememb v celični membrani, ki vodijo do povečane prepustnosti, kar omogoča lažji prehod snovi, ki drugače težko ali pa sploh ne prehajajo skozi membrano. Elektroporacija je reverzibilna, če celica preživi, in ireverzibilna, če električnimi pulzi povzročijo spremembe, ki vodijo v celično smrt. V medicini se reverzibilna elektroporacija najpogosteje uporablja kot spremljevalna metoda, ki izboljša vnos genov v celice (genska elektrotransfekcija) ali poveča prehajanje kemoterapevtikov v tumorske celice (elektrokemoterapija), medtem ko se ireverzibilna elektroporacija uporablja kot samostojna metoda za atermično ablacijo tkiv.

Čeprav je osnovni pogoj za uspešnost metod in terapij na osnovi elektroporacije preprost - pokritost ciljnega tkiva z električnim poljem, ki zagotavlja reverzibilno elektroporacijo (elektrokemoterapija in genska elektrotransfekcija) oziroma ireverzibilno elektroporacijo (atermična ablacija) - je za doseganje optimalne učinkovitosti potrebno upoštevati še vpliv spremljevalnih učinkov elektroporacije. V sklopu disertacije smo z uporabo matematičnih modelov skušali oceniti vpliv imunskega odziva pri elektrokemoterapiji, razsežnost termičnih poškodb pri elektroporaciji kože, ter vpliv porazdelitve električne poljske jakosti na učinkovitost genske elektrotransfekcije.

Nekaj vpogleda v vlogo spremljevalnih učinkov elektrokemoterapije lahko dobimo s spremljanjem velikosti tumorjev po zdravljenju. V ta namen smo razvili matematični model na osnovi diferencialnih enačb, ki opisuje spremembe v prostornini mišjih tumorjev po zdravljenju z elektrokemoterapijo ob uporabi različnih doz cisplatina in bleomicina. Za opis rasti tumorjev smo uporabili eksponentno-linearni model, pri čemer sta bila parametra, ki opisujeta hitrost rasti v eksponentni in linearni fazi, določena na osnovi podatkov kontrolne skupine. Učinek elektrokemoterapije smo vključili preko posebne funkcije, ki upošteva časovni zamik med elektrokemoterapijo in celično smrtjo. Na ta način smo prikazali dinamiko eliminacije celic iz tumorja, ki

kaže dva vrhova. Prvi vrh je dosežen kmalu po elektrokemoterapiji in ga lahko pripišemo citotoksičnosti kemoterapevtika, medtem ko je drugi vrh najverjetneje povezan z imunskim odzivom.

Ostali učinki elektroporacije, zajeti v disertaciji, so bili ovrednoteni z uporabo numeričnega modeliranja. Natančneje, zgradili smo tridimenzionalni model kože skupaj z različnimi vrstami elektrod, ki se uporabljajo pri elektroporaciji kože (ploščate, igelne in prstne elektrode). Modeliranje učinkov pri elektroporaciji kože je zajemalo izračun porazdelitve električnega polja, izračun dviga temperature oziroma razsežnosti termičnih poškodb, ter elektroforetskega gibanja plazmidne DNK v električnem polju. Rezultate modeliranja smo primerjali z *in vivo* eksperimenti. Izračuni kažejo, da so termične poškodbe, ki vodijo v celično smrt, omejene na majhno prostornino tik pod območji povečane električne prevodnosti zgornje plasti kože, ki se pojavijo zaradi elektroporacije. Okoli območja nepovratnih termičnih poškodb ležijo celice, izpostavljene zmernemu toplotnemu stresu, ki vodi do izražanja proteinov vročinskega šoka. Eksperimenti kažejo nizko raven toplotnega stresa, kar se sklada z izračuni, saj večina celic, izpostavljenih zmernemu toplotnemu stresu, leži na območju ireverzibilne elektroporacije, ki preprečuje izražanje proteinov vročinskega šoka.

Nekaj več odstopanja med modelom in eksperimenti smo dobili pri genski elektrotransfekciji. Glavni korak naprej v modeliranju genske elektrotransfekcije predstavlja simulacija elektroforetskega gibanja plazmidne DNK v nehomogenem električnem polju. Večina dosedanjih modelov namreč temelji na porazdelitvi električne poljske jakosti, gibanje plazmidne DNK pa ni upoštevano ali je kvečjemu ocenjeno z maksimalnim dosegom. V disertaciji smo predstavili model, ki prikazuje tridimenzionalno gibanje plazmidne DNK pri različnih parametrih električnih pulzov. Učinkovitost genske elektrotransfekcije smo ocenili s številom nabitih delcev, ki predstavljajo plazmidno DNK, znotraj volumna reverzibilne elektroporacije. To merilo učinkovitosti pa ni v celoti pojasnilo eksperimentalnih razlik v učinkovitosti med različnimi vrstami elektrod in pulznimi protokoli. Razhajanja so bila do neke mere pričakovana, saj je izražanje vnesenih genov odvisno od vrste parametrov, med drugim tudi od stresa, ki ga elektroporacija povzroči celicam. Ugotovili smo, da je eden izmed glavnih razlogov za razhajanja med eksperimenti in modelom pomanjkljivo poznavanje sprememb v prevodnosti zgornje, rožene plasti kože, do katerih pride zaradi elektroporacije. Torej, da bi modeliranje postalo zanesljivo orodje za napovedovanje učinkovitosti genske elektrotransfekcije, je potrebno boljše poznavanje procesa elektroporacije kože in identifikacija morebitnih drugih pomembnih procesov, ki niso bili upoštevani v modelu.

ABSTRACT

In the field of biology, the modeling is considered as an important tool, that helps to better understand responses observed in experiments. Modeling is particularly important in medicine, since it also serves for treatment planning of different therapies, including therapies, based on electroporation.

Electroporation is a phenomenon of transiently increased cell membrane permeability under the influence of external electric field. Short electric pulses with sufficiently high amplitude cause structural changes in the cell membrane, resulting in increased permeability, which enables transient enhancement of molecular transport across the membrane. Electroporation is reversible when cell survives and returns to its normal state, and irreversible when electric pulses cause irreversible changes in cell membrane leading to cell death. In the medicine, reversible electroporation is used to enhance the uptake of chemotherapeutic drug (electrochemotherapy) and as a gene delivery approach (gene electrotransfection). Irreversible electroporation is used for nonthermal ablation of undesired tissue.

Prerequisite for the succes of the methods, relying on electroporation, is to achieve a complete coverage of the target tissue with electric fields, resulting in reversible (electrochemotherapy and gene electrotransfection) or irreversible electroporation (nonthermal ablation). Despite the apparent simplicity of the concept, it is necessary to consider the influence of several effects of electroporation in order to achieve the optimal efficiency. The aim of the doctoral thesis was to evaluate the following effects of electroporation: immune response in electrochemotherapy, thermal damage due to skin electroporation and the influence of electric field distribution on gene electrotransfer efficiency.

Monitoring the time course of tumor response to electrochemotherapy can provide additional insight into the contribution of different antitumor mechanisms to the success of the therapy. Therefore, we developed a model, based on the system of four differential equations, describing the tumor volume dynamics following electrochemotherapy with different doses of cisplatin or bleomycin. An exponential-linear model was employed to describe the unperturbed tumor growth. Parameters, describing the rate of exponential and linear growth, were determined from the control group. The effect of electrochemotherapy was included in the model through a function describing the time delay between electrochemotherapy and cell death. This approach enables to visualize the dynamics of the elimination of the damaged tumor cells from the tumor volume. The results revealed two distinct peaks. The first

peak, which appears shortly after the electrochemotherapy, is related to the action of chemotherapeutic drug, whereas the second peak is presumably related to immune response.

The remaining effects of electroporation, studied in this doctoral thesis, were evaluated using numerical modeling. We built a tridimensional geometry of the skin tissue together with different types of electrodes, most commonly used for skin electroporation - plate, needle and finger electrodes. Modeling of electric field-induced effects included electric field distribution modeling, thermal damage modeling and the simulation of electrophoretic movement of plasmid DNA. Results of the modeling were compared to results of *in vivo* experiments, performed by collaborating groups. According to the model, thermal cell death is limited to a small volume of epidermis. More precisely, thermal damage occurs beneath the regions of high electrical conductivity in stratum corneum, which result from electroporation. Cells, lying around the volume of thermal damage, are also exposed to substantial heat stress, which leads to the heat shock protein synthesis. Experiments show that electric pulse parameters commonly used for gene electrotransfer to skin cause only low level of thermal stress. According to the model, however, actual thermal stress is higher than measured. Namely, the majority of the cells, exposed to the heat stress lies within the volume of irreversible electroporation and are, therefore, unable to express heat shock proteins.

The model of gene electrotransfer, presented in the thesis, simulates the two most important processess, involved in gene electrotransfer - electroporation of cells and electrophoretic movement of plasmid DNA. The simulation of electrophoretic movement represents an important step forward in modeling of gene electrotransfer efficiency, since previously published model mainly rely on electric field distribution. The measure of gene electrotransfer efficiency was based on number of charged particles representing plasmid DNA inside the volume of reversible electroporation. This measure of gene electrotransfer efficiency, however, did not completely explain the differences between the efficiency of different electrodes and pulse parameters observed in experiments. The observed inconsistencies between the model and experiments are not surprising, considering a large number of parameters affecting gene expression, including also the stress due to electroporation. The increase in electrical conductivity of the stratum corneum due to electroporation was identified as one of the critical parameters of the model. Therefore, a better understanding of stratum corneum electroporation as well as other processes involved in gene electrotransfer is required to improve the predictive power of numerical models.

1. UVOD

1.1 Elektroporacija

Pojav elektroporacije dosežemo z Izpostavitvijo bioloških celic električnemu polju dovolj visoke jakosti, ki povzroči strukturne spremembe v njihovi membrani (Neumann et al. 1982; Tsong 1991; Weaver & Chizmadzhev 1996; Weaver 2000; Kotnik et al. 2012; Rems & Miklavčič 2016). Te spremembe se odražajo v povečani prepustnosti celične membrane za molekule, ki jo sicer težko prehajajo. Celična membrana postane bolj prepustna tako za majhne molekule (Pucihar et al. 2008; Rols et al. 1998), kakor tudi za večje molekule, kot so proteini in DNK molekule (Mir et al. 1999; Golzio et al. 2004; Kotnik et al. 2015). V praksi dosežemo elektroporacijo tako, da ciljne celice ali tkivo izpostavimo kratkim, visokonapetostnim električnim pulzom. Glede na uporabljene parametre električnih pulzov lahko dosežemo reverzibilno ali ireverzibilno elektroporacijo (Weaver & Chizmadzhev 1996). O reverzibilni elektroporaciji govorimo takrat, ko celice preživijo in se začnejo po dovajanju električnih pulzov vračati v osnovno stanje. Prepustnost celične membrane se pri tem zmanjša, kar pomeni, da ostanejo molekule, ki so vstopile v celico v času povečane prepustnosti membrane, ujete znotraj celice (Weaver 2000). Pri ireverzibilni elektroporaciji so spremembe v celični membrani in celici tako obsežne, da vodijo v celično smrt (Lee & Kolodney 1987).

Reverzibilnost elektroporacije je odvisna od parametrov električnih pulzov, kot so amplituda, dolžina, število in ponavljalna frekvenca. V splošnem doživi celica ireverzibilno elektroporacijo, če jo dlje časa izpostavimo električnemu polju dovolj visoke jakosti. Z zniževanjem števila, amplitude ali trajanja pulzov dosežemo reverzibilno elektroporacijo, ob predpostavki, da kombinacija parametrov električnih pulzov presega prag elektroporacije (Yarmush et al. 2014).

Pojav elektroporacije lahko opazimo pri vseh vrstah celic - živalskih, rastlinskih in mikroorganizmih, kar omogoča razvoj številnih aplikacij elektroporacije (Haberl et al. 2013; Kotnik et al. 2015). V biotehnologiji se elektroporacija uporablja, na primer, za izboljšanje izkoristka pri ekstrakciji sokov iz sadja in zelenjave (Sack et al. 2010, MAhnič-Kalamiza et al. 2014) ali kot metoda za inaktivacijo mikroorganizmov (Álvarez et al. 2006). Široka uporabna vrednost elektroporacije se je pokazala tudi na področju biomedicine. Z metodami na osnovi reverzibilne elektroporacije lahko izboljšamo vnos genov v ciljne celice (genska elektrotransfekcija) (Wong & Neumann 1982) ali prehajanje kemoterapevtikov v tumorske celice (elektrokemoterapija) (Mir et al.

1991; Serša et al. 1995). Ireverzibilna elektroporacija se je izkazala kot učinkovita metoda za atermično ablacijo tumorjev (Davalos et al. 2005; Scheffer et al. 2014) in drugih tkiv (Maor et al. 2009).

1.2 Elektrokemoterapija

Glavna pomanjkljivost kemoterapije, ki povzroča številne neželene učinke, je neselektivnost delovanja kemoterapevtikov (zdravil, ki zavirajo celično rast in razmnoževanje). To pomeni, da kemoterapevtiki učinkujejo tako na tumorske celice kot tudi na zdrave, predvsem hitro deleče se celice. Uveljavljena metoda zdravljenja, ki omogoča omejitev delovanja kemoterapevtikov na ciljno, torej tumorsko tkivo, se imenuje elektrokemoterapija (Miklavčič et al. 2014). Elektrokemoterapija je metoda zdravljenja na osnovi reverzibilne elektroporacije, katere namen je povečati prepustnost membrane tumorskih celic in s tem povečati vnos kemoterapevtikov v celice. Za uspešnost elektrokemoterapije je potrebno zagotoviti primerno porazdelitev električnega polja, ki omogoči reverzibilno elektroporacijo tumorskih celic in hkrati omeji elektroporacijo zdravih celic (Miklavčič et al. 2006). To pomeni, da je potrebno uporabiti primerne elektrode in določiti ustrezne parametre električnih pulzov. V primeru kožnih in podkožnih tumorjev in zasevkov, za zdravljenje katerih se je elektrokemoterapija uveljavila kot standardna metoda, se parametri zdravljenja določijo v skladu s standardnimi operativnimi postopki (SOP) zdravljenja kožnih tumorjev (Mir et al. 2006). V SOP so zbrana navodila, ki določajo izbiro elektrod, vrsto in dozo kemoterapevtika, ter parametre električnih pulzov (število, amplituda, trajanje in ponavljalna frekvenca) glede na število, velikost in globino tumorskih nodulov. Elektrokemoterapija pa se začenja uveljavljati tudi na področju zdravljenja globoko ležečih tumorjev. Trenutno v Sloveniji potekajo klinične raziskave faze I/II, ki preiskujejo varnost in učinkovitost elektrokemoterapije za zdravljenje tumorjev v jetrih (Edhemović et al. 2014) in v področju glave in vratu (Grošelj et al. 2015). Drugod po svetu poteka razvoj elektrokemoterapije v smeri zdravljenja kostnih metastaz, možganskih tumorjev in raka debelega črevesa (Miklavčič et al. 2012; Stepišnik et al. 2016). Za zdravljenje globlje ležečih tumorjev se uporabljajo posebne igelne elektrode, ki omogočajo posamično vstavljanje elektrod glede na obliko in velikost posameznega tumorja. Za doseganje optimalnih rezultatov elektrokemoterapije je potrebno pripraviti načrt zdravljenja, ki je prilagojen vsakemu bolniku posebej (Miklavčič et al. 2010). Načrtovanje zdravljenja zajema izračun optimalnih pozicij elektrod ter parametrov električnih pulzov na podlagi

geometrijskega modela, pridobljenega iz medicinskih slik bolnika (Pavliha et al. 2012, Pavliha et al. 2013, Marčan et al. 2015).

Učinki elektrokemoterapije

Odgovor tumorja na elektrokemoterapijo je poleg osnovnega učinka zdravljenja (celična smrt zaradi delovanja kemoterapevtika) odvisen še vsaj od dveh spremljevalnih učinkov - učinka na prekrvitev tumorja in imunskega odziva. Elektrokemoterapija povzroči takojšnje zmanjšanje prekrvitve tumorja, ki je nepovratno (Serša et al. 2008; Jarm et al. 2010; Markelc et al. 2013). Začetno zmanjšanje prekrvitve je posledica neposrednega učinka elektroporacije na endotelijske celice tumorskega žilja. Ta učinek je začasne narave, saj se žilje tumorjev, izpostavljenih samo elektroporaciji, po nekaj urah vrne v osnovno stanje. Zmanjšanje prekrvitve po elektrokemoterapiji pa je, nasprotno, dolgotrajno, kar je posledica citotoksičnosti kemoterapevtika na endotelijske celice (Jarm et al. 2010). Zaradi zmanjšane prekrvitve se kemoterapevtik dlje časa zadržuje v tumorju, kar povečuje njegovo učinkovitost. Poleg tega so tumorske celice izpostavljene hipoksičnemu okolju, kar lahko dodatno vpliva na učinkovitost elektrokemoterapije.

Pomemben protitumorski mehanizem elektrokemoterapije je tudi imunski odziv. Pomembnost vloge imunskega sistema pri elektrokemoterapiji so potrdili eksperimenti na miših z normalnim in zavrtim imunskim sistemom. Namreč, samo pri miših z normalno razvitim imunskim sistemom so z elektrokemoterapijo dosegli popolne odgovore, medtem ko so pri miših z zavrtim imunskim sistemom dosegli kvečjemu delne odgovore (Serša et al. 1997). Še več, v nedavni študiji so dokazali posebno vrsto celične smrti po elektrokemoterapiji, ki sproži imunski odziv proti preživelim tumorskim celicam (Calvet et al. 2014).

1.3 Genska elektrotransfekcija za gensko terapijo in DNK cepljenje

Uporabnost reverzibilne elektroporacije se je pokazala tudi na področju vnašanja genov v ciljne celice. Z metodo, imenovano genska elektrotransfekcija, dosežemo povečano prepustnost celičnih membran, ter s tem olajšamo prehajanje genskega materiala (običajno plazmidne DNK) v celice. Glede na namen genske elektrotransfekcije ločimo med gensko terapijo in DNK cepljenjem (Gothelf & Gehl 2012). Pri genski terapiji želimo doseči, da celice proizvajajo terapevtsko molekulo s

sistemskim ali lokalnim učinkom, medtem ko je namen DNK cepljenja spodbujanje imunskega odziva.

Ne glede na namen genske elektrotransfekcije je potrebno zagotoviti elektroporacijo ciljnega tkiva, pri čemer je posebej pomembno, da je elektroporacija reverzibilna, saj je preživetje celic pogoj za izražanje vnesenih genov (Rosazza et al. 2016). Za uspešnost genske elektrotransfekcije je poleg elektroporacije pomemben še en mehanizem - interakcija plazmidne DNK s celično membrano. Med dovajanjem električnih pulzov na negativno nabite DNK molekule deluje elektroforetska sila, ki vpliva na porazdelitev plazmidne DNK med celicami (Klenchin et al. 1991; Wolf et al. 1994). Natančneje, elektroforetska sila omogoči več vezav med plazmidno DNK in celičnimi membranami, oziroma pripomore k tvorbi kompleksov DNK - membrana, ki so ključni za uspešnost genske elektrotransfekcije (Golzio et al. 2002; Faurie et al. 2010; Escoffre et al. 2011). Glede na to, da na uspešnost genske elektrotransfekcije vplivata dva mehanizma, ne preseneča, da se je v številnih *in vitro* in *in vivo* študijah kot najboljša izkazala kombinacija dveh vrst pulzov - kratkih visokonapetostnih (HV - high voltage) in daljših nizkonapetostnih pulzov (LV - low voltage) (Pavšelj & Préat 2005; Šautkauskas et al. 2005; André et al. 2008; Kandušer et al. 2009; Haberl et al. 2013). Visokonapetostni pulzi zagotovijo elektroporacijo membrane celice, nizkonapetostni pulzi pa vplivajo predvsem na elektroforetsko gibanje plazmidne DNK proti celicam (Haberl et al. 2013). Prednost uporabe dveh vrst pulzov je torej v tem, da omogoča optimizacijo parametrov glede na vsakega od obeh mehanizmov posebej. Čeprav je bilo pokazano, da lahko znatno izražanje vnesenih genov dosežemo že z uporabo zgolj ene vrste ustrezno prilagojenih pulzov (Heller et al. 2007), pa kombinacija dveh vrst pulzov omogoča doseganje boljše učinkovitosti.

1.4 Numerično modeliranje za načrtovanje terapij na osnovi elektroporacije

Numerično modeliranje elektroporacije lahko razdelimo na dve veji - modeliranje na nivoju celic in modeliranje na makroskopskem nivoju. Med modele elektroporacije na celičnem nivoju spadajo izračun transmembranske napetosti, modeliranje dinamike nastajanja, širjenja in krčenja por v membrani, modeliranje molekularnega transporta in simulacije molekularne dinamike (Pucihar et al. 2009; Delemotte & Tarek 2012; Rems & Miklavčič 2014). Za načrtovanje terapij se uporabljajo makroskopski modeli, saj bi bilo upoštevanje celične strukture tkiva računsko preveč zahtevno.

Makroskopski modeli predpostavljajo, da je tkivo homogeno, kar pomeni, da se v modelih uporabljajo povprečne električne in mehanske lastnosti posameznih tkiv. Glavna pomanjkljivost makroskopskih modelov je v tem, da ne upoštevajo časovne dinamike elektroporacije v tkivu. Naslednji korak v razvoju makroskopskih modelov torej predstavlja vpeljava časovne dinamike prevodnosti in porazdelitve električnega polja v tkivu. V zadnjem času se zato veliko pozornosti posveča iskanju povezave med celičnimi in makroskopskimi modeli elektroporacije (Langus et al. 2016; Voyer et al. 2018; Dermol-Černe & Miklavčič 2018).

Priprava individualnih načrtov zdravljenja globlje ležečih čvrstih tumorjev z elektrokemoterapijo temelji na numeričnih modelih elektroporacije na makroskopskem nivoju (Kos et al. 2010; Pavliha et al. 2012; Marčan et al. 2015). Postopek načrtovanja se začne z razgradnjo medicinskih slik bolnika (določitev tumorja ter relevantnih organov in struktur), na podlagi katere se zgradi tridimenzionalni geometrijski model. Ta model nato služi izračunu porazdelitve električnega polja upoštevajoč električne lastnosti posameznih tkiv in postavitev elektrod. Na koncu se z algoritmi optimizacije določijo položaji elektrod in napetosti na elektrodah, ki zagotavljajo popolno pokritost tumorja z električnim poljem dovoljšne jakosti.

Numerično modeliranje se, sicer v nekoliko manjši meri, uporablja tudi za optimizacijo parametrov genske elektrotransfekcije. Kot merilo učinkovitosti genske elektrotransfekcije se najpogosteje uporablja porazdelitev električnega polja (Miklavčič et al. 2000; Županič et al. 2010; Županič et al. 2012). Za uspešnost genske elektrotransfekcije je pomembno, da celice niso izpostavljene ireverzibilni elektroporaciji ali drugim poškodbam, ki lahko nastanejo zaradi dovajanja električnih pulzov. Z uporabo numeričnega modeliranja je bil zato ocenjen tudi vpliv poškodb zaradi Joulovega segrevanja (Lacković et al. 2009, Garcia et al. 2014) in zaradi sprememb v pH vrednostih (Olaiz et al. 2014), do katerih pride predvsem v neposredni bližini elektrod.

1.5 Cilji disertacije

Cilj doktorske disertacije je razvoj modelov za opis odziva tumorjev na elektrokemoterapijo in za opis učinkovitosti genske elektrotransfekcije. Namen razvoja modela, ki opisuje odziv tumorjev na elektrokemoterapijo, je raziskati, ali lahko na podlagi dinamike velikosti tumorjev pojasnimo razlike v uspešnosti

elektrokemoterapije z različnimi dozami cisplatina in bleomicina. Namen numeričnega modeliranja genske elektrotransfekcije pa je preveriti skladnost med eksperimenti in trenutnim razumevanjem procesov, ki pomembno vplivajo na učinkovitost genske elektrotransfekcije.

2. METODE

2.1 Modeliranje dinamike odziva mišjih tumorjev na zdravljenje z elektrokemoterapijo

Model odziva tumorjev na elektrokemoterapijo temelji na rezultatih predhodno objavljenih eksperimentalih študij o učinkovitosti elektrokemoterapije na miših (Serša et al. 1995; Serša et al. 1997; Čemažar et al. 1998). Na kratko, pri eksperimentih so uporabili naslednje tumorske modele: tumorje SA-1 na miših A/J, tumorje LPB na miših C57Bl/6 in tumorje LPB na miših Swiss nu/nu. Vrsti miši A/J in C57Bl/6 imata normalno razvit imunski sistem (miši so imunsko kompetentne), medtem ko ima vrsta miši Swiss nu/nu zavrt imunski sistem. Čvrste podkožne tumorje so zdravili s kemoterapijo ali elektrokemoterapijo z različnimi dozami kemoterapevtikov. Uporabili so dva kemoterapevtika: SA-1 tumorje so zdravili z bleomicinom ali cisplatinom, LBP tumorje pa samo s cisplatinom. Pri elektrokemoterapiji so s ploščatimi elektrodami dovedli 8 pulzov dolžine 100 µs pri frekvenci 1 Hz. Razmak med elektrodama je bil 8 mm (tumorji SA-1), oz. 6 mm (tumorji LBP), ustrezni amplitudi pulzov pa 1040 V in 780 V. Po zdravljenju (dan 0) so sledile vsakodnevne meritve volumnov tumorjev.

Model rasti tumorja

V začetnem delu rasti število tumorskih celic narašča eksponentno, nato se rast upočasni in preide v linearno fazo. V končni fazi se rast še naprej upočasnjuje vse dokler ni dosežen "plato", ko se rast popolnoma ustavi. Na eksperimentalnih podatkih lahko opazimo samo prvi dve fazi rasti (eksponentno in linearno), zato smo za modeliranje rasti tumorja uporabili eksponentno-linearni model (Koch et al. 2009):

$$\frac{dX}{dt} = \frac{2\lambda_0\lambda_1 X}{(\lambda_1 + 2\lambda_0 X)} \qquad (1)$$

X označuje število tumorskih celic, parameter λ_0 [dan^{-1}] hitrost eksponentne rasti in parameter λ_1 [celic/dan] hitrost linearne rasti. Pri pretvarjanju iz volumna tumorjev v število celic smo uporabili celično gostoto 10^9 celic/cm^3.

Model odziva tumorja na zdravljenje

Pri modeliranju odziva tumorjev na terapijo (kemoterapijo in elektrokemoterapijo) smo upoštevali naslednje procese: večanje tumorja zaradi celične delitve preživelih celic, manjšanje tumorja zaradi celične smrti ireverzibilno poškodovanih celic, aktivacija imunskih celic, ter interakcija med imunskimi in tumorskimi celicami. Celice smo razdelili na več t.i. razdelkov, ki so opisani vsak s svojo diferencialno enačbo. Model, ki smo ga razvili, je sestavljen iz štirih razdelkov, ki jih opisuje sistem štirih diferencialnih enačb:

$$\frac{dx_1}{dt} = \frac{2\lambda_0\lambda_1 x_1^2}{(\lambda_1 + 2\lambda_0 x_1)\,(x_1 + x_2)} - d\,e^{-kt}x_1 - nx_1y \qquad (2a)$$

$$\frac{dx_2}{dt} = de^{-kt}x_1 - dx_2 \qquad (2b)$$

$$\frac{dx_3}{dt} = dx_2 - bx_3 \qquad (2c)$$

$$\frac{dy}{dt} = cx_3 + p\frac{x_1y}{g + x_1} - mx_1y - ay \qquad (2d)$$

Skupno število tumorskih celic je vsota celic iz prvega in drugega razdelka:

$$X(t) = x_1(t) + x_2(t) \qquad (3)$$

Na začetku (dan 0) vse tumorske celice pripadajo prvemu razdelku (x_1). Po terapiji prehajajo poškodovane celice v drugi razdelek (x_2), kjer vse do celične smrti še vedno prispevajo k velikosti tumorja, vendar se ne delijo več. Z vpeljavo drugega razdelka torej opišemo časovni zamik med terapijo in celično smrtjo. Časovni zamik je potrebno upoštevati tudi pri aktivaciji imunskega odziva, kar opisuje tretji razdelek. Natančneje, tretji razdelek opisuje imunogeno vrsto celične smrti, kar pomeni, da lahko umirajoče celice vzbudijo lastni imunski sistem organizma. Stimulacijo imunskega odziva smo opisali z *Michaelis-Menten kinetiko,* ki upošteva zasičenost imunskega odziva. Interakcija med tumorskimi in imunskimi celicami vodi do zmanjšanja obeh celičnih populacij, kar opisujeta člena nx_1y in mx_1y. Končno, ay opisuje zmanjševanje števila imunskih celic zaradi naravne celične smrti.

2.2 Numerično modeliranje elektroporacije kože

Koža je sestavljena iz več plasti, ki se po debelini in električnih lastnostih precej razlikujejo, zato je numerično modeliranje elektroporacije kože računsko zahtevno. Še posebej računsko zahtevno je numerično modeliranje procesov v zgornjih plasteh kože, ki so zelo tanke. Pri miših je debelina zunanje, rožene plasti (stratum corneuma) le okrog 5 μm in debelina vrhnjice (epidermisa) 15 μm. Poleg omenjenih dveh plasti (rožene plasti in vrhnjice) smo v geometrijo mišje kože, uporabljene pri numeričnem modeliranju, vključili še sledeče plasti: usnjico (dermis), adipozno (maščobno) tkivo, mišično tkivo in podkožno tkivo (Tabela 1).

Posamezne plasti kože se razlikujejo tudi po električnih lastnostih. Pri dovajanju pulzov s ploščatimi elektrodami so pomembne predvsem električne lastnosti rožene plasti, od katerih je odvisna elektroporacija spodaj ležečih plasti kože. Rožena plast ima zelo visoko električno upornost, zato se ob aplikaciji električnih pulzov praktično celoten padec napetosti nahaja na tej plasti. Ob uporabi električnih pulzov dovolj visoke napetosti pa se prevodnost rožene plasti močno poveča (do 1000-krat), kar posledično omogoči elektroporacijo ostalih plasti kože (Pliquett et al. 1995). Povečanje prevodnosti rožene plasti pa ni homogeno po celotni površini, kjer je bil prag elektroporacije presežen, ampak je omejeno na majhna območja. Ta območja, tako imenovana lokalna transportna območja (ang. local transport regions – LTRs), so rezultat novih poti v roženi plasti, ki nastanejo zaradi aplikacije visokonapetostnih električnih pulzov (Pliquett et al. 1998). Velikost in gostota lokalnih transportnih območij (LTR) je odvisna od parametrov električnih pulzov. Z višanjem napetosti električnega pulza se povečuje gostota LTR, medtem ko njihova velikost narašča s trajanjem pulza. LTR so bila v geometrijo kože vključena preko majhnih cilindrov v roženi plasti, katerih gostota je ustrezala podatkom o gostoti LTR v literaturi. Velikost LTR pa ni bila fiksna, ampak je naraščala med dovajanjem pulzov. Med dovajanjem pulzov, namreč, prihaja do močnega Joulovega gretja na območju LTR, kar vodi do povečanja njihove velikosti. Pri okoli 70 stopinj Celzija pride v roženi plasti do nepovratnih sprememb v strukturi oz. do faznega prehoda (Pavšelj & Miklavčič 2011). Z vključitvijo tega faznega prehoda v model lahko spremljamo naraščanje velikosti posameznih LTR, saj se zaradi neenakomerne porazdelitve električne poljske jakosti LTR razširjajo različno hitro. Na ta način natančneje modeliramo spremembe v prevodnosti rožene plasti zaradi elektroporacije, ki vpliva na porazdelitev električne poljske jakosti v preostalih plasteh kože.

Tabela 1: *Definicija numeričnega modela kože: geometrija ter električne in termične lastnosti*

	Debelina [μm]	Električna prevodnost [S/m]	Gostota [kg/m^3]	Termična prevodnost [W/mK]	Specifična toplotna kapaciteta [J/kgK]
Lokalno transportno območje (LTR)	5	0.1	1400	0.2	3600
Rožena plast	5	0.0001	1400	0.2	3600
Vrhnjica	15	0.2 – 0.8*	1200	0.24	3600
Usnjica	200	0.2 – 0.8*	1200	0.45	3300
Maščobno tkivo	150	0.05 – 0.2*	900	0.19	2400
Mišično tkivo	90	0.5	1040	0.5	3350
Podkožno tkivo	2000	0.05	900	0.19	2400
Volumen s plazmidno DNK	-	1.4	1000	0.6	3600
Elektrode	-	1.35×10^6	7810	16.9	477

*prevodnost pod pragom elektroporacije - maksimalna prevodnost elektroporiranega tkiva

Prag reverzibilne in ireverzibilne elektroporacije

Prag elektroporacije je odvisen od parametrov električnih pulzov. V splošnem, krajši so pulzi, višja napetost je potrebna, da dosežemo prag elektroporacije. Odvisnost med dolžino pulza in mejno električno poljsko jakostjo, s katero dosežemo prag elektroporacije, je zelo nelinearna. Na območju kratkih pulzov (do 1 ms) se z večanjem dolžine pulzov mejna električna poljska jakost hitro zmanjšuje, pri daljših pulzih pa nato vedno počasneje. Za 100 μs pulze smo mejni vrednosti električnega polja, s katerim dosežemo prag reverzibilne (600 V/cm) in irreverzibilne elektroporacije (1200 V/cm), vzeli iz literature. Za daljše pulze sta bili meji postavljeni ustrezno nižje, v skladu s (Pucihar et al. 2011): za 5 ms pulze sta bili meji nižji za faktor 1.8, za 20 ms pulze za faktor 2.5 in za 400 ms pulze za faktor 6. Med procesom elektroporacije se električne lastnosti kože spremenijo. Natančneje, elektroporacija se odraža na povečani električni prevodnosti, kar pomeni, da se tudi porazdelitev električnega polja spremeni. Večanje prevodnosti tkiva med reverzibilnim in ireverzbilnim pragom elektroporacije smo v modelu opisali s sigmoidno funkcijo (Pavšelj et al. 2005; Sel et al. 2005). Z iterativnim izračunom smo določili stacionarno porazdelitev električnega polja, ki smo jo nato uporabili za določitev volumna elektroporacije in za oceno termičnih poškodb kože.

Termične poškodbe pri elektroporaciji kože

Temperatura v koži med dovajanjem pulzov narašča zaradi Joulovega gretja. Morebitne termične poškodbe tkiva zaradi elektroporacije smo ocenili z Arrheniusovim integralom, ki upošteva časovni potek temperature ($T(\tau)$) in čas izpostavljenosti povišanim temperaturam (t):

$$\Omega = \int_0^t A \exp\left(-\frac{E_a}{R\,T\,(\tau)}\right) d\tau, \qquad (4)$$

pri čemer A označuje frekvenčni faktor [s^{-1}] in E_a aktivacijsko energijo [J/mol]. Ω je merilo termičnih poškodb, ki smo ga uporabili za izračun deleža preživetih celic, ki je enak $e^{-\Omega}$.

V celicah, izpostavljenih zmernemu toplotnemu stresu, ki ne vodi v celično smrt, se sintetizirajo proteini vročinskega šoka. Vpliv različnih pulznih protokolov na sintezo proteinov vročinskega šoka je z *in vivo* eksperimenti na miših ocenila sodelujoča raziskovalna skupina. Pri eksperimentih so uporabili transgene miši, ki pod vplivom sinteze proteinov vročinskega šoka (Hsp) izražajo gen za luciferazo. Količino sintetizirane luciferaze so določili z meritvami bioluminiscence 6 ur po elektroporaciji, ko je koncentracija luciferaze najvišja. Intenziteta bioluminiscence torej predstavlja merilo za sintezo proteinov vročinskega šoka.

Eksperimentalne rezultate smo primerjali z rezultati numeričnega modeliranja. Pri modeliranju bioluminiscence smo ponovno uporabili enačbo (4), saj tudi sinteza proteinov vročinskega šoka sledi Arrheniusovemu integralu, le parametra A in E_a sta drugačna kot pri modeliranju termičnih poškodb. Za določitev vrednosti obeh parametrov, A in E_a, smo uporabili kontrolno skupino miši, katerih koža na nogi je bila za osem minut izpostavljena konstantni temperaturi. Ko je temperatura konstantna, se Arrheniusov integral poenostavi v linearno odvisnost med Ω in časom izpostavljenosti povišani temperaturi, t. Iskana parametra parametra A in E_a najlažje razberemo iz premice, ki se najbolje prilega meritvam, predstavljenim na grafu $\ln(t) - \ln(\Omega)$ v odvisnosti od $1/T$. Iz naklona premice lahko določimo aktivacijsko energijo E_a, iz presečišča z ordinato pa frekvenčni faktor A.

Genska elektrotransfekcija

Numerično modeliranje smo uporabili tudi za določanje učinkovitosti genske elektrotransfekcije. Ker je pogoj za uspešno gensko elektrotransfekcijo prisotnost

plazmidne DNK ob elektroporirani membrani, smo za vsak pulzni protokol izračunali prostornino elektroporiranega tkiva in simulirali elektroforetsko gibanje plazmidne DNK. Elektroforetski premik plazmidne DNK, L [m], je odvisen od mobilnosti plazmida, μ [m^2/Vs], lokalne električne poljske jakosti, E [V/m] in trajanja pulza, t [s] (Pavlin & Kandušer 2015):

$$L = \mu E t \tag{5}$$

Mobilnost plazmida je odvisna od števila baznih parov. Za plazmid s 4700 baznimi pari znaša mobilnost 1.5×10^4 μm^2/Vs (Pavlin & Kandušer 2015). Mobilnosti ostalih dveh plazmidov, ki sta bila uporabljena pri eksperimentih, smo izračunali glede na število baznih parov. V primeru plazmida pCMV-luc s 6233 baznimi pari smo pri simulaciji gibanja v električnem polju uporabili vrednost mobilnosti 2.0×10^4 μm^2/Vs, v primeru plazmida INVAC-1 s 7120 baznimi pari pa 2.3×10^4 μm^2/Vs.

Pri numeričnem modeliranju genske elektrotransfekcije smo v geometrijo kože vključili še volumen injicirane suspenzije s plazmidom. Pri vseh eksperimentih so uporabili 25 μl suspenzije, ki so jo injicirali intradermalno, zato smo geometrijo kože prilagodili tako, da smo na sredino dermisa dodali elipsoid z volumnom 25 mm^3.

Numerično modeliranje je potekalo v programskem okolju Comsol Multiphysics® (v5.3, Stockholm, Švedska), ki temelji na metodi končnih elementov. Pri simulaciji gibanja plazmidne DNK smo uporabili modul, ki omogoča izračun gibanja nabitih delcev v električnem polju. Nabiti delci, ki predstavljajo plazmidno DNK, so izhajali iz površine elipsoida. Na koncu zadnjega električnega pulza smo določili število nabitih delcev, ki se nahajajo znotraj volumna reverzibilno elektroporiranega tkiva.

3. REZULTATI

3.1 Modeliranje dinamike odziva mišjih tumorjev na zdravljenje z elektrokemoterapijo (Članek 1)

Parametra, ki opisujeta hitrost eksponentne in linearne rasti tumorja, λ_0 in λ_1, smo določili s prileganjem modela rasti tumorja (1) kontrolnim skupinam. Povprečne vrednosti obeh parametrov za posamezni tumorski model so zbrani v Tabeli 2:

Tabela 2: Povprečne vrednosti eksponentne in linearne hitrosti rasti tumorja za posamezni tumorski model

Tumorski model	Vrsta miši	Študija	Eksponentna hitrost rasti λ_0 (dan^{-1})	Linearna hitrost rasti λ_1 (celic/dan)
SA-1	A/J	Čemažar et al. 1998	0.346	$1.24 \cdot 10^8$
SA-1	A/J	Serša et al. 1995	0.357	$0.70 \cdot 10^8$
LPB	C57B1/6	Serša et al. 1997	0.3*	$0.57 \cdot 10^8$
LPB	Swiss nu/nu	Serša et al. 1997	0.3*	$0.62 \cdot 10^8$

* Zaradi pomanjkanja podatkov o rasti tumorja pred zdravljenjem je bila vrednost eksponentne hitrosti rasti nastavljena na 0.3/dan.

Povprečne vrednosti eksponentne in linearne hitrosti rasti smo uporabili pri prileganju modela, ki ga opisujejo enačbe $(2a) - (2d)$, posameznim odgovorom na zdravljenje. Kot je razvidno iz Slik 2, 3 in 4 v članku 1, lahko z modelom dobro opišemo raznolike odgovore na kemoterapijo in elektrokemoterapijo, kar dokazuje tudi visok povprečni R^2 : R^2 = 0.992 za prileganje modela rezultatom, objavljenim v (Čemažar et al. 1998) in R^2 = 0.989 za prileganje modela rezultatom, objavljenim v (Serša et al. 1995). Natančno prileganje modela posameznim odgovorom na zdravljenje smo dosegli z velikim številom prostih parametrov, ki pa niso natančno določljivi (Tabela 1 v članku 1). Iz tega razloga smo poskušali zmanjšati število prostih parametrov, vendar se je izkazalo, da se že z izločitvijo enega samega parametra prileganje modela bistveno poslabša (podatki niso prikazani). Slabše prileganje je bilo opaziti predvsem v primeru delnih odgovorov na elektrokemoterapijo z bleomicinom, zato je število parametrov ostalo nespremenjeno.

Namesto primerjave vrednosti posameznih parametrov smo za ocenjevanje protitumorske učinkovitosti zdravljenja uporabili bolj objektivno merilo - število odmrlih tumorskih celic. Na Slikah 2 - 4 v članku 1 je s črtkano krivuljo prikazana dinamika odmiranja tumorskih celic, iz katere lahko razberemo dva bolj ali manj

izrazita vrhova. Zgodnejši vrh predvidoma odraža citotoksičnost kemoterapevtika, kasnejši vrh pa je predvidoma posledica imunskega odziva. Ocenili smo koliko tumorskih celic odmre zaradi zgodnejših učinkov in koliko zaradi kasnejših učinkov zdravljenja. Izkaže se, da večja učinkovitost elektrokemoterapije v primerjavi s kemoterapijo ne glede na kemoterapevtik (bleomicin ali cisplatin) ni posledica samo večjega deleža celične smrti kmalu po zdravljenju, ampak je protitumorski učinek izrazitejši tudi v kasnejši fazi. Do nekoliko drugačne ugotovitve pridemo, če primerjamo učinkovitosti elektrokemoterapije z bleomicinom in cisplatinom. Doze obeh kemoterapevtikov, ki so jih uporabili pri eksperimentih, povzročijo primerljivo število odmrlih tumorskih celic kmalu po elektrokemoterapiji (Tabela 1, Sliki 5(a) in 5(b) v članku 1). Večje razlike je opaziti predvsem v kasnejši fazi, kar pomeni, da lahko večjo učinkovitost elektrokemoterapije z bleomicinom v primerjavi s cisplatinom pripišemo močnejšemu imunskemu odzivu (Tabela 1, Sliki 5(c) in 5(d) v članku 1).

Prileganje modela rezultatom študije, katere namen je bila primerjava med učinkovitostjo kemoterapije in elektrokemoterapije na miših z normalno razvitim imunskim sistemom in miših z zavrtim imunskim sistemom (Serša et al. 1997), je dalo pričakovane rezultate. Glavne razlike v odgovorih na zdravljenje med obema skupinama miši so namreč opazne šele v kasnejši fazi, ki je povezana z imunskim odzivom (Tabela 2 v članku 1).

Med Biol Eng Comput (2017) 55:1085–1096
DOI 10.1007/s11517-016-1562-1

SPECIAL ISSUE – ORIGINAL ARTICLE

Mathematical model of tumor volume dynamics in mice treated with electrochemotherapy

Tadeja Forjanič[1] · **Damijan Miklavčič**[1]

Received: 2 December 2015 / Accepted: 2 September 2016 / Published online: 22 September 2016

Abstract The effectiveness of electrochemotherapy, a local treatment using electric pulses to increase the uptake of chemotherapeutic drug, includes several antitumor mechanisms. In addition to the cytotoxic action of chemotherapeutic drug, treatment outcome also depends on antitumor immune response. In order to assess the contribution of different antitumor mechanisms to the observed treatment outcome, we designed a model of tumor volume dynamics, which is able to quantify early and late treatment effects. Model integrates characteristics of both main posttreatment processes, namely removal of lethally damaged cells from tumor volume and tumor–immune interaction. Fitting to individual responses gives the insight into the dynamics of tumor cell elimination. Two more or less clearly separable peaks can be observed from these dynamics. Model was used to quantify responses obtained after chemotherapy and electrochemotherapy with bleomycin and cisplatin in immunocompetent and immunodeficient mice. As expected, electrochemotherapy resulted in higher number of lethally damaged cells as well as in stronger immune response compared to chemotherapy alone. Additionally, bleomycin-treated tumors proved to be more immunogenic than cisplatin-treated tumors in the given range of doses.

✉ Damijan Miklavčič
damijan.miklavcic@fe.uni-lj.si

Tadeja Forjanič
tadeja.forjanic@fe.uni-lj.si

[1] Department for Biomedical Engineering, Faculty of Electrical Engineering, University of Ljubljana, Trzaska 25, 1000 Ljubljana, Slovenia

Keywords Electroporation · Electrochemotherapy · Mathematical model · Tumor growth

1 Introduction

Electrochemotherapy is a local anticancer treatment achieving an improved chemotherapeutic action by increasing cell membrane permeability [19, 22, 31, 33]. This increased permeability is achieved by local application of short, high-intensity electric pulses which induce changes in cell membrane resulting in transient enhancement of molecular transport across the membrane. Thus, electrochemotherapy relies on electroporation [13], a phenomenon of increased membrane permeability achieved by electric pulses, which enables enhanced uptake of chemotherapeutic drug into the treated cells. Electrochemotherapy is used in daily clinical practice for treatment of primary and metastatic skin tumors. Comparison between different treatments of cutaneous metastasis showed that electrochemotherapy is at least as efficient as other standard treatments (photodynamic therapy, intralesional therapy, topical therapy and radiotherapy) [32]. Moreover, electrochemotherapy is also very effective for the treatment of internal tumors, as confirmed by first clinical experiences [8, 20].

Tumor response to electrochemotherapy should be considered as the result of several mechanisms, contributing to the beneficial treatment outcome. In addition to the chemotherapeutic cytotoxicity, there are at least two mechanisms, affecting final treatment outcome—antivascular action and immune response.

Electrochemotherapy affects the tumor perfusion leading to increased hypoxia levels and extended exposure to chemotherapeutic drug, which remains entrapped in the tumor area [28]. In addition to immediate, but transient

vascular lock, electrochemotherapy also has a prolonged reduction of tumor blood flow due to cytotoxic effect on endothelial cells (vascular disruption action) [11, 17, 28]. The long-term lack of oxygen and nutrients enhances the cell death of surviving cells supplied by the damaged blood vessels. On the other hand, tumor cells in hypoxic environment can become more resistant and can repopulate tumors after chemotherapy and radiotherapy [34]. Increased tumor hypoxia after application of electric pulses was also demonstrated by enhanced antitumor effectiveness of tirapazamine, a hypoxia-activated drug [5].

Additional antitumor mechanism is the immune response, which plays vital role in eradication of surviving tumor cells, thus preventing tumor regrowth. This was confirmed by studies showing that complete responses could only be obtained in immunocompetent mice, whereas in immunodeficient mice only partial responses were achieved [3, 27]. The immune system seems to play important role also in other cancer treatment modalities [1], among others chemotherapy [2, 35] and radiotherapy [10]. Although the exact mechanisms of the so-called immunogenic cell death [15] are not yet fully understood, it is clear that surface exposure and release of certain molecules from dying tumor cells activate the immune cell recruitment [29]. Local immune response was demonstrated also by histological analyses confirming the immune cell infiltration in the tumor area [16].

Evaluation of anticancer treatments, including electrochemotherapy, is often limited to the observation of long-term outcomes [18]. Monitoring the time course of tumor response can, however, provide additional information regarding the treatment effectiveness and enables a more comprehensive comparison between individual responses. Through the development of models describing tumor volume dynamics, we can obtain cell survival fraction or other measures of treatment efficacy. Modeling of the tumor volume dynamics is already extensively used in oncology drug development [23, 25] and in radiotherapy [9, 26].

In human patients, it is often difficult to obtain sufficient information needed for model development due to limited follow-up examinations after electrochemotherapy. However, the results of preclinical studies conducted on animal tumor models are usually presented by daily measurements of tumor size. In this paper, we present a mathematical model describing the dynamics of the number of tumor cells in mice tumor model following electrochemotherapy. Such model enables estimating the contribution of early (direct cell kill) and delayed treatment effect (immune response) on the observed dynamics. Thus, the model can serve as a tool to compare different tumor responses and to better understand the effects of a specific type of the treatment.

2 Methods

2.1 Animal studies

The data used in this study were in detail described in [4, 27, 30]. Subcutaneous SA-1 sarcoma tumors in A/J mice were subjected to a treatment with BLM [4] or CDDP [30] alone or in combination with high-voltage electric pulses. Electrochemotherapy was performed by eight 100-μs electric pulses of 1040 V amplitude and 1 Hz repetition frequency delivered by two plate electrodes separated by 8 mm. This protocol resulted in sufficiently high electric field throughout the tumor so most of the cells were permeabilized [21, 24]. After the day of the treatment (day 0), tumor volume was determined by daily measurements of three mutually orthogonal diameters (e_1, e_2 and e_3) according to the formula: $V = \frac{\pi}{6} e_1 e_2 e_3$. In the third study, [27], LPB sarcoma was treated in immunocompetent C57B1/6 and immunodeficient Swiss *nu/nu* mice. Chemotherapy and electrochemotherapy with different doses of cisplatin were performed on 25 mm^3 tumors using parallel plate electrodes, spaced 6 mm apart. Pulse parameters (8 pulses of 100 μs width and amplitude of 780 V, delivered at 1 Hz) again assured a successful permeabilization of the majority of tumor cells [6]. In all experiments, drug was injected only on day 0 and pulses were delivered 3 min later, which was demonstrated to be the optimal timing for achieving the highest electrochemotherapy effectiveness of BLM [7] as well as CDDP [30].

2.2 Unperturbed growth

In general, after tumor cell inoculation, tumor begins to grow exponentially, and then, the growth slows down to linear rate, eventually reaching a plateau phase. Since only exponential and linear growth phases can be observed in our experimental data, we adopted a function originally proposed by Koch et al. [12] with smooth transition between exponential and linear growth:

$$\frac{\mathrm{d}X}{\mathrm{d}t} = \frac{2\lambda_0\lambda_1 X}{(\lambda_1 + 2\lambda_0 X)} \tag{1}$$

2.3 Tumor response modeling

Tumor volume was converted to the number of tumor cells assuming a cell density of 10^9 cells/cm^3 in order to model tumor–immune interaction. The model consists of four differential equations. At the day of the treatment (day 0), all tumor cells belong to the first compartment (x_1). Tumor cells, damaged by the treatment, move to the second compartment (x_2), where they still contribute to the total tumor volume, but do not divide anymore. Since

dead-cell resolving takes place soon after the treatment, an exponentially decaying function was employed to limit this process to a first few days after the treatment. Tumor cells die, at least partially, in an immunogenic manner, thereby stimulating the recruitment of immune cells (y) [36]. Since we were specifically interested in the treatment-induced immune response, the initial number of immune cells, y_0, is set to 0. In order to account for the time required to stimulate the immune response, we introduced the third compartment in the model. With parameter b, we also enabled some flexibility at the initial phase of immune response. Equation (2d) describes the dynamics of immune cell population, present at the tumor site, y. Since we wanted to keep the model simple, y includes all types of immune cells. Nevertheless, Eq. (2d), based on the model describing the dynamics of immunogenic tumors by Kuznetsov et al. [14], captures all main characteristics of tumor–immune interaction. Treatment-induced immune response is initiated through the process of immunogenic cell death, meaning that parameter c can be interpreted as a measure for immunogenicity of dying tumor cells. Subsequent recruitment of immune cells is modeled by Michaelis–Menten dynamics to include the saturation effect of the immune response. Further, immune-mediated tumor cell killing leads to mutual decrease in both cell populations. Finally, the number of immune cells decreases due to natural death. Hence, complete system of differential equations reads:

$$\frac{\mathrm{d}x_1}{\mathrm{d}t} = \frac{2\lambda_0\lambda_1 x_1^2}{(\lambda_1 + 2\lambda_0 x_1)(x_1 + x_2)} - de^{-kt}x_1 - nx_1 y \tag{2a}$$

$$\frac{\mathrm{d}x_2}{\mathrm{d}t} = de^{-kt}x_1 - \mathrm{d}x_2 \tag{2b}$$

$$\frac{\mathrm{d}x_3}{\mathrm{d}t} = \mathrm{d}x_2 - bx_3 \tag{2c}$$

$$\frac{\mathrm{d}y}{\mathrm{d}t} = cx_3 + p\frac{x_1 y}{g + x_1} - mx_1 y - ay, \tag{2d}$$

with initial conditions:

$$x_1(0) = x_{10}, \quad x_2(0) = 0, \quad x_3(0) = 0, \quad y(0) = 0$$

Total number of tumor cells is described by the sum of the first and second compartment:

$$X(t) = x_1(t) + x_2(t) \tag{3}$$

Parameter n describes tumor cell killing by immune cells, whereas m describes the immune cell inactivation as a result of this interaction. Further, parameter p denotes the rate of immune cell recruitment, whereas g denotes the steepness of the recruitment curve. The value for g was taken from the literature ($g = 2.019 \times 10^7$ cells) [14]. In order to distinguish between early and late treatment effect, we limited the death of directly damaged cells to a first few days following the treatment by setting a minimum value of parameter k to 0.2 day^{-1}. Parameters were estimated for each individual response, except for the data of immunodeficiency study, where only average data were available. Estimation of parameters was performed using *fitnlm*, a MATLAB's nonlinear model fitting tool.

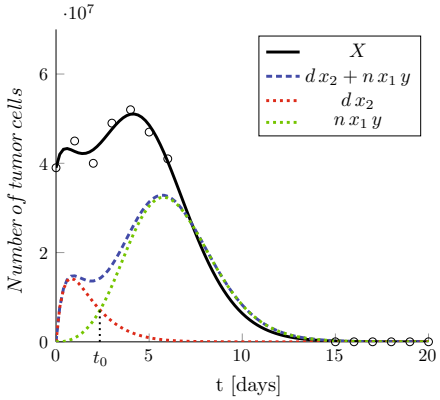

Fig. 1 Complete response with two distinctive peaks, corresponding to dying process of damaged cells ($d\,x_2$) and immune-mediated cell killing ($n\,x_1\,y$)

3 Results

Fitting tumor growth curves to the control group data gave exponential and linear growth rates. Average values were $\lambda_0 = 0.346$ day^{-1} and $\lambda_1 = 1.24 \times 10^8$ cells/day for the mice treated with BLM and $\lambda_0 = 0.357$ day^{-1} and $\lambda_1 = 0.70 \times 10^8$ cells/day for the mice treated with CDDP. From the data of immunodeficiency study, we obtained two linear growth rates: 0.57×10^8 cells/day for immunocompetent mice and 0.62×10^8 cells/day for *nu / nu* mice. However, due to lack of pretreatment growth data, exponential growth rate was fixed to 0.3 day^{-1}.

The proposed model fitted individual responses very well (average $R^2 = 0.992$ for BLM study and average $R^2 = 0.989$ for CDDP study). However, high number of free parameters resulted in high dispersion of parameter estimates (Table 1). Therefore, we estimated a total number of tumor cells, killed directly or by immune mechanisms, as a more valuable and objective measure of treatment efficacy. The contribution of each cell killing mechanism can be assessed from the tumor volume dynamics. By some complete and also partial responses, we can observe two distinctive peaks in a first few days after the treatment (Fig. 1). This dynamics is successfully captured by our model, indicating that first peak corresponds to dying of directly damaged cells and second

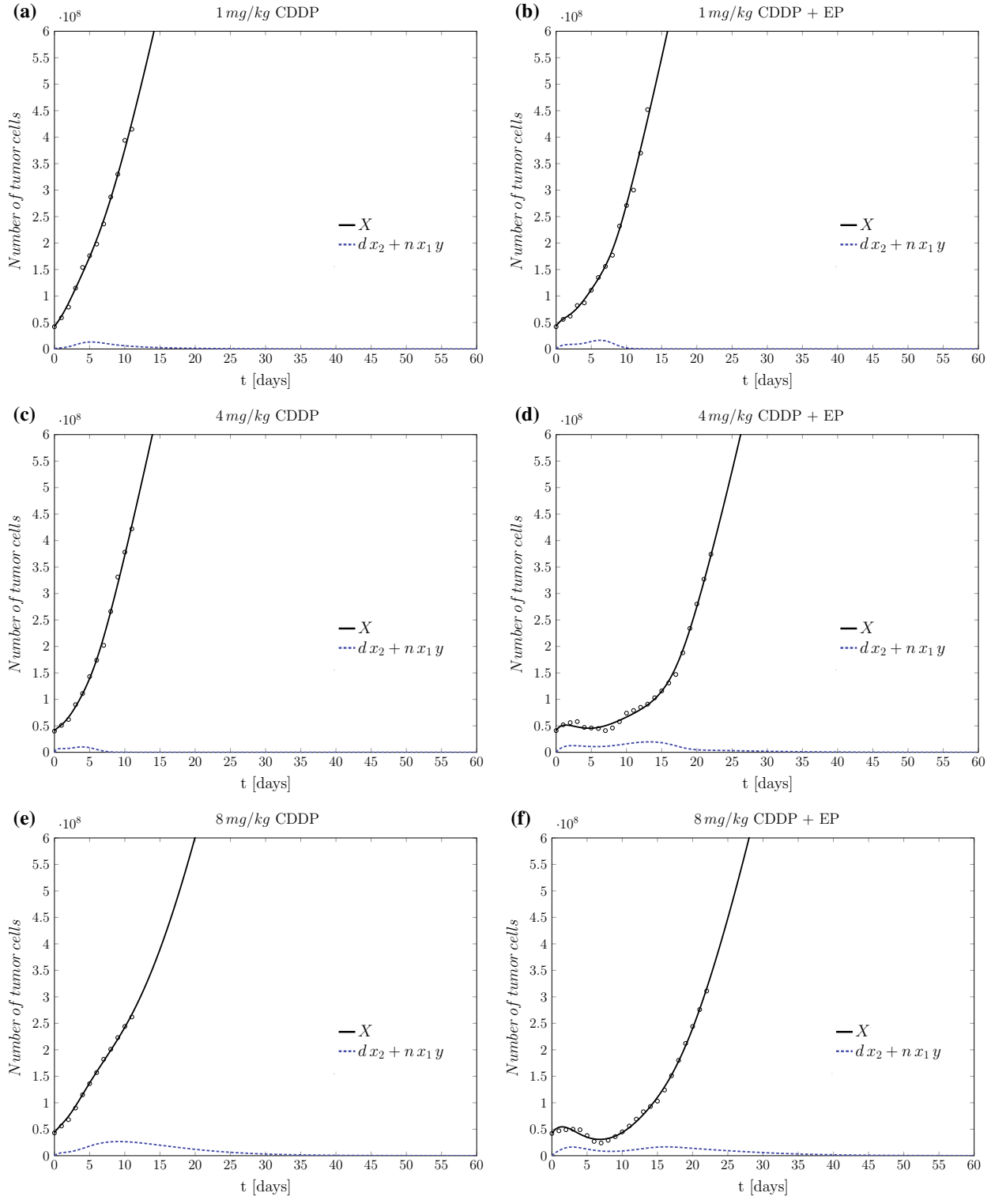

Fig. 2 Selected responses of mice treated with CDDP together with fitted curves. The *left column* shows typical responses obtained after chemotherapy with different doses of CDDP: 1 mg/kg (**a**), 4 mg/kg (**c**) and 8 mg/kg (**e**), whereas the *right column* shows corresponding responses after electrochemotherapy. *Solid line* represents the total number of tumor cells while *dashed line* represents the number of dying tumor cells either due to drug cytotoxicity or immune response

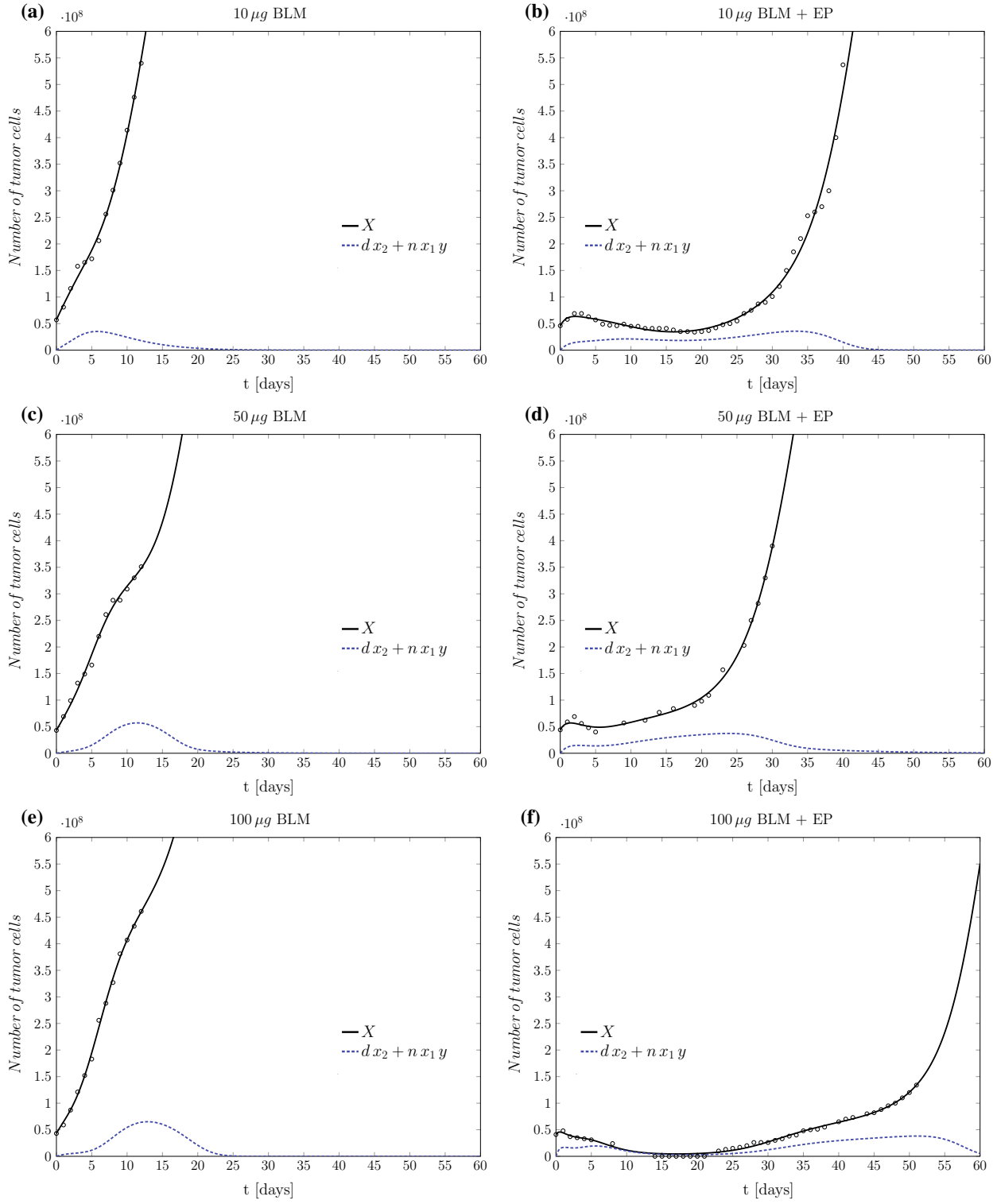

Fig. 3 Selected responses of mice treated with BLM-based chemotherapy and electrochemotherapy together with fitted curves. Similar to Fig. 2, *left column* shows typical responses obtained after chemotherapy and the *right column* shows corresponding responses after electrochemotherapy

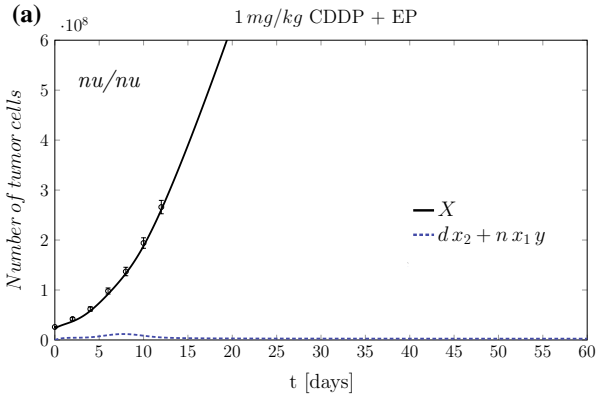
(a)
1 mg/kg CDDP + EP
nu/nu
Number of tumor cells
t [days]
X
d x2 + n x1 y

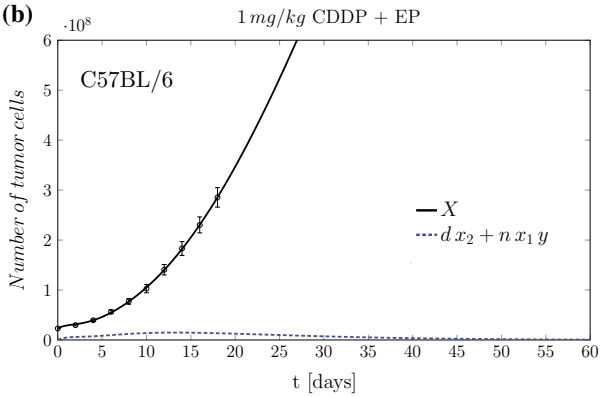
(b)
1 mg/kg CDDP + EP
C57BL/6
Number of tumor cells
t [days]
X
d x2 + n x1 y

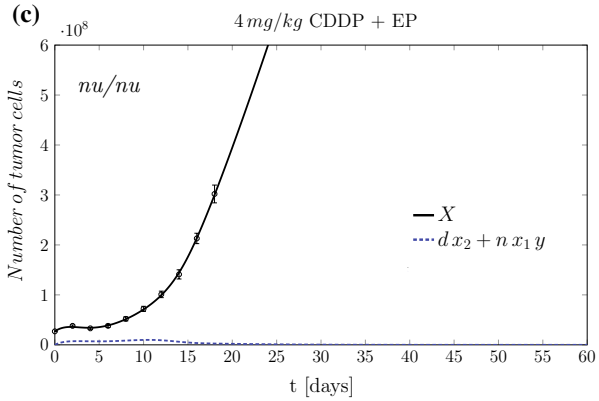
(c)
4 mg/kg CDDP + EP
nu/nu
Number of tumor cells
t [days]
X
d x2 + n x1 y

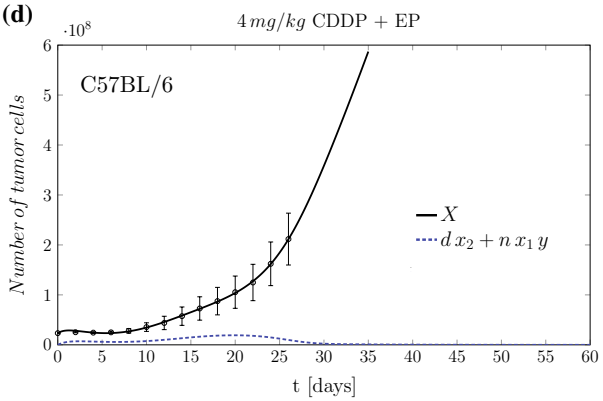
(d)
4 mg/kg CDDP + EP
C57BL/6
Number of tumor cells
t [days]
X
d x2 + n x1 y

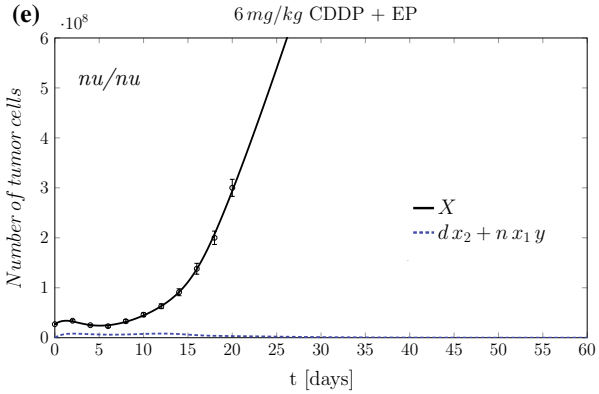
(e)
6 mg/kg CDDP + EP
nu/nu
Number of tumor cells
t [days]
X
d x2 + n x1 y

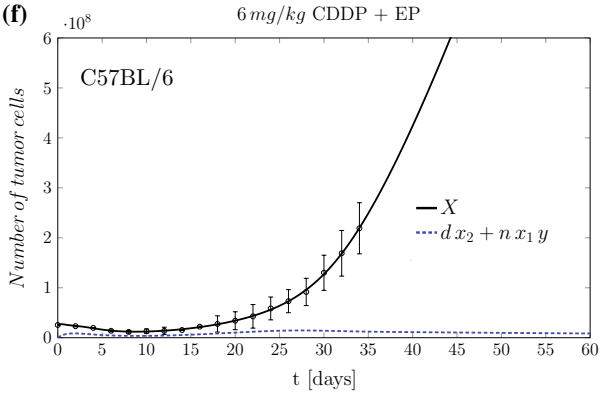
(f)
6 mg/kg CDDP + EP
C57BL/6
Number of tumor cells
t [days]
X
d x2 + n x1 y

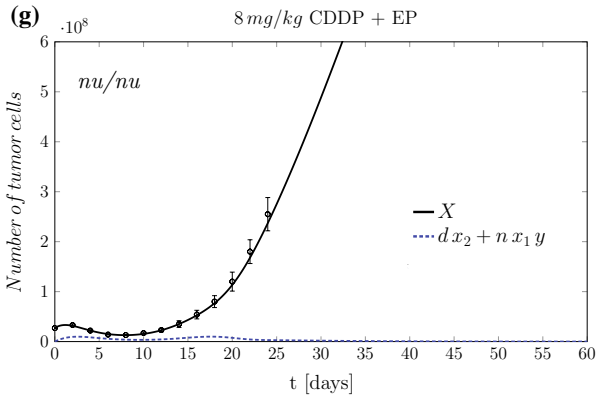
(g)
8 mg/kg CDDP + EP
nu/nu
Number of tumor cells
t [days]
X
d x2 + n x1 y

Fig. 4 Comparison of average responses obtained after CDDP-based electrochemotherapy in immunodeficient *nu/nu* mice (*left column*) and immunocompetent C57B1/6 mice (*right column*). Doses of CDDP used in the study were: 1 mg/kg (**a**, **b**), 4 mg/kg (**c**, **d**), 6 mg/kg (**e**, **f**) and 8 mg/kg (**g**)

peak to immune-mediated cell killing. Moreover, both peaks of cell killing activity are easy distinguishable also in other cases by plotting the time course of killed tumor cells (Figs. 2, 3, 4). Of course, in the cases of weak partial responses peaks become less pronounced, making the separation between both causes of cell death less reliable. In order to objectively separate between both effects, we calculated the time point of equal cell killing efficiency of both antitumor mechanisms according to the model and used it as a limit for integration. More precisely, this time point represented the upper limit for directly killed tumor cells and lower limit for tumor cells killed by immune system.

The calculation of total tumor cell kill is subject to uncertainty arising from the assumption that all animals in each experiment share the same tumor growth parameters.

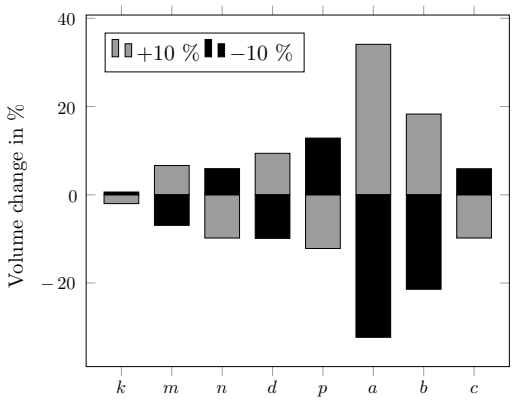

Fig. 6 Percent change in the tumor volume of a selected partial response with 33 days of growth delay after changing each of the parameters for 10 %, one at a time

In order to assess this uncertainty, we first performed the calculation of tumor cell kill on control groups. Average values, obtained from BLM study [4] and CDDP study [30], respectively, were: 0.079×10^8 cells and 0.067×10^8

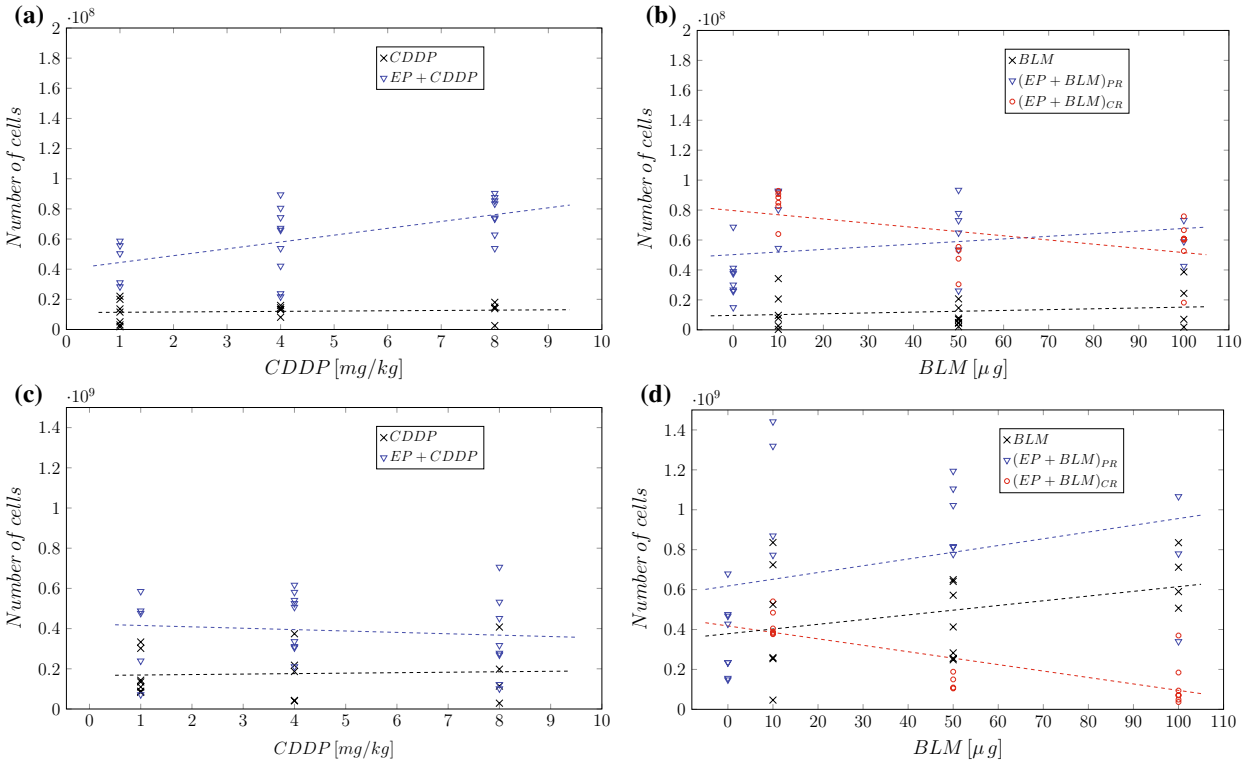

Fig. 5 Number of tumor cells killed directly (**a**, **b**) and number of tumor cells eliminated by immune system (**c**, **d**). Results show that electrochemotherapy effectiveness relies on improved drug action as well as stronger immune response. Complete responses (CR) were achieved only by BLM-based electrochemotherapy, which elicited stronger immune response than CDDP-based electrochemotherapy. Total number of tumor cells killed by immune system is lower by complete responses than partial responses (PR) due to successful elimination of all surviving cells

Table 1 Estimated model parameters obtained by fitting the responses of (a) BLM-treated mice [4] and (b) CDDP-treated mice [30]. Average parameter estimates are given along with their coefficients of variation (between brackets). Additionally, average total number of cells killed due to drug cytotoxicity, $\int_0^{t_0}(\mathrm{d}x_2 + nx_1y)\,\mathrm{d}t$, and immune activity, $\int_{t_0}^{\infty}(\mathrm{d}x_2 + nx_1y)\,\mathrm{d}t$, are presented

(a)

Dose [μg]	BLM			EP
	10	50	100	
N	6 PR	5 PR	4 PR	8 PR
k [day^{-1}]	0.576 (46)	0.286 (25)	0.706 (38)	0.618 (50)
m [cells^{-1} day^{-1}]	6.00×10^{-9} (83)	4.61×10^{-9} (75)	1.42×10^{-9} (8)	5.82×10^{-9} (100)
n [cells^{-1} day^{-1}]	4.16×10^{-6}(95)	2.18×10^{-6}(32)	1.38×10^{-6} (74)	1.65×10^{-6} (90)
d [day^{-1}]	0.201 (33)	0.199 (21)	0.253 (36)	0.478 (28)
p [day^{-1}]	0.344 (68)	0.463 (75)	0.519 (46)	0.925 (22)
a [day^{-1}]	0.096 (141)	0.192 (140)	0.078 (162)	8×10^{-5} (120)
b [day^{-1}]	0.337 (78)	0.528 (59)	0.608 (157)	0.686 (61)
c [day^{-1}]	0.0035 (95)	0.0018 (32)	0.0017 (39)	0.0014 (90)
$\int_0^{t_0}(\mathrm{d}x_2 + nx_1y)\,\mathrm{d}t$	0.13×10^8 (102)	0.09×10^8 (75)	0.18×10^8(94)	0.35×10^8 (45)
$\int_{t_0}^{\infty}(\mathrm{d}x_2 + nx_1y)\,\mathrm{d}t$	4.41×10^8 (69)	4.37×10^8 (42)	6.61×10^8 (22)	3.53×10^8 (53)

Dose [μg]	BLM + EP					
	10	10	50	50	100	100
N	4 PR	6 CR	6 PR	4 CR	3 PR	7 CR
k [day^{-1}]	0.240 (29)	0.200 (0.2)	0.543 (106)	0.639 (50)	0.416 (60)	0.706 (135)
m [cells^{-1} day^{-1}]	2.44×10^{-9} (76)	8.71×10^{-9} (138)	1.43×10^{-9} (125)	3.56×10^{-9} (138)	1.60×10^{-9} (25)	2.66×10^{-9} (173)
n [cells^{-1} day^{-1}]	1.68×10^{-6} (50)	1.43×10^{-6} (70)	2.16×10^{-6} (38)	2.16×10^{-6} (30)	2.69×10^{-6} (14)	1.67×10^{-6} (106)
d [day^{-1}]	0.575 (2)	0.577 (8)	0.870 (37)	0.952 (14)	0.870 (25)	0.986 (36)
p [day^{-1}]	0.332 (92)	0.177 (94)	0.156 (104)	0.435 (69)	0.293 (49)	1.042 (64)
a [day^{-1}]	0.201 (117)	0.170 (197)	0.091 (82)	0.026 (199)	0.155 (52)	0.0004 (168)
b [day^{-1}]	0.326 (124)	0.071 (245)	0.367 (78)	0.231 (176)	0.382 (35)	0.099 (107)
c [day^{-1}]	0.0014 (50)	0.0012 (70)	0.0018 (38)	0.0018 (30)	0.0022 (14)	0.0014 (106)
$\int_0^{t_0}(\mathrm{d}x_2 + nx_1y)\,\mathrm{d}t$	0.80×10^8 (22)	0.84×10^8 (12)	0.65×10^8 (36)	0.47×10^8 (24)	0.58×10^8 (26)	0.56×10^8 (32)
$\int_{t_0}^{\infty}(\mathrm{d}x_2 + nx_1y)\,\mathrm{d}t$	11.01×10^8 (30)	4.29×10^8 (16)	9.54×10^8 (18)	1.38×10^8 (28)	7.29×10^8 (50)	1.25×10^8 (95)

(b)

Dose [mg/kg]	CDDP			CDDP + EP		
	1	4	8	1	4	8
N	7 PR	5 PR	4 PR	5 PR	9 PR	8 PR
k [day^{-1}]	1.893 (38)	2.020 (28)	1.662 (21)	0.681 (76)	0.476 (89)	0.282 (34)
m [cells^{-1} day^{-1}]	2.77×10^{-9} (178)	4.14×10^{-9} (106)	8.95×10^{-9} (89)	10.33×10^{-9} (40)	5.37×10^{-9} (62)	8.78×10^{-9} (50)
n [cells^{-1} day^{-1}]	2.58×10^{-6} (59)	2.34×10^{-6} (37)	4.29×10^{-6} (75)	0.78×10^{-6} (56)	2.15×10^{-6} (70)	2.19×10^{-6} (105)
d [day^{-1}]	0.490 (28)	0.682 (74)	0.634 (40)	0.680 (17)	0.654 (25)	0.730 (16)
p [day^{-1}]	0.161 (145)	0.451 (82)	0.744 (80)	1.502 (12)	0.349 (87)	1.475 (122)
a [day^{-1}]	0.587 (87)	0.270 (119)	0.116 (200)	0.00001 (214)	0.067 (157)	0.806 (176)
b [day^{-1}]	1.52 (52)	0.477 (114)	0.709 (134)	0.309 (129)	0.361 (97)	0.480 (162)
c [day^{-1}]	0.0025 (59)	0.0019 (37)	0.0035 (75)	0.0006 (56)	0.0018 (70)	0.0018 (105)
$\int_0^{t_0}(\mathrm{d}x_2 + nx_1y)\,\mathrm{d}t$	0.11×10^8 (73)	0.13×10^8 (23)	1.12×10^8 (55)	0.45×10^8 (32)	0.58×10^8 (42)	0.76×10^8 (17)
$\int_{t_0}^{\infty}(\mathrm{d}x_2 + nx_1y)\,\mathrm{d}t$	1.71×10^8 (61)	1.72×10^8 (81)	1.87×10^8 (87)	3.72×10^8 (32)	4.37×10^8 (33)	3.47×10^8 (59)

N is the number of successfully fitted partial (PR) or complete responses (CR)

Table 2 Results of parameter estimation using the data of study [27], demonstrating the involvement of the immune response in the antitumor effectiveness of CDDP-based electrochemotherapy. Calculated parameter values were used to estimate the contribution of direct and immune-mediated cell kill

(a)

Dose [mg/kg]	Immunocompetent mice (C57B1/6)						
	CDDP			CDDP + EP			EP
	1	4	6	1	4	6	
k [day^{-1}]	0.779	0.771	0.240	0.629	0.217	0.168	3.138
m [cells^{-1} day^{-1}]	8.13×10^{-9}	2.1×10^{-15}	7.1×10^{-12}	1.0×10^{-13}	4.25×10^{-9}	8.91×10^{-9}	0.96×10^{-9}
n [cells^{-1} day^{-1}]	2.76×10^{-6}	3.90×10^{-6}	2.19×10^{-6}	3.89×10^{-6}	1.96×10^{-6}	1.54×10^{-6}	5.94×10^{-6}
d [day^{-1}]	0.653	0.702	0.462	0.622	0.622	0.720	1.137
p [day^{-1}]	0.115	0.562	0.518	0.562	0.943	0.541	0.002
a [day^{-1}]	0.162	0.668	0.717	0.670	0.501	0.387	0.273
b [day^{-1}]	0.116	0.484	1.230	0.7054	0.4539	0.0141	0.273
c [day^{-1}]	0.0023	0.0032	0.0018	0.0032	0.0016	0.0013	0.0049
$\int_0^{t_0}(dx_2 + nx_1y)\,dt$	0.17×10^8	0.16×10^8	0.58×10^8	0.19×10^8	0.47×10^8	0.49×10^8	0.07×10^8
$\int_{t_0}^{\infty}(dx_2 + nx_1y)\,dt$	1.37×10^8	3.76×10^8	3.02×10^8	3.44×10^8	2.85×10^8	4.53×10^8	1.57×10^8
TGD [days]	1.4	2.1	2.2	2.3	16.5	21.4	0.8

(b)

Dose [mg/kg]	Immunodeficient mice (*nu/nu*)				EP
	CDDP				
	1	4	6	8	
k [day^{-1}]	0.772	1.007	0.616	0.502	3.692
m [cells^{-1} day^{-1}]	9.34×10^{-9}	7.68×10^{-9}	9.62×10^{-9}	7.32×10^{-9}	1×10^{-14}
n [cells^{-1} day^{-1}]	1.90×10^{-6}	6.32×10^{-6}	1.53×10^{-6}	0.95×10^{-6}	5.55×10^{-6}
d [day^{-1}]	0.385	0.486	0.450	0.393	1.075
p [day^{-1}]	1.340	2.166	1.414	1.213	0.031
a [day^{-1}]	7.3×10^{-6}	1.157	7×10^{-7}	0.295	0.468
b [day^{-1}]	1.88	3.83	2.11	4.4×10^{-6}	0.554
c [day^{-1}]	0.0016	0.0052	0.0013	0.0008	0.0046
$\int_0^{t_0}(dx_2 + nx_1y)\,dt$	0.12×10^8	0.10×10^8	0.19×10^8	0.21×10^8	0.06×10^8
$\int_{t_0}^{\infty}(dx_2 + nx_1y)\,dt$	0.47×10^8	0.67×10^8	0.75×10^8	1.45×10^8	0.90×10^8
TGD [days]	0.1	0.5	0.7	0.6	0.5

Dose [mg/kg]	Immunodeficient mice (*nu/nu*)			
	CDDP + EP			
	1	4	6	8
k [day^{-1}]	0.732	0.263	0.224	0.200
m [cells^{-1} day^{-1}]	11.38×10^{-9}	10.47×10^{-9}	11.30×10^{-9}	13.26×10^{-9}
n [cells^{-1} day^{-1}]	1.22×10^{-6}	1.29×10^{-6}	1.32×10^{-6}	5.64×10^{-6}
d [day^{-1}]	0.508	0.580	0.650	0.581
p [day^{-1}]	1.248	0.562	0.393	1.571
a [day^{-1}]	0.100	1×10^{-4}	1×10^{-4}	0.619
b [day^{-1}]	3.8×10^{-6}	0.40	0.33	13.71
c [day^{-1}]	0.0010	0.0011	0.0011	0.0032
$\int_0^{t_0}(dx_2 + nx_1y)\,dt$	0.17×10^8	0.49×10^8	0.54×10^8	0.54×10^8
$\int_{t_0}^{\infty}(dx_2 + nx_1y)\,dt$	1.14×10^8	0.93×10^8	1.02×10^8	1.25×10^8
TGD [days]	0.8	5.8	8.4	13.2

cells, killed directly, and 0.659×10^8 cells and $0.723 \cdot 10^8$ cells, killed by immune system.

Keeping these uncertainties in mind, we proceeded to the calculation of tumor cell kill in treated animals. As expected, electrochemotherapy achieved higher number of tumor cells killed directly as well as higher number of tumor cells killed by immune system than chemotherapy. Moreover, both drugs show similar cell killing efficiency over the range of doses used in experiments. However, there are substantial differences in immune response. BLM-based electrochemotherapy elicited substantially stronger immune response compared to CDDP-based electrochemotherapy (Fig. 5). Complete responses resulted in lower number of tumor cells killed by immune system due to successful elimination of all surviving cells. A key role of immune response is further confirmed by results of immunodeficiency study. Nude mice, lacking T lymphocytes, show significantly weaker immune response compared to immunocompetent mice, explaining the difference in tumor growth delays (Table 2).

Due to high number of free parameters, we considered simplifying the model by combining first two compartments or by eliminating certain parameters. Simplified models were compared to the original model using Akaike information criterion (AIC) and Bayesian information criterion (BIC). In most cases, certain simplifications (elimination of the third compartment and $b = d$) turned out to be justified (data not shown). However, these simplified models could not follow the dynamics of highly responsive tumors to BLM-based electrochemotherapy and were therefore excluded from further analysis and discussion.

3.1 Sensitivity analysis

The impact of individual model parameters on the number of tumor cells at day 40 was evaluated by modifying parameter values for 10 % (Fig. 6). Initial parameter values were taken from a case showing partial response from the group of mice treated with BLM-based electrochemotherapy.

4 Discussion

A high variability of tumor responses can be observed not only between different treatment groups, but also within the same group, particularly in the case of BLM-based electrochemotherapy. This variability is visible in terms of differences in tumor growth delays as well as in differences regarding the shape of tumor volume dynamics. Having in mind presumably different mechanisms of immune response depending on the type of the treatment, we had to design a flexible model, able to follow the individual response curves. On the other hand, model had to be robust enough to allow a reliable estimation of direct and immune-mediated cell killing. While the robustness was achieved by following the characteristics of both cell killing mechanisms, flexibility was added by additional compartment, allowing for the differences at the initiation of immune response.

Results are in agreement with existing knowledge that treatment outcome depends on drug cytotoxicity as well as immune response. Mice treated with CDDP-based electrochemotherapy showed only limited level of immune response, and no complete responses were obtained in given range of doses. On the other hand, BLM-based electrochemotherapy induced more potent antitumor immune responses, which again proved to be the key factor for obtaining complete responses. A decrease in number of killed tumor cells with increasing dose observed by complete responses can be explained by faster regression of tumors and thus lower number of surviving cells that have to be eliminated. Interestingly, also tumors treated by electric pulses only showed a weak immune response, comparable to low-dose chemotherapy.

More important than each cell killing mechanism by itself, is their cooperative action. Electrochemotherapy-treated tumors induce a certain level of immune response, which is capable to control a limited number of tumor cells. Therefore, in addition to efficient direct cell kill, it is important that immune response is initiated fast to eliminate surviving tumor cells. Namely, during the time required for immune cell recruitment, surviving tumor cells continue to proliferate, thus enhancing the possibilities to escape from immune control.

Using a single model to analyze such a wide range of tumor responses leads to poor parameter identifiability by weak tumor responses. Nevertheless, estimated parameters related to tumor–immune competition agree well with the values reported in Kuznetsov et al. [14] ($m = 3.422 \times 10^{-10}$ cells^{-1} day^{-1}, $n = 1.101 \times 10^{-7}$ cells^{-1} day^{-1}, $p = 0.1245\,\text{day}^{-1}$, $d = 0.0412\,\text{day}^{-1}$). It is important to keep in mind, however, that we developed our model to reveal the dynamics of treatment-induced tumor cell killing rather than describe the exact mechanisms involved in the tumor response. For improving the identifiability of model parameters, further experiments about the types and the dynamics of immune cells involved are needed. Our work should therefore be seen as the first step toward assessing drug-, treatment- and tumor-dependent immunogenicity and other factors contributing to tumor response to electrochemotherapy.

5 Conclusions

Tumor response to electrochemotherapy is a complex phenomenon. In this paper, we presented a model that is able to capture the dynamics of two main antitumor effects, namely drug cytotoxicity and immune response. Thus, the model can serve as a tool to quantify the tumor response in terms of direct and immune-mediated cell killing. However, modeling should be considered as a testing hypothesis and thus complementary to experimental work. More profound understanding of immune dynamics would enable to further extend the presented model.

Acknowledgments This work was supported by the Slovenian Research Agency (ARRS) and conducted within the scope of Electroporation in Biology and Medicine (EBAM) European Associated Laboratory (LEA) and the COST Action TD1104 (in particular by a short-term scientific mission COST-STSM-TD1104-21001). Authors would like to thank Gregor Sersa from Institute of Oncology Ljubljana for providing us with the raw data.

References

1. Adkins I, Fucikova J, Garg AD, Agostinis P, Spisek R (2015) Physical modalities inducing immunogenic tumor cell death for cancer immunotherapy. Oncoimmunology 3:e968434
2. Bugaut H , Bruchard M, Berger H, Derangere V, Odoul L, Euvrard R, Ladoire S, Chalmin F, Vegran F, Rebe C, Apetoh L, Ghiringhelli F, Mignot G (2013) Bleomycin exerts ambivalent antitumor immune effect by triggering both immunogenic cell death and proliferation of regulatory T cells. PLoS One 8:e65181
3. Calvet CY, Famin D, Andre FM, Mir LM (2014) Electrochemotherapy with bleomycin induces hallmarks of immunogenic cell death in murine colon cancer cells. Oncoimmunology 3:e28131
4. Cemazar M, Miklavcic D, Sersa G (1998) Intrinsic sensitivity of tumor cells to bleomycin as an indicator of tumor response to electrochemotherapy. Jpn J Cancer Res 89:328–333
5. Cemazar M, Parkins CS, Holder AL, Kranjc S, Chaplin DJ, Sersa G (2001) Cytotoxicity of bioreductive drug tirapazamine is increased by application of electric pulses in SA-1 tumours in mice. Anticancer Res 21:1151–1156
6. Corovic S, Lackovic I, Sustaric P, Sustar T, Rodic T, Miklavcic D (2013) Modeling of electric field distribution in tissues during electroporation. Biomed Eng Online 12:16
7. Domenge C, Orlowski S, Luboinski B, De Baere T, Schwaab G, Belehradek J, Mir LM (1996) Antitumor electrochemotherapy: new advances in the clinical protocol. Cancer 77:956–963
8. Edhemovic I, Brecelj E, Gasljevic G, Marolt Music M, Gorjup V, Mali B, Jarm T, Kos B, Pavliha D, Grcar Kuzmanov B, Cemazar M, Snoj M, Miklavcic D, Gadzijev EM, Sersa G (2014) Intraoperative electrochemotherapy of colorectal liver metastases. J Surg Oncol 110:320–327
9. Gay HA, Taylor QQ, Kiriyama F, Dieck GT, Jenkins T, Walker P, Allison RR, Ubezio P (2013) Modeling of non-small cell lung cancer volume changes during CT-based image guided radiotherapy: patterns observed and clinical implications. Comput Math Methods Med 2013:637181
10. Golden EB, Apetoh L (2015) Radiotherapy and immunogenic cell death. Semin Radiat Oncol 25:11–17
11. Jarm T, Cemazar M, Miklavcic D, Sersa G (2010) Antivascular effects of electrochemotherapy: implications in treatment of bleeding metastases. Expert Rev Anticancer Ther 10:729–746
12. Koch G, Walz A, Lahu G, Schropp J (2009) Modeling of tumor growth and anticancer effects of combination therapy. J Pharmacokinet Pharmacodyn 36:179–197
13. Kotnik T, Kramar P, Pucihar G, Miklavcic D, Tarek M (2012) Cell membrane electroporation- Part 1: The phenomenon. IEEE Electr Insul Mag 28:14–23
14. Kuznetsov V, Makalkin I, Taylor M, Perelson A (1994) Nonlinear dynamics of immunogenic tumors: parameter estimation and global bifurcation analysis. Bull Math Biol 56:295–321
15. Krysko DV, Garg AD, Kaczmarek A, Krysko O, Agostinis P, Vandenabeele P (2012) Immunogenic cell death and DAMPs in cancer therapy. Nat Rev Cancer 12:860–875
16. Markelc B, Bellard E, Sersa G, Pelofy S, Teissie J, Coer A, Golzio M, Cemazar M (2012) In vivo molecular imaging and histological analysis of changes induced by electric pulses used for plasmid DNA electrotransfer to the skin: a study in a dorsal window chamber in mice. J Membr Biol 245:545–554
17. Markelc B, Sersa G, Cemazar M (2013) Differential mechanisms associated with vascular disrupting action of electrochemotherapy: intravital microscopy on the level of single normal and tumor blood vessels. PLoS One 8:e59557
18. Marty M, Sersa G, Garbay JR, Gehl J, Collins CG, Snoj M, Billard V, Geertsen PF, Larkin JO, Miklavcic D, Pavlovic I, Paulin-Kosir SM, Cemazar M, Morsli N, Soden DM, Rudolf Z, Robert C, O'Sullivan GC, Mir LM (2006) Electrochemotherapy—an easy, highly effective and safe treatment of cutaneous and subcutaneous metastases: results of ESOPE (European Standard Operating Procedures of Electrochemotherapy) study. Eur J Cancer Suppl 4:3–13
19. Miklavcic D, Mali B, Kos B, Heller R, Sersa G (2014) Electrochemotherapy: from the drawing board into medical practice. Biomed Eng Online 13:29
20. Miklavcic D, Sersa G, Brecelj E, Gehl J, Soden D, Bianchi G, Ruggieri P, Rossi CR, Campana LG, Jarm T (2012) Electrochemotherapy: technological advancements for efficient electroporation-based treatment of internal tumors. Med Biol Eng Comput 50:1213–1225
21. Miklavcic D, Beravs K, Semrov D, Cemazar M, Demsar F, Sersa G (1998) The importance of electric field distribution for effective in vivo electroporation of tissues. Biophys J 74:2152–2158
22. Mir LM, Orlowski S, Belehradek J, Paoletti C (1991) Electrochemotherapy potentiation of antitumour effect of bleomycin by local electric pulses. Eur J Cancer 27:68–72
23. Mould DR, Walz A-C, Lave T, Gibbs JP, Frame B (2015) Developing exposure/response models for anticancer drug treatment: special considerations. CPT Pharmacomet Syst Pharmacol 4:e00016
24. Pavselj N, Bregar Z, Cukjati D, Batiuskaite D, Mir LM, Miklavcic D (2005) The course of tissue permeabilization studied on a mathematical model of a subcutaneous tumor in small animals. IEEE Trans Biomed Eng 52:1373–1381
25. Rocchetti M, Poggesi I, Germani M, Fiorentini F, Pellizzoni C, Zugnoni P, Pesenti E, Simeoni M, De Nicolao G (2005) A pharmacokinetic-pharmacodynamic model for predicting tumour growth inhibition in mice: a useful tool in oncology drug development. Basic Clin Pharmacol Toxicol 96:265–268

26. Rockne R, Alvord EC, Rockhill JK, Swanson KR (2009) A mathematical model for brain tumor response to radiation therapy. J Math Biol 58:561–578
27. Sersa G, Miklavcic D, Cemazar M, Belehradek J, Jarm T, Mir LM (1997) Electrochemotherapy with CDDP on LPB sarcoma: comparison of the anti-tumor effectiveness in immunocompotent and immunodeficient mice. Bioelectrochem Bioenerg 43:279–283
28. Sersa G, Jarm T, Kotnik T, Coer A, Podkrajsek M, Sentjurc M, Miklavcic D, Kadivec M, Kranjc S, Secerov A, Cemazar M (2008) Vascular disrupting action of electroporation and electrochemotherapy with bleomycin in murine sarcoma. Br J Cancer 98:388–398
29. Sersa G, Teissie J, Cemazar M, Signori E, Kamensek U, Marshall G, Miklavcic D (2015) Electrochemotherapy of tumors as in situ vaccination boosted by immunogene electrotransfer. Cancer Immunol Immunother 64:1315–1327
30. Sersa G, Cemazar M, Miklavcic D (1995) Antitumor effectiveness of electrochemotherapy with cis-diamminedichloroplatinum(II) in mice. Cancer Res 55:3450–3455
31. Sersa G, Miklavcic D, Cemazar M, Rudolf Z, Pucihar G, Snoj M (2008) Electrochemotherapy in treatment of tumours. Eur J Surg Oncol 34:232–240
32. Spratt DE, Gordon Spratt EA, Wu S, DeRosa A, Lee NY, Lacouture ME, Barker CA (2014) Efficacy of skin-directed therapy for cutaneous metastases from advanced cancer: a meta-analysis. J Clin Oncol 32:3144–3155
33. Todorovic V, Sersa G, Flisar K, Cemazar M (2009) Enhanced cytotoxicity of bleomycin and cisplatin after electroporation in murine colorectal carcinoma cells. Radiol Oncol 43:264–273
34. Trdan O, Galmarini CM, Patel K, Tannock IF (2007) Drug resistance and the solid tumor microenvironment. J Natl Cancer Inst 99:1441–1454
35. Zitvogel L, Apetoh L, Ghiringhelli F, Kroemer G (2008) Immunological aspects of cancer chemotherapy. Nat Rev Immunol 8:59–73
36. Zitvogel L, Kepp O, Kroemer G (2011) Immune parameters affecting the efficacy of chemotherapeutic regimens. Nat Rev Clin Oncol 8:151–160

Tadeja Forjanič received a B.S. degree in Physics and a M.S. degree in Medical Physics from the University of Ljubljana in 2011 and 2013, respectively. She is a Ph.D. student in the field of Biomedical Engineering at the University of Ljubljana. Her field of interest is mathematical modeling of biological responses to electroporation-based therapies.

Damijan Miklavčič was born in Ljubljana, Slovenia, in 1963. He received a Masters and a Doctoral degree in Electrical Engineering from University of Ljubljana in 1991 and 1993, respectively. He is currently Professor and the Head of the Laboratory of Biocybernetics at the Faculty of Electrical Engineering, University of Ljubljana. His research areas are biomedical engineering and study of the interaction of electromagnetic fields with biological systems. In the last years, he has focused on the engineering aspects of electroporation as the basis of drug delivery into cells in tumor models in vitro and in vivo. His research includes biological experimentation, numerical modeling and hardware development for electrochemotherapy, irreversible electroporation and gene electrotransfer.

3.2 Numerično modeliranje termičnih poškodb tkiva zaradi elektroporacije in primerjava z meritvami bioluminiscence (Članek 2 - oddan v objavo)

Za modeliranje toplotnega stresa pri elektroporaciji smo najprej določili parametre Arrheniusovega integrala s pomočjo kontrolne skupine. Najnižja temperatura, ki je povzročila povečanje bioluminiscenčnega signala po osemminutni izpostavitvi mišje noge vodni kopeli, je bila 41˚C. Vrednost Ω, merila za bioluminiscenčni signal, je bila postavljena na 1 pri temperaturi 45˚C, ki je povzročila maksimalno biolumiscenco. Iz premice, ki se najbolje prilega meritvam, predstavljenim na grafu $\ln(t) - \ln(\Omega)$ v odvisnosti od $1/T$, smo dobili naslednji vrednosti Arrheniusovih parametrov: 359 kJ/mol za aktivacijsko energijo (E_a) in 2.39 x 10^{56} s^{-1} za frekvenčni faktor (A) (Slika 3 v članku 2).

Eksperimenti, ki so jih naredili v sodelujoči raziskovalni skupini, so pokazali, da elektroporacija povzroča nizko raven bioluminiscence, ki je le štirikrat večja od ozadja. Za primerjavo, intenziteta bioluminiscence, ki so jo izmerili po osemminutni izpostavitvi kože vodni kopeli z 41˚C, je bila kar 20-krat višja od ozadja. Kljub nizkim intenzitetam bioluminiscence pa ne moremo zaključiti, da elektroporacija ne povzroča lokalnih termičnih poškodb. Nasprotno, rezultati numeričnega modeliranja kažejo, da vsi uporabljeni pulzni protokoli povzročijo termično razširjanje lokalnih transportnih območij (LTR). Izmed vseh pulznih protokolov (HV, MV, EGT in HV+MV; Dodatna slika 1 v članku 2) je EGT pulzni protokol povzročil največje gretje, zaradi česar je velikost LTR narasla do 180 µm v premeru. Pri ostalih protokolih so zaradi krajših pulzov ali nižje napetosti velikosti LTR narasle do kvečjemu 55 µm v premeru. Pri numeričnem modeliranju smo uporabili dve gostoti LTR - 4 LTR/mm^2 in 8 LTR/mm^2, ki ležita blizu spodnje in zgornje meje gostot LTR, najdenih v literaturi (Pavšelj & Miklavčič 2011). Velikosti LTR po koncu dovajanja pulzov niso enake, saj je gretje neenakomerno. Kot lahko vidimo iz Slik 4A in 4B v članku 2, velikosti LTR naraščajo proti sredini med obema elektrodama. Izkaže se, da noben izmed pulznih protokolov ne povzroči razsežnejših termičnih poškodb. Vse termično poškodovane celice se nahajajo tik pod LTR in ležijo znotraj mnogo večjega območja ireverzibilne elektroporacije (Slika 4C v članku 2). Ireverzibilna elektroporacija je torej glavni razlog za nizko raven bioluminiscence, saj preprečuje sintezo proteinov vročinskega šoka tudi celicam, ki so izpostavljene zmernemu toplotnemu stresu. K bioluminiscenčnemu signalu tako prispevajo samo celice iz ozkega območja poleg volumna ireverzibilne

elektroporacije, ki so izpostavljene povišanim temperaturam, vendar ne doživijo znatnejših poškodb zaradi elektroporacije (Slika 4D v članku 2).

Rezultati numeričnega modeliranja so torej skladni z nizko izmerjeno bioluminiscenco. Kot je razvidno iz Slike 5 v članku 2, kaže model z višjo gostoto LTR nekoliko višjo raven bioluminiscence in večje razlike med pulznimi protokoli. Bioluminiscenčni profili, pridobljeni z numeričnim modeliranjem kažejo, tako kot eksperimentalni, dva vrhova. V primeru večje gostote LTR je dobro ujemanje med modelom in eksperimenti opaziti tudi v intenziteti profilov, saj je najvišja intenziteta dosežena pri EGT pulznem protokolu, ki mu sledijo HV+MV, MV, ter HV pulzni protokol.

Zaradi nizkih intenzitet bioluminiscence in negotovosti, katerim je podvrženo numerično modeliranje, ni bilo mogoče določiti, koliko k bioluminiscenčnemu signalu prispeva stres zaradi elektroporacije same. Med glavne negotovosti spadata gostota LTR, ki je odvisna od električnega polja in kompleksnost odziva na toplotni stres. Arrheniusova parametra sta bila, namreč, določena na podlagi dolgotrajnejše izpostavljenosti zmernim temperaturam, medtem ko so pri elektroporaciji celice izpostavljene višjim temperaturam za krajši čas. Poleg tega je vrh sinteze proteinov vročinskega šoka pri bolj poškodovanih celicah zakasnjen v primerjavi z manj poškodovanimi celicami, ki dosežejo vrh po 6 urah. Ker je bil bioluminiscenčni signal zajet 6 ur po elektroporaciji, prispevek bolj poškodovanih celic pri meritvah najverjetneje ni zajet.

3.3 Določanje učinkovitosti genske elektrotransfekcije na osnovi numeričnega modeliranja in primerjava z izražanjem reporterskih genov

3.3.1. Genska elektrotransfekcija s ploščatimi elektrodami (Članek 2 - oddan v objavo)

Učinkovitost genske elektrotransfekcije kože je močno odvisna od parametrov električnih pulzov, kar so pokazali tudi eksperimenti, ki so jih izvedli v sodelujoči raziskovalni skupini. Najvišjo učinkovitost genske elektrotransfecije so dosegli v primeru kombinacije HV in MV pulzov, najmanjšo pa v primeru HV pulznega protokola, ne glede na uporabljen plazmid (EGFP ali tdTomato; Slika 7 v članku 2). Eksperimentalne rezultate smo primerjali z rezultati numeričnega modeliranja, ki je vključevalo izračun električnega polja in simulacijo elektroforetskega gibanja plazmidne DNK. Kot merilo učinkovitosti genske elektrotransfekcije smo uporabili število nabitih delcev, ki predstavljajo plazmidno DNK, znotraj volumna reverzibilne elektroporacije. Rezultati modeliranja so potrdili, da so HV pulzi sami neprimerni za gensko elektrotransfekcijo, saj je elektroforetski premik plazmidne DNK zelo kratek (Slika 9A v članku 2). MV pulzni protokol se je izkazal kot učinkovitejši kljub manjšemu volumnu reverzibilne elektroporacije (Tabela III v članku 2). Razlog za večjo učinkovitost MV pulznega protokola leži v večjem elektroforetskem premiku (Slika 9B v članku 2), ki je posledica daljšega trajanja pulzov. Največjo učinkovitost pa, kljub krajši skupni dolžini pulzov, kaže HV-MV pulzni protokol. HV pulzi namreč dosežejo večji volumen reverzibilne elektroporacije, če jih kombiniramo z MV pulzi, ki povzročajo večje segrevanje znotraj LTR. Z MV pulzi torej dosežemo večje velikosti LTR in s tem večjo prevodnost rožene plasti (levi stolpec Slike 9 v članku 2). Na ta način lahko s primerno kombinacijo HV in MV pulzov povečamo volumen reverzibilne elektroporacije in izboljšamo učinkovitost genske elektrotransfekcije.

Numerical model of the *in vivo* determined electroporation induced thermal stress and gene electrotransfer in the skin

Journal:	*Transactions on Biomedical Engineering*
Manuscript ID	TBME-00291-2018
Manuscript Type:	Paper
Date Submitted by the Author:	21-Feb-2018
Complete List of Authors:	Forjanič, Tadeja; University of Ljubljana, Faculty of Electrical Engineering Markelc, Bostjan; University of Oxford, Dept. of Radiation Oncology; Institut de Pharmacologie et de Biologie Structurale Marčan, Marija; University of Ljubljana, Faculty of Electrical Engineering Bellard, Elisabeth; Institut de Pharmacologie et de Biologie Structurale Couillaud, Franck; University of Bordeaux, Molecular Imaging and Innovative therapies in Oncology Golzio, Muriel; Institut de Pharmacologie et de Biologie Structurale Miklavcic, Damijan; University of Ljubljana, Faculty of Electrical Engineering

Numerical model of the *in vivo* determined electroporation induced thermal stress and gene electrotransfer in the skin

Tadeja Forjanič[1,*], Boštjan Markelc[2, 3,*], Marija Marčan[1], Elisabeth Bellard[2], Franck Couillaud[4], Muriel Golzio[2, †] and Damijan Miklavčič[1, †].

***Abstract*— *Objective:* Skin is an attractive target tissue for gene transfer due to its size and accessibility. One of the promising delivery methods is gene delivery by means of electroporation (EP), i.e. gene electrotransfer. To assess the importance of different effects of electroporation for successful gene electrotransfer we investigated: i) the stress response to electroporation, ii) transfection efficiency of different pulse protocols for gene electrotransfer. Moreover, numerical modelling was used to explain experimental results and to test the agreement of experimental results with current knowledge about gene electrotransfer. *Methods:* A double transgenic mice Hspa1b-LucF (+/+) Hspa1b-mPlum (+/+) were used to determine the level of stress sensed by the cell in the tissue *in vivo* that was exposed to EP. The effect of five different pulse protocols on the stress levels sensed by the exposed cells and their efficacy for gene electrotransfer for two plasmids pEGFP-C1 (EGFP) and pCMV-tdTomato was tested. *Results:* Quantification of the bioluminescence signal intensity showed that EP, regardless of the electric pulse parameters used, increased mean bioluminescence compared to the baseline bioluminescence signal of the non-exposed skin. Out of the tested electric pulse protocols the highest expression of EGFP and tdTomato was achieved with HV-MV (high voltage – medium voltage) protocols. *Significance:* Although EP is now widely used as a method for gene delivery, we show that the use of mathematical modelling could benefit the field by helping to increase the efficiency of gene electrotransfer while minimizing the damage caused to the tissue.**

***Index Terms*—electroporation, gene electrotransfer, numerical modelling, skin electroporation, local transport region**

I. Introduction

SKIN is an attractive target tissue for gene transfer and DNA vaccination due to its size and accessibility. Moreover, skin contains antigen-presenting cells and is, thus, a particularly suitable target for DNA vaccination [1], [2]. However, in order to reach the cellular nucleus of the target cell in the tissue, naked DNA has to overcome several barriers/limitations. These include poor mobility of DNA and its rapid degradation in the extracellular space of the tissue, low permeability of the cellular membrane which prevents naked DNA to enter the cell, and poor mobility of the DNA inside the cell [3]. One of the promising delivery methods is gene delivery by means of electroporation [4]- [7]. This delivery method, termed gene electrotransfer (GET), is based on the application of electric pulses, which generate sufficiently high electric fields to achieve increased cell membrane permeability due to the phenomenon, called electroporation (EP). Moreover, electric pulses also generate electrophoretic force, which promotes directional movement of naked DNA within the extracellular space and pushes DNA towards the cell membrane [8]-[11]. Efficient gene electrotransfer requires a careful control of pulse parameters and appropriate choice of electrode configuration [12], [13]. In order to achieve successful gene expression, it is also necessary to avoid excessive cellular damage. Moreover, electroporation itself represents stress for the cell, which together with membrane resealing is energy consuming and, therefore, can compete with the ability of the cell to start expressing the transfected gene. Recently it was shown that gene electrotransfer can upregulate the expression of cytosolic DNA sensors which can in turn lead to inflammation, thus

*These authors contributed equally to this work
† Corresponding authors
*T. Forjanič is with the Department for Biomedical Engineering, Faculty of Electrical Engineering, University of Ljubljana, Tržaška 25, 1000, Ljubljana, Slovenia (email: tadeja.forjanic@fe.uni-lj.si).
*B. Markelc was with the Institut de Pharmacologie et Biologie Structurale, IPBS, Université de Toulouse, CNRS, UPS, BP 64182, 205 Route de Narbonne, F-31077, Toulouse, France. He is now with CRUK/MRC Oxford Institute for Radiation Oncology, Old Road Campus Research Building, Roosevelt Drive, Oxford, OX3 7DQ (email: bostjan.markelc@oncology.ox.ac.uk).
M. Marčan is with the Department for Biomedical Engineering, Faculty of Electrical Engineering, University of Ljubljana, Tržaška 25, 1000, Ljubljana, Slovenia (email: marija.marcan@gmail.com).
E.Bellard is with the Institut de Pharmacologie et Biologie Structurale, IPBS, Université de Toulouse, CNRS, UPS, BP 64182, 205 Route de Narbonne, F-31077, Toulouse, France (email: bellard@ipbs.fr).
F. Couillaud is with the Molecular Imaging and Innovative therapies in Oncology (IMOTION), EA 7435/University of Bordeaux, 146 rue Leo Saignat, 33076 Bordeaux, France (email: franck.couillaud@u-bordeaux.fr).
†M. Golzio is with the Institut de Pharmacologie et Biologie Structurale, IPBS, Université de Toulouse, CNRS, UPS, BP 64182, 205 Route de Narbonne, F-31077, Toulouse, France (correspondence email: muriel.golzio@ipbs.fr, Telephone: +33(0)561175812, Fax: +33(0)561175994).
†D. Miklavčič is with the Department for Biomedical Engineering, Faculty of Electrical Engineering, University of Ljubljana, Tržaška 25, 1000, Ljubljana, Slovenia (correspondence email: damijan.miklavcic@fe.uni-lj.si, Telephone: +386 1 4768 456).

adding additional level of stress that the electroporated cell is exposed to [14].

Expression of heat shock proteins (HSP) is observed when cells are exposed to elevated temperatures. Heat shock proteins are, however, non-specific proteins, meaning their synthesis is not induced only by elevated temperatures, but also by variety of other stressful conditions, including EP [15], [16]. One can determine the expression of HSP's *in vivo* by using transgenic mouse models where bioluminescent or fluorescent reporter genes are linked to HSP promoters. In these models the level of the expression of HSP's can be readily determined by measuring the emitted bioluminescent or fluorescent signal [17], [18]. It is important to distinguish between thermal damage and bioluminescence intensity as a measure of heat shock protein (HSP) expression, which are two fundamentally different processes. The first Arrhenius relationship describes temperature- and time- dependency of the thermal damage, which is usually quantified in terms of cell survival or protein denaturation while the second describes HSP promoter activation. It has been namely shown that HSP expression caused by thermal stress also follows Arrhenius relationship *in vitro* [19] as well as *in vivo* [20]. The relationship between EP and upregulation of HSP expression, however, remains unknown.

To assess the importance of different effects of electroporation on successful gene electrotransfer, the aims of our study included: i) evaluating the stress response to electroporation using a transgenic mouse model that allows firefly luciferase (LucF) expression under the control of the thermo-inducible heat-shock protein (Hsp70) promoter 1B (Hspa1b), ii) comparing transfection efficiency of different pulse protocols for gene electrotransfer of plasmids coding for fluorescent proteins. Moreover, numerical modelling was used as a tool to explain experimental results and to challenge the agreement of experimental results with current knowledge about gene electrotransfer.

II. Materials and Methods

A. *In vivo experiments*

1) Mice

Animal experiments were performed in agreement with European directives and conducted in accordance with French procedural guidelines for animal handling and with approval from the Regional Ethical Review Committee (MP/02/36/10/10). The double transgenic mice Hspa1b-LucF (+/+) Hspa1b-mPlum (+/+) [17], [18] were maintained under 12 h light/dark cycle with water and food ad libitum. One day before the experiments, mice were shaved with clippers and a depilatory cream was applied to remove the hair.

2) Reagents

D-luciferin Na salt (OZBIOSCEINCES) was dissolved in 1x Dulbecco's phosphate-buffered saline (DPBS, Gibco) without $MgCl_2$ and $CaCl_2$ to a final concentration of 30 mg/mL, filtered through a 0.2 µm filter and stored at -80°C until further use. Plasmids pEGFP-C1 (EGFP) and pCMV-tdTomato (tdTomato) (both Clontech) were isolated from competent *E. coli* with EndoFree Plasmid Mega Kit (Qiagen) according to manufacturers' instructions. Quality of isolated plasmid DNA was confirmed with NanoDrop (ThermoFisher). The isolated plasmid DNA was dissolved in sterile H_2O and stored at -20°C.

3) Electroporation and gene electrotransfer

EP was carried out one day after shaving and depilating the mouse. Electric pulses were delivered by contact electrodes (4 mm apart, length 10 mm, 2 mm diameter) connected to electropulsator (ELECTRO cell B10 HVLV (βtech-Leroy biotech, France)). Good contact was assured by means of conductive gel (Eko-gel, Egna, Italy). Except in control mice where nothing was injected, either 25 µL of phosphate buffered saline (PBS, Gibco) or plasmid DNA (tdTomato or EGFP, 25 µg (1 µg/µL)) was injected intradermally immediately (5 s) prior to the delivery of electric pulses. Five different pulse protocols were used in experiments: 1) short, high voltage pulses used in electrochemotherapy (HV) [21], 2) long, high voltage pulses used for gene electrotransfer (EGT) [12], [22], [23], 3) long, medium voltage pulses used in skin electrotransfer (MV) [24], [25], 4) HV + MV unipolar pulses and 5) HV + MV bipolar pulses (Table I, Supp. Fig. 1).

B. *Image acquisition and analysis*

1) Bioluminescence

In vivo bioluminescence (BLI) imaging was performed 6h after EP or control treatment, when the expression of Hspa1b-induced LucF is highest [17], [18]. As a positive control, the right back leg of a mouse was submerged for 8 min in a water bath with automatic temperature regulation while the rest of their body was lying on isolation material to prevent heating of the mouse. Mice were injected with 100 µL of luciferin (3 mg/mouse) intraperitoneally (*ip*) 5 min prior to imaging. Animals were anaesthetized with inhalation anaesthesia (2% Isofluran in air, Vetflurane, VIRBAC-France) delivered by a MiniHub station (TEM-Sega) throughout the experiment. Bioluminescence imaging was performed using a home-built system comprising of a Light box (Photek) equipped with a cooled CCD camera (Andor iKon M, Belfast, UK), a Schneider objective VIS-NIR (Cinegon 1.4/12-0515) and a heating blanket (Harvard Apparatus) to maintain the temperature of mice. Images were acquired with Solis acquisition software (Andor technology) with the following parameters: 16bit, 4x4 binning, 5 min exposure, 6 consecutive images in a series.

Bioluminescence images were processed using FIJI [26] in the following way: i) from each image in a series a fixed value of 300 was subtracted to correct for background pixel intensity, ii) two regions of interest (ROI) were drawn on each mouse, one around the position of electrodes (ROI EP) and the second one on a part of the skin that was not exposed to EP (ROI ctrl), iii) mean pixel intensity from ROI ctrl was used as a threshold in ROI EP to determine the area exhibiting BLI signal above baseline, iv) the ratio of mean pixel intensity ROI EP/ROI ctrl was calculated for each image in a series to give a normalized increase of BLI intensity, v) the highest ROI EP/ROI ctrl ratio from an image series was used in subsequent analysis. To determine average bioluminescence intensity profiles we first drew a line parallel to the original direction of the electrodes.

Then, this line was shifted from the beginning to the end of the region of interest (ROI) one pixel at a time. At each step, we calculated the average intensity along the line, which represents an individual data point of the profile. The same procedure was used to obtain the average simulated profiles.

2) Fluorescence

In vivo fluorescence microscopy was carried out using an upright "Macrofluo" fluorescence macroscope (Leica Microsystems SA, Rueil-Malmaison, France), equipped with a Cool Snap HQ Camera (Roper Scientific, Photometrics, Tucson, AZ, USA). Animals were anaesthetized with inhalation anaesthesia (Isoflurane, Belamont) throughout the experiment. EGFP and tdTomato expression was imaged by fluorescence using specific filters (excitation filters; BP 480/40 nm (EGFP), BP 560/40 nm (tdTomato), emission filters: BP 527/30 nm (EGFP), BP 630/75 nm (tdTomato)). Exposure was kept constant between mice and neutral density (ND) filters were used to prevent overexposure. Each mouse was imaged daily for 16 days.

The expression of EGFP and tdTomato in mice after EP was measured as mean pixel intensity in the transfected area. The transfected area was determined using Otsu thresholding and morphological operations (image opening, image closing) in Matlab. The mean pixel intensity of the thresholded area was then measured for each image, adjusted to account for any ND filters used, and background intensity (determined as mean pixel intensity of the non-transfected skin). The obtained value was then normalized to the highest value in the entire dataset for tdTomato and EGFP separately to give the fraction of the maximum measured mean intensity (fraction of Imax). For each mouse, the highest determined fraction of Imax from the daily imaging series was used in the subsequent analysis. To determine average fluorescence intensity profiles after EP, a 400 pixels thick line was drawn perpendicularly to the position of electrodes on the image obtained 1 day after EP in FIJI software and the mean pixel intensity (of the 400 pixels) for each pixel on the length of the line was calculated.

C. Numerical model of the skin

1) Bioluminescence

Skin was modelled as a three-dimensional multilayered structure with following layers [4], [27]: stratum corneum, epidermis, dermis, adipose tissue, muscle tissue and subcutaneous tissue (Table II). The thickness of the subcutaneous layer was increased in order to reduce the effect of boundary on simulation results. To achieve successful skin EP using non-invasive electrodes, appropriate electric pulses have to be selected to overcome the high resistance of stratum corneum, the superficial layer of the skin. After exceeding EP threshold, resistance of stratum corneum drops for 2-3 orders of magnitude, thus enabling EP of underlying layers [28]. This drop in resistance occurs due to formation of so-called local transport regions (LTRs) [29], which were introduced in the model as small cylinders with initial diameter of 10 µm. During the pulses, the size of LTRs increases if the local temperature rises to around 70 °C [30], a phase transition temperature of stratum corneum lipids. LTR expansion due to Joule heating was modelled as an irreversible phase change at the temperature range 65 – 75 °C with the latent heat of 5300 J/kg [31]. The size of LTRs was assumed constant during each pulse and was updated at the beginning of the next pulse to account for the changes in electric field distribution due to the LTR expansion. Although LTR density increases with the pulse amplitude, the exact relationship is not known. Thus, we modelled two different LTR densities, 4/mm^2 and 8/mm^2, which lie near the low and the high end of the range of reported LTR densities (3-9/mm^2) in the literature [30].

The contact electrodes were modelled as two cylinders with the diameter of 2 mm and center-to-center distance of 4 mm. Conductive gel (Eko Gel, Italy) with the conductivity of 0.155 S/m [32] was introduced in the model as a 2 mm wide layer, placed between each electrode and the skin. To limit the computational cost of numerical simulations, we reduced the size of the model along the electrodes to 1 mm (Fig. 1).

The electric field distribution was calculated by solving the Laplace equation:

$$\nabla \cdot (\sigma(E)\nabla\varphi), \quad (1)$$

where σ is the electrical conductivity and V is the electric potential. The boundary conditions were as follows: one of the electrodes was set to ground (φ = 0 V), while the other electrode was set to electric potential equal to the applied voltage. All outer boundaries of the geometry were treated as electrically insulated. Static electric field distribution was then used to calculate the resistive heat generated during the delivery of the pulses. Resistive heating was included as a source term in the Pennes' bioheat equation which, by neglecting the contribution of metabolism and blood flow [30], simplifies to:

$$\rho c \frac{\partial T}{\partial t} = \nabla \cdot (k\nabla T) + \sigma|\nabla\varphi|^2, \quad (2)$$

where ρ and c are mass density and specific heat capacity of the material, respectively, T is the temperature and k is the thermal conductivity of the material. Before electrodes were placed on the skin, the temperature of the skin tissue was assumed to be 37 ˚C, whereas the temperature of the electrodes and gel was assumed to be 22 ˚C. Since pulse delivery does not begin immediately after placing electrodes on the skin, we first calculated the temperature distribution, established after 30 s of the contact between electrodes, gel and skin tissue (Supp. Fig. 2). This temperature distribution was then used as initial condition at the beginning of the first pulse. A convective heat flux boundary condition was applied at the electrode and tissue top faces, representing the heat dissipation into surrounding air with the temperature of 22 ˚C. The heat transfer coefficient was 5 W/(m^{2}K). Remaining faces of electrodes and skin tissue were treated as thermally insulated.

2) Gene electrotransfer

Modelling of gene transfection efficiency did not involve computationally demanding thermal stress analysis based on the Arrhenius' law, which allowed us to increase the size of the geometry of the model. The length of cylinders representing the

two electrodes, was increased to 10 mm, the complete length of the electrodes used in experiments. Correspondingly, the size of the skin volume was extended to 14 mm in the direction parallel to the electrodes (Fig. 1C). An ellipsoid with the volume of 25 mm^3 was placed in the middle of the dermis, representing the intradermally injected plasmid volume (Fig. 1C). Due to the size of ellipsoid and to reduce the effect of boundary, the thickness of subcutaneous layer was increased to 4 mm. The conductivity of the plasmid solution was set to 1.4 S/m [33], [34] and the LTR density was set to 4 /mm^2.

3) Electroporation of the skin

Five different pulse protocols were used in experiments: HV, EGT, MV, HV + MV unipolar and HV + MV bipolar (Table 1, Supp Fig 1). The duration and number of electric pulses determine the threshold for EP. In general, shorter pulses require higher electric field amplitudes to achieve the same level of EP [35]. Despite this straightforward relationship, EP threshold proved to be rather complex function of pulse amplitude, width and number of pulses. In the literature, we only found the data on EP thresholds for HV pulse protocol. The reversible and irreversible thresholds were set to 600 V/cm and 1200 V/cm [28], respectively. We reduced both thresholds for 5 ms (EGT protocol) and 20 ms pulses (MV protocol) to 1.8- and 2.5-times lower values, respectively, according to Pucihar et al. [36]. The increase in electrical conductivity observed at local electric fields above the reversible threshold, was represented in the model through the sigmoid curve. The temperature dependency of electrical conductivity was neglected, since it is negligible compared to the conductivity changes due to EP. All properties of the skin tissue used in the model are given in Table 2.

4) Arrhenius relationship

Arrhenius relationship was used to determine cell death due to excessive thermal damage [37] and to predict the bioluminescent intensity associated with each of the pulse protocols:

$$\Omega = \int_0^t A \exp\left(-\frac{E_a}{R\,T}\right) d\tau, \qquad (3)$$

where Ω indicates the damage factor, A the frequency factor (s^{-1}) and Ea the activation energy (J/mol). The first set of Arrhenius parameters, describing the thermal damage, was taken from the literature [20], [38], while the second set of parameters, regarding HSP expression, was determined from the mice in the control group (Fig. 2C, Fig. 3). More precisely, it was determined from the bioluminescence intensity measurements resulting from 8 minutes long exposures to constant-temperature water baths. When the temperature is constant, the damage factor, or in our case the bioluminescence intensity, becomes a linear function of heating time. Therefore, both Arrhenius parameters can be determined from the linear regression of ln(t)- ln(Ω) versus 1/T.

5) Numerical simulations of bioluminescence intensity

Excessive cellular stress can cause irreparable damage to the structures involved in the protein synthesis, resulting in reduced bioluminescence intensity. In fact, it has been shown that when the cell surviving fraction following a thermal stress is below 0.4, even the surviving cells are unable to produce heat shock proteins [19], [39]. To account for the reduced heat shock protein production due to mild thermal stress, bioluminescence intensity was assumed to be proportional to the cell surviving fraction. If, however, cell surviving fraction dropped below 0.4, bioluminescence intensity was set to zero. Further, the cells experiencing irreversible EP are also unable to express heat shock proteins and emit any light, thus they were excluded from further calculation. Finally, cells can only emit a limited amount of light due to the expression of heat shock proteins. Therefore, we implemented the restriction on the maximum bioluminescence intensity, which was determined from the heating protocol of 40 minutes at 44 °C. This heating protocol, namely, was shown to result in maximum HSP expression in an *in vitro* study [19].

6) Light propagation

Bioluminescence light is very suitable for *in vivo* applications, since large portion of its broad emission spectrum lies above 600 nm, with an emission peak at 612 nm at 37°C [40]. Below 600 nm, namely, strong haemoglobin absorption limits the transmission of light through the tissue [41]. Scattering, on the other hand, is less wavelength-dependent and limits the spatial resolution of bioluminescence images. In the highly scattering media, such as skin tissue, where scattering dominates over absorption, a diffusion approximation can be used to model the light propagation:

$$-\nabla \cdot \big(D(r)\nabla\Phi(r)\big) + \mu_a\Phi(r) = S(r), \quad r \in \Omega \qquad (4)$$

$$\Phi(r) + 2A(r)D(r)\hat{n} \cdot \nabla\Phi(r) = 0, \quad r \in \partial\Omega \qquad (5)$$

D and μ_a represent the diffusion and absorption coefficient, respectively. $\Phi(r)$ denotes photon power density, $S(r)$ denotes the source distribution and A denotes a factor accounting for the difference in refractive indices across the boundary. The diffusion coefficient is given by $D = 1/(3\,(\mu_a + \mu_s'))$, where μ_s' is the reduced scattering coefficient. Both optical parameters, absorption and reduced scattering coefficient for the mouse skin tissue were taken from the literature [27].

7) Gene expression

Gene electrotransfer is a complex multistep process, which requires the presence of plasmid DNA in the immediate vicinity of reversibly electroporated cell membrane [42]. In addition to increasing the cell membrane permeability, electric pulses also bring DNA molecules in close contact with the membrane due to electrophoresis. Electrophoretic force namely drags the negatively charged DNA molecules toward the side of the cell membrane facing the cathode. The distance that DNA molecules travel due to electrophoresis [10], [43] can be expressed by:

$$L = \mu\, E\, t, \qquad (6)$$

where μ represents electrophoretic mobility, E electric field and t the duration of electric pulses.

In order to evaluate three pulse protocols (HV, MV, HV-MV) in terms of their relative transfection efficiencies, we compared

the number of particles inside the volume of reversible EP. Since the volume of reversible as well irreversible EP increases with LTR expansion, we used electric field distribution resulting from the last pulse to determine the volume of reversibly electroporated cells. For practical reasons and due to limitations of the software, the same electric field distribution was used to simulate the trajectories of charged particles representing plasmid DNA. In the case of HV-MV protocol, the determination of reversible EP volume was based on the last HV pulse, whereas electrophoretic movement simulation was based on the last MV pulse. The simulation of electrophoretic movement was performed using the Charged particle tracing module provided by Comsol. The same number of charged particles was released uniformly from the surface of the bleb every 1 ms to simulate continuous flux of DNA molecules from the bleb to the skin tissue during the pulse delivery. The number of simulated charged particles was chosen arbitrarily, however, it was large enough to obtain accurate estimates of relative transfection efficiencies. The time of simulation was equal to complete duration of electric pulses (0.8 ms, 160 ms and 80 ms for HV, MV and HV-MV pulse protocol, respectively).

Numerical simulations were performed in Comsol Multiphysics® (v5.3, Stockholm, Sweden), except for thermal damage calculation, which was performed in Matlab® (R2017a; The MathWorks, Inc., Natick, MA, USA). The time dependent temperature distribution from the model was imported into Matlab using the Comsol's Livelink with Matlab feature. We used physics-controlled mesh with finer or fine element size for thin layers (stratum corneum with LTRs, epidermis and dermis) and normal element size elsewhere.

8) Statistical analysis

Statistical analysis was carried out using Prism 5 Statistical software (GraphPad Software Inc). A one-way ANOVA with Tukey's test or Pearson test (correlation analysis) were used. A value of $p < 0.05$ was considered to represent a significant difference between groups. Data represents mean ± SEM unless specified otherwise.

III. Results

A. Electroporation induces expression of Hspa1b-dependent LucF resulting in bioluminescence signal

To determine the level of heat stress/HSP expression due to EP, we used transgenic Hspa1b-LucF (+/+) Hspa1b-mPlum (+/+) mice [17], [18], where the exposure of mice to external stress (heat) results in expression of LucF due to activation of Hspa1b promoter, which can be measured as a bioluminescence signal due to luciferase activity of LucF after injection of luciferin and in expression of mPlum protein which can be measured by its emitted fluorescence signal. Bioluminescence signal under the position of electrodes could be readily detected 6 h after EP (Fig. 2A), in contrast, we were unable to detect mPlum fluorescence signal at any time point after EP, most likely due to low levels of expression (data not shown). Quantification of the bioluminescence signal intensity showed that EP, regardless of the electric pulse parameters used increased mean bioluminescence up to 4 fold compared to the baseline bioluminescence signal of the non-exposed skin (Fig. 2B). There was no statistical difference in the bioluminescence intensities after EP between the different electric pulse parameters that we used in the study. However, there was a trend showing that higher bioluminescence intensities could be measured when longer pluses were used. To characterize our transgenic mouse model, we exposed the right back leg of mice to a constant temperature (8 min in a water bath) and performed the same bioluminescence imaging as for EP treated mice (Fig. 2C). Exposure of the leg for 8 min to 41°C resulted in a 20-fold increase in mean bioluminescence compared to the baseline bioluminescence signal of the non-exposed part of the mouse and higher temperatures resulted in even higher increase in mean bioluminescence, showing a temperature dependency of the bioluminescence signal. Altogether, this shows that EP induced bioluminescence can be detected in the transgenic Hspa1b-LucF (+/+) Hspa1b-mPlum (+/+) mice, however, the overall increase of the bioluminescence signal is low compared to the induction achieved by exposing the leg of mice for 8 min to an increased temperature. Of interest it is to note, that even though the detected increase in bioluminescence signal was low compared to the positive control (8 min heating), it was achieved in a very short time, which is 6000 to 600000 shorter than total electric pulse duration (from 80 ms to 800 µs).

B. Numerical modelling of electroporation induced bioluminescence signal due to the expression of Hspa1b-LucF

To better understand how can EP in a such a short time induces the activation of Hspa1b and subsequent expression of LucF resulting in the measured increase in the bioluminescence signal (Fig. 2) and the spatial relationship between the position of the electrodes and the induction of Hspa1b-LucF (Fig. 2A), we employed numerical modelling.

First, we determined the relationship between bioluminescence signal intensity and temperature from our positive control group (Fig. 2C). As the first temperature protocol resulting in an elevated bioluminescence signal was 8 min exposure to 41°C, we therefore performed linear fitting on three data points, corresponding to 41°, 43° and 45°C (Fig. 3). The correlation coefficient of 0.93 suggests that bioluminescence intensity follows Arrhenius relationship in the temperature range of 41°-45°C. The frequency factor and activation energy, obtained from linear regression analysis are 2.39×10^{56} s^{-1} and 359 kJ/mol, respectively. These parameters were then used in numerical model.

All of the tested EP protocols (HV, EGT, MV, HV-MV uni, HV-MV bi) resulted in a very low bioluminescence signal intensities, achieving only up to 4-fold increase in the signal from the treated area with respect to the background (Fig. 2B, Fig. 4). Compared to the positive control group, EP-induced bioluminescence signal equals up to 25% of the bioluminescence signal resulting from the 8 min exposure to 41°C, the threshold temperature for thermal stress response activation. However, since bioluminescence images actually show the mean intensity within each pixel, we cannot conclude there was no local thermal damage. On the contrary, our simulations show that all pulse protocols resulted in formation

of so-called local transport regions (LTRs) expansion (Fig. 4). The EGT pulse protocol shows the largest LTR expansion (180 μm in diameter at the density 4 LTRs/mm^2). Other protocols resulted in significantly smaller LTR expansion (up to 55 μm in diameter) either due to short duration or due to low amplitude of the pulses.

As we can observe from our model (Fig. 4A, B), the distribution of LTR sizes after the last pulse is not uniform across the skin surface. The size of the LTRs increases in the direction towards the opposite electrode, meaning that thermal damage, which follows the evolution of LTRs, is maximal near the inner edges of the gel layer. Nevertheless, the effect of thermal damage on the bioluminescence signal is only minor, since the affected volume is rather small. Moreover, the volume of thermal damage lies within much larger volume of irreversible EP (Fig. 4C), which is therefore the main factor affecting the bioluminescence signal.

If we take a closer look on the distribution of the bioluminescence emission, we can observe that the majority of bioluminescence signal originates from the round-shaped volume of cells below the LTRs (Fig. 4D). The cells inside this volume are unable to emit any light either because of irreversible EP or because the cells were not exposed to sufficiently high temperatures to induce the activation of Hspa1b and subsequent expression of LucF as it is the case for the cells outside this volume. It turns out that the volume of cells, contributing to bioluminescence signal increases with the size of the LTR. Therefore, the peak of bioluminescence signal is located near the largest LTR (Fig 4D).

According to numerical model results, the density of 4 LTRs /mm^2 shows similar bioluminescence intensities for all pulse protocols (Fig. 5A). The density of 8 LTRs/mm^2, on the other hand, shows the highest bioluminescence intensity for EGT pulse protocol, followed by HV-MV, MV and HV protocols, respectively (Fig. 5B), which is in line with experiments. It is important to emphasize, however, that all bioluminescence intensities are rather low due to small volume of light-emitting cells, making the results sensitive to changes in model parameters. Nevertheless, small volume of light-emitting cells explains for the low bioluminescence intensity observed in experiments compared to the positive control. This indicates, that the heat shock response induced by all 5 pulse protocols used is modest at best. Also, a good agreement can be observed in terms of the shape of the profiles, showing two distinctive peaks (Fig. 5A, B).

C. Efficacy of gene electrotransfer of EGFP and tdTomato plasmid DNA depends on the pulse parameters

Electroporation can be successfully used to deliver plasmid DNA into cells and tissue, thus inducing the expression of genes of interest [44]. However, the efficacy of gene electrotransfer varies with pulse parameters used and with the target organ [45]. To determine whether the efficacy of gene electrotransfer to skin can be improved and whether there is a correlation between electroporation induced heat shock response and subsequent gene expression we used two different plasmids, one coding for EGFP and the other for tdTomato, both under constitutive CMV promoter, and measured their expression after gene electrotransfer with four different electric pulse parameters commonly used for gene electrotransfer to skin [4].

Out of the four tested electric pulse protocols (HV, MV, HV-MV uni and HV-MV bi) the highest expression of EGFP and tdTomato was achieved with both HV-MV protocols (Fig. 6), with no statistically significant difference between them, thus demonstrating that reversing the polarity of electric pulses within the train of pulses does not improve gene electrotransfer efficacy *in vivo* in skin. Interestingly, the MV electric pulse protocol proved as efficient as the HV-MV protocols in the group of mice where EGFP plasmid DNA was used (Fig. 6B), whereas in the group of mice where tdTomato plasmid DNA was used it's efficacy was only about 50% of the HV-MV pulse protocols (Fig. 6A), indicating that the plasmid DNA also plays a role in the efficacy of gene electrotransfer. To note is that in both cases the HV pulse parameters were able to induce only low levels of gene expression regardless of the plasmid DNA used (Fig. 6).

Our results on Hspa1b-LucF induction after EP suggest that the skin directly under the electrodes should also have the highest level of gene expression after gene electrotransfer of plasmid DNA. The fluorescence intensity profiles (indicating the level of expression) of EGFP and tdTomato measured 1 day after EP (Fig. 7) showed a remarkable similarity to the experimentally measured bioluminescence intensities (Fig. 2 and Fig. 5) with the majority of expression detected under the electrodes, with a more pronounced peak under the anode except when HV pulse protocol was used to deliver tdTomato plasmid DNA (Fig. 7). The injection of plasmid DNA without EP resulted in barely detectable expression of either EGFP or tdTomato (Fig. 7) demonstrating the need for EP to enable plasmid DNA to enter the cells. Although the similarity between the measured fluorescence intensity profiles of EGFP and tdTomato expression and bioluminescence signal would suggest a strong correlation between the Hspa1b-LucF induction after EP and gene electrotransfer efficacy, our results did not confirm this. We were only able to detect a modest correlation (Pearson r=0.401, P=0.047) between the expression levels of tdTomato and bioluminescence signal resulting from Hspa1b-LucF induction after EP, whereas there was no correlation in the group where EGFP plasmid DNA was used (Fig. 8). A possible explanation could be found in the localization of expression of tdTomato and EGFP at later time points after EP (Fig. 6) where the expression was no longer localized only under the electrodes, but more homogeneously in the entire electroporated area of the skin and in the muscle fibres under the skin (Fig. 6A), indicating that, although the initial expression is observed mainly under the electrodes, there is a large volume of cells between the electrodes that is also transfected with plasmid DNA.

All together, these results show that HV-MV electric pulse protocols, with our without reversing the polarity of pulses, can achieve higher levels of expression compared to MV and HV electric pulse protocols, however, their efficacy also depends on the plasmid DNA used. Although, the initial expression of fluorescent proteins resembles the pattern of LucF induction after EP, the overall expression of the gene of interest is not

correlated with the level of LucF induction.

D. Numerical modelling of gene electrotransfer efficacy

To further explore the relationship between electric field distribution and gene expression due to introduction of plasmid DNA, after EP, we once again used numerical modelling. The presence of a plasmid volume affects the electric field distribution resulting in higher temperatures and larger LTR expansion (Fig. 9) compared to bioluminescence experiments with no plasmid injection. Despite higher temperatures, thermal damage was not evaluated, since it overlaps with larger volume of irreversible EP, as shown in the case of bioluminescence. Right column of the Fig. 9 shows the side of the bleb facing the anode. Electrophoretic movement towards the cathode is negligible, thus explaining the pronounced peak of expression under the anode, observed in experiments.

Gene transfection efficiencies of the three pulse protocols used in experiments were evaluated in terms of the number of plasmid DNA molecules inside the volume of reversible EP. After the completion of the pulse delivery, the lowest number of plasmid DNA molecules present inside the volume of reversible EP was obtained in the case of HV pulse protocol (Table 3), which agrees with experiments. MV pulses, on the contrary, achieve better transfection efficiency due to larger electrophoretic distance. According to our numerical model, even better transfection efficiency is expected from the combination of 4 HV and 4 MV pulses, although plasmid DNA travels only about half a distance compared to MV protocol. The use of HV pulses, namely, results in larger volume of reversible EP, particularly in combination with longer pulses, which cause larger thermal expansion of LTRs. However, with larger LTRs increases also the volume of irreversible EP, which prevents successful transfection. This double effect is clearly visible from the Fig. 9, which presents the movement of plasmid DNA through the volume of reversible EP. Namely, in the region between the center of larger LTRs and the surface of the bleb, only initial part of the movement is presented, meaning that only those cells, lying near the surface of the bleb contribute to the transfection efficiency. The difference in mobility of both plasmids due to their different length has only minor effect on the expected transfection efficiency.

IV. Discussion

Optimizing pulse parameters for gene electrotransfer means finding a compromise between optimal electric field distribution, providing sufficient volume of reversibly electroporated cells, optimal plasmid DNA distribution and minimal tissue damage. In this study, we examined the relative importance of electroporated volume, electrophoresis, stress response and thermal damage on transfection efficiency. For this purpose, we used bioluminescence imaging and numerical modeling in addition to measuring the expression levels of two plasmids (coding for EGFP and tdTomato) after gene electrotransfer with different pulse protocols.

Despite the advances in computer power and software tools, skin electroporation remains challenging for numerical simulations. The main reasons are very fine meshing due to complexity of the skin structure and very fine time stepping, which is required to catch the rapid changes in temperature distribution during the pulse delivery. Therefore, we built only a 1 mm thick slice of complete geometry. Namely, we had to reduce the number of LTRs, which make the simulations very time consuming, especially in combination with the thermal damage calculation. However, 1 mm thickness proved to be sufficient to obtain accurate results, since further increase in size did not affect the results. Thermal damage calculation was not included in gene electrotransfer simulations, thus the reduction of geometry was not necessary.

Numerical model shows the thermal expansion of individual LTRs, which depends on the local electric field. In addition to size, the distribution of LTRs also affects EP of underlying layers and electrophoretic movement of plasmid DNA. Better understanding of LTR formation is, therefore, required for improving the accuracy of simulations. We modelled LTRs as predefined structures, thus neglecting any dynamics in LTR formation. Also, we assumed a uniform distribution of LTRs across the part of the stratum corneum, exposed to high electric fields (below the gel). Actual distribution of LTRs is probably not uniform, since their density depends on the local electric field. Nevertheless, model is still able to explain the transfection efficiencies of different pulse protocols. Moreover, model enables visualization of the volume of cells transfected with plasmid DNA. Therefore, model can be used as a tool to optimize pulse parameters and site of administration for targeted transfection of different skin layers. By regulating the depth of transfection in the skin we can, namely, achieve local or systemic action of gene and control the duration of gene expression [46].

A. Bioluminescence (stress response to EP)

Bioluminescence imaging was performed in order to evaluate the stress response to five different EP pulse protocols. Despite the small differences between treated groups, our aim was to explore whether these differences can be explained by thermal and electroporation-induced stress in the skin using numerical modelling.

All tested pulse protocols resulted in similar, low bioluminescence intensity. Numerical simulations suggest that bioluminescence intensity is low due to small volume of cells exposed to sufficiently high temperatures, which are not irreversibly electroporated. The small volume of light emitting cells was also a reason we were unable to discriminate between thermal and electroporation-induced stress.

Simulated bioluminescence intensities resulting from the model with higher LTR density agree with experiments. However, we cannot conclude that thermal stress alone explains the differences in measured bioluminescence considering low level of bioluminescence and relatively large number of model parameters. First, bioluminescence intensity is affected by the uncertainty in EP threshold determination, especially the irreversible threshold, which served as an indicator of cell death [47]. Another source of uncertainty in numerical model results is the complexity of heat shock response. Bioluminescence images were acquired 6 hours after EP, since this time delay has

been determined as optimal for achieving maximum bioluminescence intensity after long exposures to moderate temperatures [18]. In our case, however, hyperthermia was achieved by short exposures to high temperatures, which results in delayed bioluminescence peak. This delay was observed *in vitro* [48] as well as *in vivo* [49]- [51] and depends on the severity of the thermal stress and therefore on the time required to repair the damaged cell mechanisms. Moreover, we have to keep in mind possible limited validity of Arrhenius parameters at high temperatures, since regression analysis was performed in the temperature range from 41° do 45°C. Nevertheless, the temperature rises above 60°C are very limited. Also, these areas are usually too severely affected by either thermal damage or irreversible EP to emit any light. Moreover, pulse protocols used in irreversible electroporation (IRE) where much higher voltages and number of pulses are used than in our study, is still considered as a non-thermal ablation method [52].

Finally, there is a limited knowledge on the cellular stress due to EP itself. Similar observation in terms of treatment (by ultrasound) related stress was reported [48], showing increased levels of HSP even below the thermal stress threshold, presumably due to ultrasound treatment itself. Increased levels of HSP were demonstrated also in the case of EP [15], [16], indicating the upregulating effect of EP on bioluminescence. On the other hand, permeabilization of cells may cause leakage of ATP, which represents the source of energy for the chemical reaction, leading to bioluminescence. The overall effect of EP on bioluminescence is probably dependent on the severity of the stress and the cells' ability to recover from stress.

B. Gene expression of genes introduced into the cells by EP

As suggested in the literature, short HV pulses alone are not most suitable for gene electrotransfer due to short electrophoretic distance. However, HV pulses proved to be efficient in combination with MV pulses (also named LV - low voltage pulses), which is in agreement with experimental observations. Moreover, our simulations support the presumable role of HV pulse as permeabilizing pulse and MV pulse as electrophoretic pulse. Despite the shorter electrophoretic distance and smaller LTR sizes achieved by 4 MV pulses, the HV-MV protocol proved to be more efficient than MV protocol with twice as many MV pulses. This confirms the importance of increasing the volume of reversible EP. The difference in electroporated volume between MV and HV-MV protocols may be even larger taking into account the higher LTR density achieved by HV pulses, which was neglected in our simulations.

The differences regarding unipolar and bipolar pulses cannot be explained by our numerical model, since both parameters, EP and electrophoresis, depend only on the norm of the electric field. The reason for better transfection efficiency of bipolar pulses, which is evident in the case of Tomato plasmid, may lie in different sizes of electroporated areas on each side of the cell. The side of the cell facing the anode is hyperpolarized, meaning it reaches the threshold transmembrane potential for EP before the other side of the cell, which is depolarized [53]. By increasing the electric field intensity, the threshold is also reached at the other side of the cell, but the area being electroporated is always smaller than the one on the hyperpolarized side [54], [55]. When using unipolar pulses, plasmid DNA encounters the depolarized size of the cell. The bipolar pulses, on the other hand, enable the contact with the larger electroporated area on the hyperpolarized side, therefore improving the transfection efficiency. We have to keep in mind, however, that changing the orientation of electric field can also have a negative impact on the transfection efficiency. The action of electrophoretic forces in the opposite direction can, namely, lead to partial removal of the DNA from the cell membrane. Due to this effect, unipolar pulses proved to be better choice than bipolar at delays shorter than 100 μs between subsequent pulses [56]. The lag between the electrophoretic MV pulse and the next HV pulse, which is close to 1 s in our experiments, is sufficient for formation of a stable plasmid-membrane complex, but still enables a partial loss of DNA-cell membrane interactions [56].

The low level of HSP induction after EP regardless of the pulse parameters used show that although the cells exposed to EP sense stress, it is at a very low level. Interestingly, although all of the tested pulse parameters induced similar level of HSP expression, there were significant differences in their transfection efficiency for plasmid DNA. Implying, that there is no connection between the induced stress levels and transfection efficiency. Furthermore, although EP is now widely used as a method for gene delivery, we show that there are still possibilities for improving its efficacy by modulating pulse parameters.

V. Conclusion

The application of electric pulses, commonly used for gene electrotransfer to skin, results in the low level of HSP induction. This indicates that surviving cells experience low level of thermal and electroporation-induced stress. According to the model, however, measurements underestimate the overall thermal stress caused by electric pulses. Namely, the volume of cells experiencing thermal stress partially overlaps with the volume of irreversible EP, which prevents HSP expression. In contrast to similar levels of HSP expression, induced by all tested electric pulse protocols, significant differences were observed in transfection efficiencies. As expected, the combination of HV and MV pulses achieved higher levels of expression compared to MV and HV electric pulse alone. However, the efficacy of electric pulse protocols depends also on the plasmid DNA used. Therefore, deeper understanding of the processes involved in electroporation mediated gene delivery is required to further improve the efficacy of gene electrotransfer.

Acknowledgment

This work was supported by grants of the InterRegion Aquitaine-Midi-Pyrénées Project (N°12050112), by grants of the Region Midi-Pyrénées (N°11052700 and N°13050740) and by the Slovenian Research Agency (Research programme P2-0249 and funding to TF). Research was conducted within the

scope of the Electroporation in Biology and Medicine European Associated Laboratory (LEA EBAM) and resulted from the networking efforts of the COST Action TD1104 (http://www.electroporation.net). We thank the Toulouse Réseau Imagerie and Anexplo core IPBS facilities (Genotoul, Toulouse, France).

REFERENCES

[1] S. H. T. Jorritsma, E. J. Gowans, B. Grubor-Bauk, and D. K. Wijesundara, "Delivery methods to increase cellular uptake and immunogenicity of DNA vaccines," *Vaccine*, vol. 34, no. 46, pp. 5488–5494, Nov. 2016.

[2] S. Pierini *et al.*, "Trial watch: DNA-based vaccines for oncological indications," *Oncoimmunology*, vol. 6, no. 12, p. e1398878, Dec. 2017.

[3] J.-M. Escoffre *et al.*, "Gene electrotransfer: from biophysical mechanisms to in vivo applications," *Biophys. Rev.*, vol. 1, no. 4, pp. 177–184, Dec. 2009.

[4] Gothelf and J. Gehl, "Gene electrotransfer to skin; review of existing literature and clinical perspectives.," *Curr. Gene Ther.*, vol. 10, no. 4, pp. 287–99, Aug. 2010.

[5] L. C. Heller and R. Heller, "In Vivo Electroporation for Gene Therapy," Hum. Gene Ther., vol. 17, no. 9, pp. 890–897, Sep. 2006.

[6] R. Heller, Y. Cruz, L. C. Heller, R. A. Gilbert, and M. J. Jaroszeski, "Electrically Mediated Delivery of Plasmid DNA to the Skin, Using a Multielectrode Array," *Hum. Gene Ther.*, vol. 21, no. 3, pp. 357–362, Mar. 2010.

[7] N. Pavselj and V. Préat, "DNA electrotransfer into the skin using a combination of one high- and one low-voltage pulse," *J. Control. Release*, vol. 106, no. 3, pp. 407–415, Sep. 2005.

[8] M. Golzio, J. Teissie, and M.-P. Rols, "Direct visualization at the single-cell level of electrically mediated gene delivery," *Proc. Natl. Acad. Sci.*, vol. 99, no. 3, pp. 1292–1297, Feb. 2002.

[9] C. Faurie, M. Golzio, P. Moller, J. Teissié, and M.-P. Rols, "Cell and Animal Imaging of Electrically Mediated Gene Transfer," *DNA Cell Biol.*, vol. 22, no. 12, pp. 777–783, Dec. 2003.

[10] A. Paganin-Gioanni, E. Bellard, J. M. Escoffre, M. P. Rols, J. Teissié, and M. Golzio, "Direct visualization at the single-cell level of siRNA electrotransfer into cancer cells.," *Proc. Natl. Acad. Sci. U. S. A.*, vol. 108, no. 26, pp. 10443–7, Jun. 2011.

[11] C. Rosazza, H. Deschout, A. Buntz, K. Braeckmans, M.-P. Rols, and A. Zumbusch, "Endocytosis and Endosomal Trafficking of DNA After Gene Electrotransfer In Vitro.," *Mol. Ther. Nucleic Acids*, vol. 5, no. 2, p. e286, Feb. 2016.

[12] G. Tevz *et al.*, "Gene Electrotransfer into Murine Skeletal Muscle: A Systematic Analysis of Parameters for Long-term Gene Expression," *Technol. Cancer Res. Treat.*, vol. 7, no. 2, pp. 91–101, Apr. 2008.

[13] F. André *et al.*, "Efficiency of high-and low-voltage pulse combinations for gene electrotransfer in muscle, liver, tumor, and skin. Efficiency of high-and low-voltage pulse combinations for gene electrotransfer in muscle, liver, tumor, and skin," *Hum Gene Ther*, vol. 19, no. 11, pp. 1261–71, 2008.

[14] K. Znidar, M. Bosnjak, M. Cemazar, and L. C. Heller, "Cytosolic DNA Sensor Upregulation Accompanies DNA Electrotransfer in B16.F10 Melanoma Cells," *Mol. Ther. - Nucleic Acids*, vol. 5, no. 6, p. e322, Jun. 2016.

[15] V. Mlakar, V. Todorovic, M. Cemazar, D. Glavac, and G. Sersa, "Electric pulses used in electrochemotherapy and electrogene therapy do not significantly change the expression profile of genes involved in the development of cancer in malignant melanoma cells.," *BMC Cancer*, vol. 9, p. 299, 2009.

[16] V. Todorovic, G. Sersa, V. Mlakar, D. Glavac, K. Flisar, and M. Cemazar, "Metastatic potential of melanoma cells is not affected by electrochemotherapy," *Melanoma Res.*, vol. 21, no. 3, pp. 196–205, Jun. 2011.

[17] X. de la Rosa *et al.*, "In vivo imaging of induction of heat-shock protein-70 gene expression with fluorescence reflectance imaging and intravital confocal microscopy following brain ischaemia in reporter mice," *Eur. J. Nucl. Med. Mol. Imaging*, vol. 40, no. 3, pp. 426–438, Feb. 2013.

[18] P.-Y. Fortin, C. Genevois, M. Chapolard, T. Santalucía, A. M. Planas, and F. Couillaud, "Dual-reporter in vivo imaging of transient and inducible heat-shock promoter activation," *Biomed. Opt. Express*, vol. 5, no. 2, p. 457, Feb. 2014.

[19] J. T. Beckham *et al.*, "Assessment of Cellular Response to Thermal Laser Injury Through Bioluminescence Imaging of Heat Shock Protein 70," *Photochem. Photobiol.*, vol. 79, no. 1, pp. 76–85, Jan. 2004.

[20] R. Deckers, C. Debeissat, P.-Y. Fortin, C. T. W. Moonen, and F. Couillaud, "Arrhenius analysis of the relationship between hyperthermia and Hsp70 promoter activation: a comparison between ex vivo and in vivo data.," *Int. J. Hyperthermia*, vol. 28, no. 5, pp. 441–50, Jan. 2012.

[21] G. Bertino *et al.*, "European Research on Electrochemotherapy in Head and Neck Cancer (EURECA) project: Results of the treatment of skin cancer," *Eur. J. Cancer*, vol. 63, pp. 41–52, Aug. 2016.

[22] M. Cemazar *et al.*, "Control by pulse parameters of DNA electrotransfer into solid tumors in mice," *Gene Ther.*, vol. 16, no. 5, pp. 635–644, May 2009.

[23] S. Chabot *et al.*, "LNA-based oligonucleotide electrotransfer for miRNA inhibition.," *Mol. Ther.*, vol. 20, no. 8, pp. 1590–8, Aug. 2012.

[24] S. Pedron-Mazoyer, J. Plouet, L. Hellaudais, J. Teissie, and M. Golzio, "New anti angiogenesis developments through electro-immunization: Optimization by in vivo optical imaging of intradermal electrogenetransfer," *Biochim. Biophys. Acta - Gen. Subj.*, vol. 1770, no. 1, pp. 137–142, Jan. 2007.

[25] S. Mazères *et al.*, "Non invasive contact electrodes for in vivo localized cutaneous electropulsation and associated drug and nucleic acid delivery," *J. Control. Release*, vol. 134, no. 2, pp. 125–131, Mar. 2009.

[26] J. Schindelin *et al.*, "Fiji: an open-source platform for biological-image analysis," *Nat. Methods*, vol. 9, no. 7, pp. 676–682, Jul. 2012.

[27] C. P. Sabino *et al.*, "The optical properties of mouse skin in the visible and near infrared spectral regions," *J. Photochem. Photobiol. B Biol.*, vol. 160, pp. 72–78, Jul. 2016.

[28] N. Pavselj, V. Préat, and D. Miklavcic, "A Numerical Model of Skin Electropermeabilization Based on In Vivo Experiments," *Ann. Biomed. Eng.*, vol. 35, no. 12, pp. 2138–2144, Nov. 2007.

[29] U. F. Pliquett, T. E. Zewert, T. Chen, R. Langer, and J. C. Weaver, "Imaging of fluorescent molecule and small ion transport through human stratum corneum during high voltage pulsing: localized transport regions are involved.," *Biophys. Chem.*, vol. 58, no. 1–2, pp. 185–204, Jan. 1996.

[30] N. Pavselj and D. Miklavcic, "Resistive heating and electropermeabilization of skin tissue during in vivo electroporation: A coupled nonlinear finite element model," *Int. J. Heat Mass Transf.*, vol. 54, no. 11–12, pp. 2294–2302, May 2011.

[31] S. Becker, B. Zorec, D. Miklavcic, and N. Pavselj, "Transdermal transport pathway creation: Electroporation pulse order," *Math. Biosci.*, vol. 257, pp. 60–68, Nov. 2014.

[32] A. Ivorra, B. Al-Sakere, B. Rubinsky, and L. M. Mir, "Use of conductive gels for electric field homogenization increases the antitumor efficacy of electroporation therapies.," *Phys. Med. Biol.*, vol. 53, no. 22, pp. 6605–18, Nov. 2008.

[33] D. E. Chafai, A. Mehle, A. Tilmatine, B. Maouche, and D. Miklavcic, "Assessment of the electrochemical effects of pulsed electric fields in a biological cell suspension," *Bioelectrochemistry*, vol. 106, pp. 249–257, 2015.

[34] A. Silve, I. Leray, C. Poignard, L. M. Mir, and L. M. Mir, "Impact of external medium conductivity on cell membrane electropermeabilization by microsecond and nanosecond electric pulses," *Sci. Rep.*, vol. 6, no. 1, p. 19957, Apr. 2016.

[35] G. Saulis, R. Saule, A. Bitinaite, N. Zurauskiene, V. Stankevic, and S. Balevicius, "Theoretical Analysis and Experimental Determination of the Relationships Between the Parameters of the Electric Field Pulse Required to Electroporate the Cells," *IEEE Trans. Plasma Sci.*, vol. 41, no. 10, pp. 2913–2919, Oct. 2013.

[36] G. Pucihar, J. Krmelj, M. Rebersek, T. Napotnik, and D. Miklavcic, "Equivalent Pulse Parameters for Electroporation," *IEEE Trans. Biomed. Eng.*, vol. 58, no. 11, pp. 3279–3288, Nov. 2011.

[37] F. C. Henriques, "Studies of thermal injury; the predictability and the significance of thermally induced rate processes leading to irreversible epidermal injury.," *Arch. Pathol.*, vol. 43, no. 5, pp. 489–502, May 1947.

[38] A. M. Stoll and L. C. Greene, "Relationship between pain and tissue damage due to thermal radiation.," *J. Appl. Physiol.*, vol. 14, no. 3, pp. 373–82, May 1959.

[39] M. N. Rylander *et al.*, "Optimizing heat shock protein expression induced by prostate cancer laser therapy through predictive computational models," *J. Biomed. Opt.*, vol. 11, no. 4, p. 041113, 2006.

[40] H. Zhao, T. C. Doyle, O. Coquoz, F. Kalish, B. W. Rice, and C. H. Contag, "Emission spectra of bioluminescent reporters and interaction with mammalian tissue determine the sensitivity of detection in vivo," *J. Biomed. Opt.*, vol. 10, no. 4, p. 041210, 2005.

[41] B. W. Rice, M. D. Cable, and M. B. Nelson, "In vivo imaging of light-emitting probes.," *J. Biomed. Opt.*, vol. 6, no. 4, pp. 432–40, Oct. 2001.
[42] S. Haberl *et al.*, "Effect of different parameters used for in vitro gene electrotransfer on gene expression efficiency, cell viability and visualization of plasmid DNA at the membrane level," *J. Gene Med.*, vol. 15, no. 5, pp. 169–181, May 2013.
[43] M. Pavlin and M. Kandušer, "New insights into the mechanisms of gene electrotransfer--experimental and theoretical analysis.," *Sci. Rep.*, vol. 5, p. 9132, Mar. 2015.
[44] C. L. Trimble *et al.*, "Safety, efficacy, and immunogenicity of VGX-3100, a therapeutic synthetic DNA vaccine targeting human papillomavirus 16 and 18 E6 and E7 proteins for cervical intraepithelial neoplasia 2/3: a randomised, double-blind, placebo-controlled phase 2b trial.," *Lancet (London, England)*, vol. 386, no. 10008, pp. 2078–2088, Nov. 2015.
[45] L. Lambricht, A. Lopes, S. Kos, G. Sersa, V. Préat, and G. Vandermeulen, "Clinical potential of electroporation for gene therapy and DNA vaccine delivery," *Expert Opin. Drug Deliv.*, vol. 13, no. 2, pp. 295–310, 2016.
[46] S. Kos *et al.*, "Electrotransfer parameters as a tool for controlled and targeted gene expression in skin.," *Mol. Ther. Nucleic Acids*, vol. 5, no. 8, p. e356, Aug. 2016.
[47] M. Kranjc, S. Kranjc, F. Bajd, G. Serša, I. Serša, and D. Miklavčič, "Predicting irreversible electroporation-induced tissue damage by means of magnetic resonance electrical impedance tomography," *Sci. Rep.*, vol. 7, no. 1, p. 10323, Dec. 2017.
[48] W. Hundt, C. E. O'Connell-Rodwell, M. D. Bednarski, S. Steinbach, and S. Guccione, "In Vitro Effect of Focused Ultrasound or Thermal Stress on HSP70 Expression and Cell Viability in Three Tumor Cell Lines," *Acad. Radiol.*, vol. 14, no. 7, pp. 859–870, 2007.
[49] C. E. O'Connell-Rodwell *et al.*, "In vivo analysis of heat-shock-protein-70 induction following pulsed laser irradiation in a transgenic reporter mouse," *J. Biomed. Opt.*, vol. 13, no. 3, p. 030501, 2008.
[50] G. J. Wilmink *et al.*, "In-vivo optical imaging of hsp70 expression to assess collateral tissue damage associated with infrared laser ablation of skin," *J. Biomed. Opt.*, vol. 13, no. 5, p. 054066, 2008.
[51] M. A. Mackanos and C. H. Contag, "Pulse duration determines levels of Hsp70 induction in tissues following laser irradiation.," *J. Biomed. Opt.*, vol. 16, no. 7, p. 078002, Jul. 2011.
[52] D. Miklavcic and R. V Davalos, "Electrochemotherapy (ECT) and irreversible electroporation (IRE) -advanced techniques for treating deep-seated tumors based on electroporation," *Biomed. Eng. Online*, vol. 14, no. Suppl 3, p. I1, 2015.
[53] T. Kotnik, L. M. Mir, K. Flisar, M. Puc, and D. Miklavcic, "Cell membrane electropermeabilization by symmetrical bipolar rectangular pulses. Part I. Increased efficiency of permeabilization.," *Bioelectrochemistry*, vol. 54, no. 1, pp. 83–90, Aug. 2001.
[54] K. Schwister and B. Deuticke, "Formation and properties of aqueous leaks induced in human erythrocytes by electrical breakdown.," *Biochim. Biophys. Acta*, vol. 816, no. 2, pp. 332–48, Jun. 1985.
[55] C. Rosazza, S. H. Meglic, A. Zumbusch, M.-P. Rols, and D. Miklavcic, "Gene Electrotransfer: A Mechanistic Perspective.," *Curr. Gene Ther.*, vol. 16, no. 2, pp. 98–129, 2016.
[56] C. Faurie *et al.*, "Electro-mediated gene transfer and expression are controlled by the life-time of DNA/membrane complex formation," *J. Gene Med.*, vol. 12, no. 1, pp. 117–125, Jan. 2010.

TABLE I
PULSE PROTOCOLS USED IN EXPERIMENTS.

Electric pulse protocol	Voltage [V]	Duration of pulses [ms]	Frequency [Hz]
HV	400	8 × 0.1	1
EGT	240	8 × 5	1
MV	100	8 × 20	1
HV+MV*	400 + 100	4 × 0.1; 4 × 20	1; 1

*HV + MV protocol consisted of 4 HV pulses, each followed by one MV pulse with 50 ms delay. Altogether 8 pulses were delivered, as in other protocols

TABLE II
DEFINITION OF SKIN MODEL: GEOMETRY, ELECTRICAL AND THERMAL PROPERTIES

	Thickness [μm]	Electrical conductivity [S/m]	Density [kg/m^3]	Thermal conductivity [W/mK]	Heat capacity [J/kgK]
Local Transport Region	5	0.1	1400	0.2	3600
Stratum Corneum	5	0.0001	1400	0.2	3600
Epidermis	15	0.2 – 0.8*	1200	0.24	3600
Dermis	200	0.2 – 0.8*	1200	0.45	3300
Adipose tissue	150	0.05 – 0.2*	900	0.19	2400
Muscle tissue	90	0.5	1040	0.5	3350
Subcutaneous tissue	2000	0.05	900	0.19	2400

**nonpermeabilized - fully permeabilized tissue*

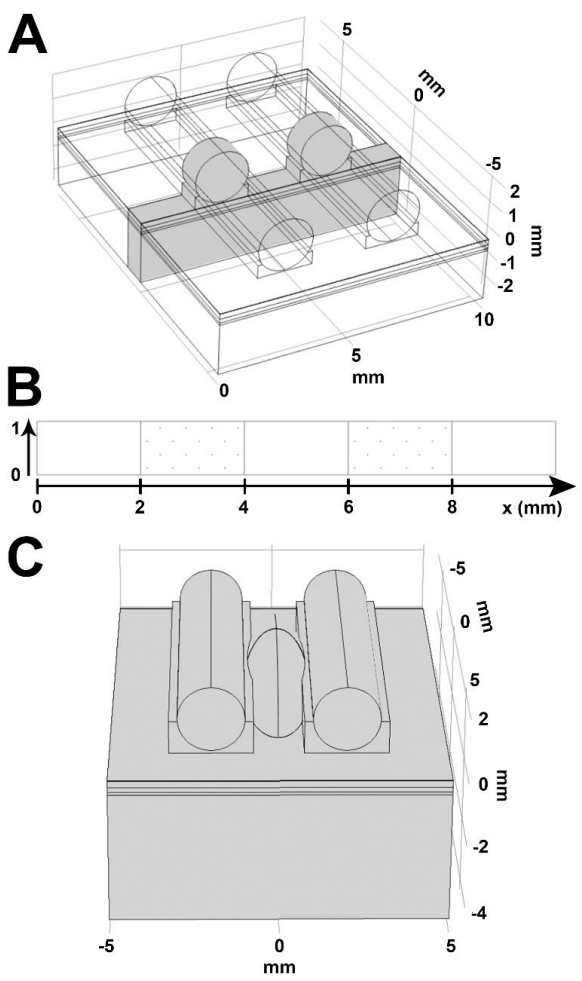

Fig. 1. Geometries used in numerical modelling. In A) and B) the geometry used in numerical modelling of heat shock response and subsequent bioluminescence emission. A) 3D geometry representing layered structure of mouse skin tissue together with the electrodes and the layer of conductive gel. The size of the subcutaneous tissue layer was increased to reduce the influence of the bottom boundary. Small size of the LTRs (the initial diameter is 10 μm) and the thin layer of the stratum corneum (5 μm) require very fine meshing, thus making the simulations computationally demanding. To make simulations feasible, the size of the geometry was reduced to 1 mm thick slice (gray), which was found to be a good compromise between computational efficiency and accuracy of results. B) Top view on the stratum corneum showing local transport regions (LTRs) with the density of 8/mm^2. In C) geometry used in numerical modelling of gene expression. The intradermally injected plasmid volume is represented by an ellipsoid with the volume of 25 mm^3, placed in the middle of the dermis and between the electrodes. Electrodes were in contact with the skin through the gel. In the areas where the gel was in contact with the skin, the LTRs were distributed throughout the stratum corneum with the density of 4 LTRs/ mm^2.

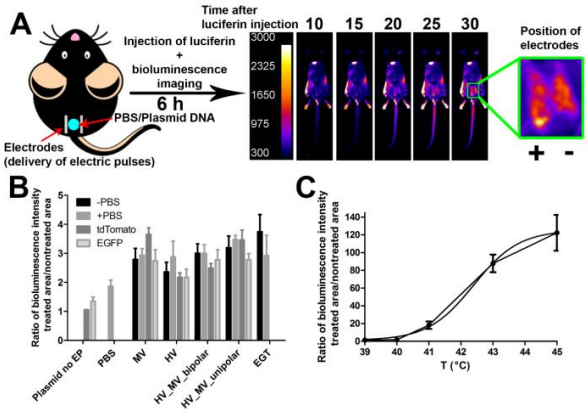

Fig. 2. Electroporation induces bioluminescence in Hspa1b-LucF (+/+) Hspa1b-mPlum (+/+) mice. Experimental design in (A): Double transgenic mice Hspa1b-LucF (+/+) Hspa1b-mPlum (+/+) were injected with PBS/plasmid DNA immediately before EP and bioluminescence 6 h after EP due to the expression of Hspa1b-LucF after the injection of luciferin was imaged. Green square shows a magnified image of the bioluminescence directly under the position of electrodes. Representative heat map images of bioluminescence 6h after EP are shown (scale on the left side). The + and - denote the position of anode and cathode, respectively. In (B) the ratio of bioluminescence intensity in treated vs non-treated area is shown for groups receiving either no injection (-PBS), vehicle (PBS), vehicle and tdTomato plasmid DNA (tdTomato), vehicle and EGFP plasmid DNA (EGFP) and receiving either one of the EP pulse parameters (x axis, Table 1) or no EP (x axis; Plasmid no EP, PBS). The ratio of bioluminescence intensity in treated vs non-treated area is shown for the control group (C), i.e. 8 min in water bath at designated temperatures with superimposed non-linear fit (sigmoidal dose-response curve). Data represents mean values ±SEM

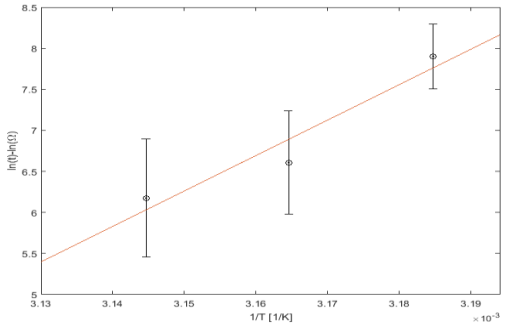

Fig. 3. Bioluminescence signal increase determined 6 h after the exposure to constant-temperature water bath follows the Arrhenius relationship. The solid line is a linear fit of the three data points, which was used to determine the Arrhenius parameters describing the expression of LucF resulting in the measured increase in the bioluminescence signal.

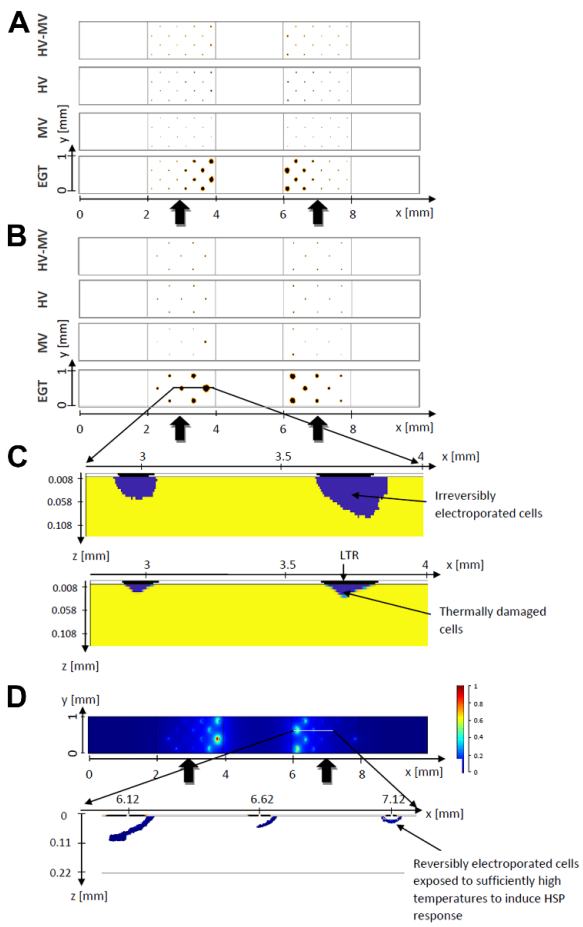

Fig. 4. Distribution of the expanded LTR sizes and position of cells emitting bioluminescence signal after the last pulse. The distribution of the expanded LTR sizes at the surface of the stratum corneum after the last pulse for HV-MV, HV, MV and EGT pulse parameters for 2 different pre-pulse LTR densities, (A) 8 LTR/mm^2 and (B) 4 LTR/mm^2. Pre-pulse LTRs with diameter of 10 µm were uniformly distributed throughout the volume of stratum corneum lying directly beneath the gel (areas between 2 - 4 mm and 6 - 8 mm). (C) The volume of cells not being able to emit light due to irreversible EP (above) is much larger than volume of thermally damaged cells (below). In (D) the distribution of cells contributing to the bioluminescence signal after EGT pulse protocol (below). These cells lie far enough from the center of the LTRs to avoid irreversible EP yet close enough to induce the thermal response. Corresponding distribution of the bioluminescence signal intensity at the surface of the stratum corneum (above). The arrows indicate the central position of electrodes. HV-MV denotes both, unipolar and bipolar protocols, since they show no difference in terms of thermal response

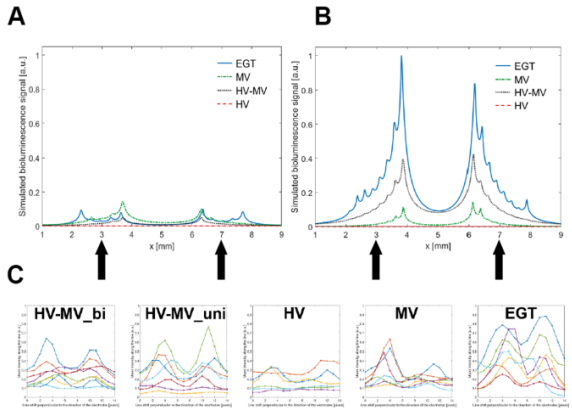

Fig. 5. Profiles of simulated and experimentally measured bioluminescence intensities corresponding to different pulse protocols. Profiles of simulated bioluminescence intensities, resulting from the LTR density of 4 LTR/mm^2 (A) and 8 LTR/mm^2 (B) as predicted by numerical model. HV+MV denotes both, unipolar and bipolar protocols, since they show no difference in terms of thermal stress levels. Position of the electrodes position is indicated by arrows. Profiles of experimentally measured bioluminescence intensities corresponding to different pulse protocols (C). Each curve shows the average profile of an individual mouse. Each data point on the curve represents the average intensity along the line, parallel to the electrodes, which was shifted from the beginning to the end of the region of interest (ROI)

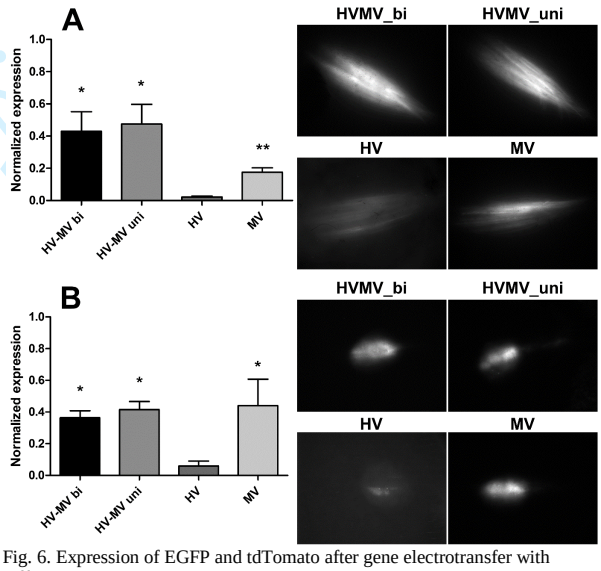

Fig. 6. Expression of EGFP and tdTomato after gene electrotransfer with different electric pulse parameters. Double transgenic mice Hspa1b-LucF (+/+) Hspa1b-mPlum (+/+) were injected with plasmid DNA immediately before EP and the expression of tdTomato (A) and EGFP (B) was imaged daily with a fluorescent stereomicroscope and quantified as a fraction of the maximum mean fluorescence intensity signal of all the mice in the entire imaging period (A and B). The representative fluorescent images of tdTomato and EGFP expression taken 14 days after transfection are shown. The contrast on the images was adjusted to correct for the use of ND filters and the large differences in fluorescence intensity between different electric pulse parameters. Data represents mean values ±SEM. In (A) * P<0.05 compared to HV and MV, ** P<0.05 compared to HV. In (B) * P<0.05 compared to HV.

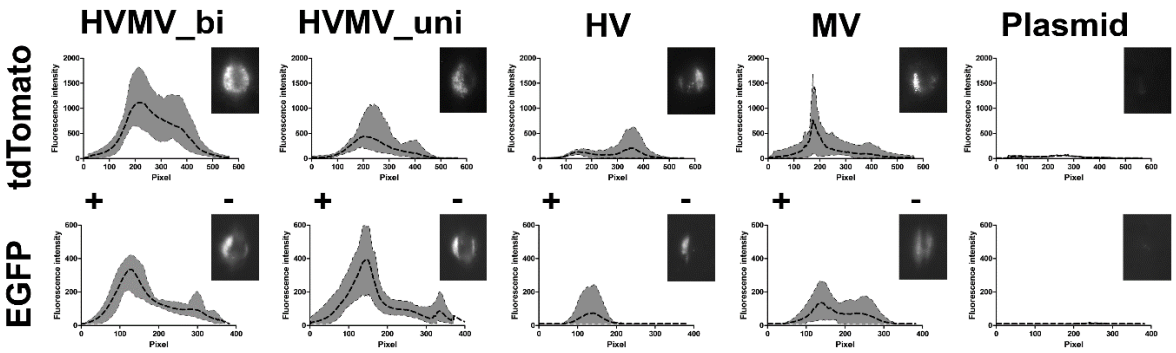

Fig. 7. Fluorescence intensity profiles of tdTomato and EGFP after gene electrotransfer. Double transgenic mice Hspa1b-LucF (+/+) Hspa1b-mPlum (+/+) were injected with plasmid DNA immediately before EP and the fluorescence intensity profiles 1 day after gene electrotransfer of tdTomato (top panel) and EGFP (bottom panel) were determined from images (inserts) obtained with a fluorescent stereomicroscope and quantified as mean pixel intensity on a 400 pixel thick line. 4 different electric pulse parameters were used (HV-MV bi, HV-MV uni, HV and MV). The + and – signs denote the position of anode and cathode, respectively. Data are presented as mean fluorescent intensity at each pixel (thick dashed lines) and the range (grey area between thin dashed lines) for each pixel on the line.

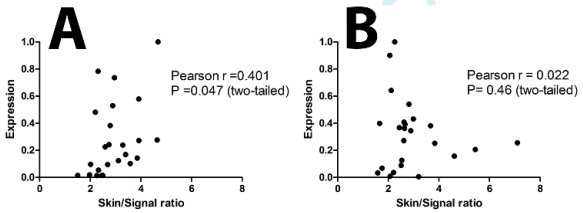

Fig. 8. Correlation of the expression of tdTomato or EGFP and bioluminescence signal intensity. Correlation plot of the ratio of bioluminescence intensity in treated vs non-treated area (x axis) vs relative maximum expression (y axis) for tdTomato (A) and EGFP (B). Double transgenic mice Hspa1b-LucF (+/+) Hspa1b-mPlum (+/+) were injected with plasmid DNA immediately before EP and the bioluminescence 6 h after EP due to the expression of Hspa1b-LucF after the injection of luciferin was imaged. The expression of tdTomato (A) and EGFP (B) was quantified as a fraction of the maximum mean fluorescence intensity signal of all the mice in the entire imaging period. Pearson r correlation, $P<0.05$ was considered statistically significant.

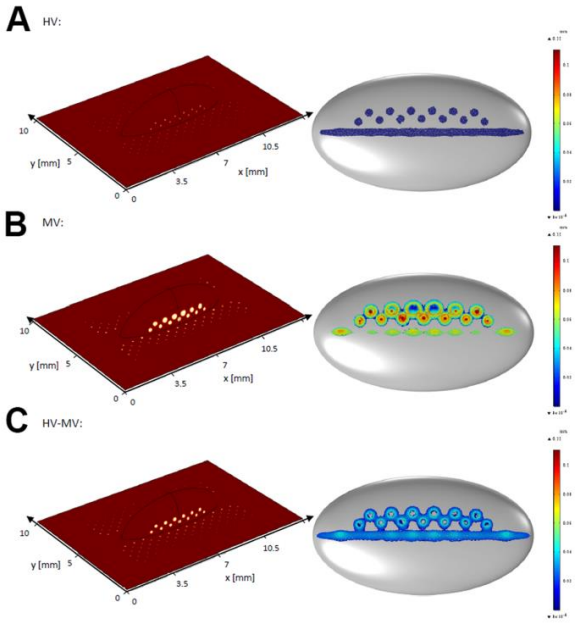

Fig. 9. Left column: Stratum corneum (red) with LTRs (white) after the last pulse of A) HV, B) MV and C) HV-MV pulse protocols. The distribution of the size of LTRs beneath the electrodes is symmetrical. Right column: Electrophoretic movement of EGFP (4.7 kbp) plasmid DNA through reversibly electroporated volume of the skin tissue. Presented are trajectories of the plasmid DNA movement due to nonuniform electric field resulting from A) HV, B) MV and C) HV-MV pulse protocols inside the volume of reversible EP. Gray ellipsoid represents the injected volume of plasmid DNA (bleb). The colors of trajectories represent the distance of the plasmid DNA from the surface of the bleb. The maximum electrophoretic distance by MV pulse protocol is more than 100 μm meaning that plasmid DNA can travel through dermis and reach the epidermis. As we can see from the images, the majority of the volume where gene transfection is expected, lies near the edges of LTRs since irreversible EP prevents successful transfection near the center of the LTRs. Represented is the side of the bleb facing the anode. Electrophoretic movement in the opposite direction (toward the cathode) is negligible.

TABLE III
RELATIVE NUMBER OF PLASMID DNA MOLECULES PRESENT IN THE VOLUME OF REVERSIBLE EP DUE TO ELECTROPHORETIC MOVEMENT AS A MEASURE OF GENE ELECTROTRANSFER EFFICIENCY

	HV	MV	HV - MV
Volume of reversible EP (mm^3)	2.58	1.70	3.29
Number of EGFP (4.7 kbp) plasmid DNA molecules present in the volume of reversible EP at the end of pulse delivery normalized to HV-MV protocol	0.14	0.74	1
Number of tdTomato (5.4 kbp) plasmid DNA molecules present in the volume of reversible EP at the end of pulse delivery normalized to HV-MV protocol	0.14	0.71	1

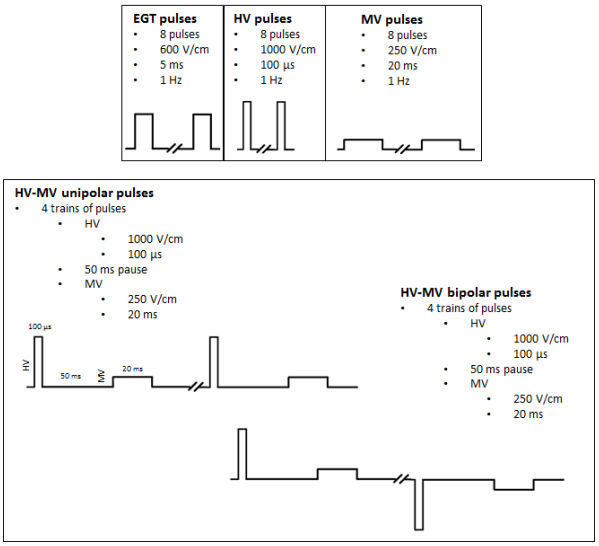

Supp. Fig. 1. Pulse protocols used in experiments. HV + MV protocol consisted of 4 HV pulses, each followed by one MV pulse 50 ms later. Altogether 8 pulses were delivered, as in other protocols. Voltages delivered were 100 V (MV pulses – 250 V/vm) 250 V (EGT pulses – 600 V/cm) and 400 V (HV pulses – 1000 V/cm).

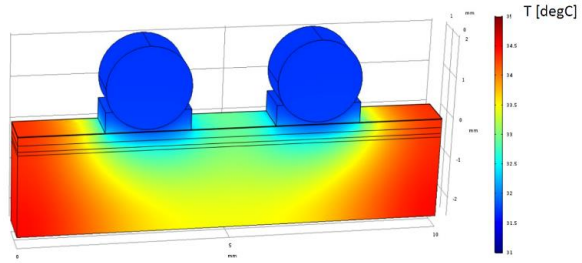

Supp. Fig. 2. Temperature distribution established after 30 s of the contact between electrodes, gel and the skin. This temperature distribution was used as an initial condition at the beginning of the pulse delivery.

3.3.2. Genska elektrotransfekcija s ploščatimi, igelnimi in prstnimi elektrodami (Članek 3 -oddan v objavo)

V okviru članka 3 smo na podlagi numeričnega modeliranja določili učinkovitost genske elektrotransfekcije kože glede na vrsto elektrod in različne parametre električnih pulzov, ter rezultate primerjali z eksperimenti, objavljenimi v (Calvet et al. 2014). Zgradili smo tri geometrije, saj so bile pri eksperimetnih uporabljene tri vrste elektrod: ploščate, prstne in igelne (Slika 1 v članku 3). Kot merilo učinkovitosti genske elektrotransfekcije smo uporabili število nabitih delcev, ki predstavljajo plazmidno DNK, znotraj volumna reverzibilne elektroporacije. V nasprotju z eksperimenti, kjer je bila največja učinkovitost genske elektrotransfekcije dosežena s ploščatimi elektrodami, numerični model predvideva večjo učinkovitost prstnih in igelnih elektrod (Tabela 2 v članku 3). Obe vrsti invazivnih elektrod (prstne in igelne) namreč dosegata večji volumen reverzibilne elektroporacije v primerjavi s ploščatimi elektrodami. Izkaže se, da je za učinkovitost genske elektrotransfekcije pomembna predvsem elektroporacija usnjice, saj zaradi kratkega elektroforetskega premika plazmidna DNK ne doseže sosednjih plasti. Eden izmed glavnih vzrokov za neskladnje med modelom in eksperimenti je nezadostno poznavanje elektroporacije rožene plasti. Prevodnost rožene plasti ima namreč velik vpliv na elektroporacijo spodaj ležečih plasti kože. Že ob povečanju začetnega premera LTR iz 10 µm na 20 µm število nabitih delcev, ki pridejo v stik z elektroporiranimi celicami, naraste za približno 30 % (Tabela 2 v članku 3). To nakazuje, da je dejanska gostota LTR ali njihova velikost večja od vrednosti, ki jih najdemo v literaturi ali pa na učinkovitost genske elektrotransfekcije vplivajo tudi drugi, še neidentificirani faktorji.

Določena neskladja med modelom in eksperimenti lahko opazimo tudi pri primerjavi različnih kombinacij HV in LV pulzov, pri čemer je bila amplituda HV pulza 1000 V/cm ali 1400 V/cm in amplituda LV pulza 60 V/cm, 100 V/cm, 140 V/cm ali 180 V/cm. Numerični model po pričakovanjih predvideva večjo učinkovitost genske elektrotransfekcije pri višji amplitudi HV pulza (1400 V/cm), saj je volumen reverzibilne elektroporacije večji (Tabela 3 v članku 3). Presenetljivo je učinek amplitude LV pulza precej manj izrazit, kar je v nasprotju z eksperimenti, ki kažejo, da je pri elektrotransfekciji plazmida pCMV-luc pomembna predvsem amplituda LV pulza. Neskladja med eksperimenti in modelom nakazujejo na pomanjkljivo poznavanje elektroporacije kože in procesov pri genski elektrotransfekciji. Za večjo napovedno moč modela je potrebno preučiti tudi vpliv drugih dejavnikov, npr. vpliv pH sprememb v bližini elektrod, globine injiciranja plazmida in količine nanešenega kontaktnega gela.

BioMedical Engineering OnLine

Numerical study of gene electrotransfer efficiency based on electroporation volume and electrophoretic movement of plasmid DNA

--Manuscript Draft--

Manuscript Number:	BMEO-D-18-00067
Full Title:	Numerical study of gene electrotransfer efficiency based on electroporation volume and electrophoretic movement of plasmid DNA
Article Type:	Research
Funding Information:	Slovenian Research Agency (ARRS) — Ms. Tadeja Forjanic
Abstract:	BACKGROUND The efficiency of gene electrotransfer, an electroporation-based method for delivery of pDNA into target tissues, depends on several processes. The method relies on application of electric pulses with appropriate amplitude and pulse duration. A careful choice of electric pulse parameters is required to obtain the appropriate electric field distribution, which not only controls the electroporated volume, but also affects the movement of pDNA. We used numerical modeling to assess the influence of different types of electrodes and pulse parameters on reversibly electroporated volume and on the extent of pDNA - membrane interaction, which is necessary for successful gene electrotransfer. METHODS A 3D geometry was built representing the mice skin tissue and intradermally injected plasmid volume. The geometry of three different types of electrodes (plate, finger, needle) was built according to the configuration and placement of electrodes used in previously reported in vivo experiments of gene electrotransfer. Electric field distribution, resulting from different pulse protocols was determined, which served for calculation of reversible electroporation volume and for simulation of electrophoretic movement of pDNA. The efficiency of gene electrotransfer was evaluated in terms of predicted amount of pDNA present inside the volume of reversible electroporation at the end of pulse delivery. RESULTS According to results of our numerical study, finger and needle electrodes provide larger amount of pDNA inside the volume of reversible electroporation than plate electrodes However, these results are not consistent with the experiments showing that plate electrodes achieve the best transfection efficiency. Some inconsistencies were observed also by comparing the efficiencies of different high and low voltage pulse combinations, delivered by plate electrodes. The reason for inconsistencies probably lies in insuffient knowledge regarding the electroporation of stratum corneum. Namely, the size of the regions with high electrical conductivity, created by electroporation, was found to strongly affect the predicted transfection efficiency. CONCLUSIONS The presented numerical model simulates the two most important processess involved in gene electrotransfer: electroporation of cells, and electrophoretic movement of pDNA. The incosistencies between the model and experiments indicate incomplete knowledge of skin electroporation, or the involvement of other mechanisms, whose importance has not been yet identified.
Corresponding Author:	Damijan Miklavcic University of Ljubljana SLOVENIA
Corresponding Author Secondary Information:	
Corresponding Author's Institution:	University of Ljubljana
Corresponding Author's Secondary Institution:	

First Author:	Tadeja Forjanic
First Author Secondary Information:	
Order of Authors:	Tadeja Forjanic
	Damijan Miklavcic
Order of Authors Secondary Information:	
Opposed Reviewers:	
Manuscript Classifications:	150: Computational Biology

NUMERICAL STUDY OF GENE ELECTROTRANSFER EFFICIENCY BASED ON ELECTROPORATION VOLUME AND ELECTROPHORETIC MOVEMENT OF PLASMID DNA

Tadeja Forjanič[1] and Damijan Miklavčič[1]

[1]University of Ljubljana, Faculty of Electrical Engineering, Trzaska 25, SI-1000 Ljubljana, Slovenia

KEYWORDS: skin electroporation, gene electrotransfer, numerical modeling

ABSTRACT

BACKGROUND

The efficiency of gene electrotransfer, an electroporation-based method for delivery of pDNA into target tissues, depends on several processes. The method relies on application of electric pulses with appropriate amplitude and pulse duration. A careful choice of electric pulse parameters is required to obtain the appropriate electric field distribution, which not only controls the electroporated volume, but also affects the movement of pDNA. We used numerical modeling to assess the influence of different types of electrodes and pulse parameters on reversibly electroporated volume and on the extent of pDNA - membrane interaction, which is necessary for successful gene electrotransfer.

METHODS

A 3D geometry was built representing the mice skin tissue and intradermally injected plasmid volume. The geometry of three different types of electrodes (plate, finger, needle) was built according to the configuration and placement of electrodes used in previously reported *in vivo* experiments of gene electrotransfer. Electric field distribution, resulting from different pulse protocols was determined, which served for calculation of reversible electroporation volume and for simulation of electrophoretic movement of pDNA. The efficiency of gene electrotransfer was evaluated in terms of predicted amount of pDNA present inside the volume of reversible electroporation at the end of pulse delivery.

RESULTS

According to results of our numerical study, finger and needle electrodes provide larger amount of pDNA inside the volume of reversible electroporation than plate electrodes However, these results are not consistent with the experiments showing that plate electrodes achieve the best transfection efficiency. Some inconsistencies were observed also by comparing the efficiencies of different high and low voltage pulse combinations, delivered by plate electrodes. The reason for inconsistencies probably lies in insuffient knowledge regarding the electroporation of stratum corneum. Namely, the size of the regions with high electrical conductivity, created by electroporation, was found to strongly affect the predicted transfection efficiency.

CONCLUSIONS

The presented numerical model simulates the two most important processess involved in gene electrotransfer: electroporation of cells, and electrophoretic movement of pDNA. The incosistencies between the model and experiments indicate incomplete knowledge of skin electroporation, or the involvement of other mechanisms, whose importance has not been yet identified.

BACKGROUND

Low permeability of the cell membrane represents a major barrier to successful gene transfer. One of the physical methods that can be employed to overcome this barrier is based on cell membrane electroporation. The method, termed gene electrotransfer, relies on the delivery of electric pulses with appropriate amplitude, duration and repetition frequency, which results in increased permeability of the cell membrane, a phenomenon known as electroporation [1, 2]. In addition to increasing the cell membrane permeability, electric pulses play an important role in transporting of pDNA towards cell membrane. Negatively charged DNA molecules move under the influence of electrophoretic force, generated by an external electric field [3, 4]. Due to the action of electrophoretic force, DNA molecules are brought in contact with more cells compared to free diffusion, thus increasing the probability of DNA-membrane complex formation, which are necessary for successful gene electrotransfer [4-6].

Therefore, electric pulses intended for gene electrotransfer have to be optimized in terms of electroporation volume and in terms of DNA-membrane interaction, while preserving cell viability [7]. As shown in several studies *in vivo* and *in vitro* [8-11], the best transfection efficiency is achieved by a combination of short high voltage (HV) and long low voltage (LV) pulses. This is not surprising, since the use of different pulses enables to separately control both factors of gene electrotransfer efficiency - HV pulses control the electroporation volume and LV pulses control the extent of pDNA-membrane interaction.

The optimization of pulse parameters for gene electrotransfer into the skin has been performed mainly experimentally [12]. So far, a few numerical models have been developed to investigate the gene electrotransfer efficiency in terms of electric field distribution [13-15] and Joule heating [16]. In this paper, we present a numerical model including additional parameter of gene electrotransfer efficiency – distribution of plasmid DNA due to action of electrophoretic force. More specifically, we were interested in the amount of plasmid DNA inside the volume of reversible electroporation depending on the electrode configuration (plate, finger, needle) and pulse parameters used. The predictive power of the model was tested on experiments published by Calvet et al [17].

METHODS

A three dimensional numerical model was developed to simulate the experiments of Calvet et al [17]. Three geometries were built considering the configuration of three different types of electrodes used in experiments – finger, needle and plate. Tips of needle and finger electrodes were positioned 5 mm below the skin surface. The geometry of the skin consisted of the following layers: stratum corneum, epidermis, dermis, adipose tissue, muscle tissue and subcutaneous tissue (Table 1). An ellipsoid with the volume of 25 mm^3 was placed in the middle of the dermis representing the intradermally injected plasmid volume. Since electrodes were placed in such a way they surrounded the bleb

formed by the plasmid volume and were in contact with it [17], we adjusted the dimensions of the ellipsoid for each electrode configuration. In the case of plate electrodes, for instance, the size of ellipsoid in the direction perpendicular to the electrodes was the largest, 1.8 mm. Finger and needle electrodes had narrower gap between both rows of electrodes, therefore, the corresponding size of the bleb was reduced to 1.3 mm in order to fit between the electrodes (Figure 1).

A steady-state Laplace equation was employed to calculate electric field distribution:

$$\nabla \cdot (\sigma(E)\, \nabla\varphi) = 0, \tag{1}$$

where σ is the electrical conductivity and φ is the electric potential. All boundaries of the geometry, except for electrodes, were treated as electrically insulated. In the case of plate electrodes, the applied voltage amplitude (φ_0) was prescribed as a boundary condition at the surface of one of the electrodes ($\varphi = \varphi_0$). The surface of the other electrode was set to ground ($\varphi = 0\ V$). Similar boundary conditions were assigned to needle and finger electrodes - one row of electrodes was set to applied voltage, while the other row was set to ground.

When pulses are delivered with plate electrodes, electrical properties of stratum corneum dictate the electroporation of underlying skin layers. The high resistance of stratum corneum begins to drop after exceeding electroporation threshold [18]. The reduced resistance is related to the formation of small regions with high electrical conductivity, so called local transport regions (LTRs) [19]. A small cylinders were introduced in the geometry to simulate the LTRs at the beginning of the HV pulse. Cylinders were distributed throughout the area of stratum corneum beneath the gel, which was applied between the electrodes and skin to improve the contact. Two different initial diameters of LTRs were used in simulation to investigate the effect of stratum corneum conductivity – 10 µm and 20 µm. The density of LTRs, which enable the electroporation of underlying tissue, increases with the pulse amplitude. In the model, we used the density of 60 LTRs per 0.1 cm^2, which lies in the middle of the reported range of LTR densities [20]. The size of LTRs increases during the pulse delivery due to lipid melting caused by Joule heating. The phase transition of stratum corneum lipids occurs at around 70 °C. In the numerical model, stratum corneum was assumed to undergo an irreversible phase transition locally in the LTR in the temperature range between 65 and 75 °C with the latent heat of 5300 J/kg [21]. Since finger and needle electrodes penetrate into the skin, the impact of stratum corneum on electric field distribution is decreased with respect to plate electrodes. Except for the stratum corneum, which was treated as a bulk layer without LTRs, electrical properties of other layers were the same as in the case of plate electrodes.

The electric field amplitude required to achieve electroporation, decreases with the duration of pulses in a strongly nonlinear fashion [22]. For pulses shorter than about 1 ms, threshold electric field decreases sharply with pulse duration, while for longer pulses (above 1 ms), this decrease becomes progressively smaller. The reversible and irreversible electroporation threshold of the skin for 100 µs pulse (600 V/cm and 1200 V/cm, respectively) were taken from literature [23]. To determine both thresholds for LV pulse, we selected the best two fits describing the relation between electric field and pulse duration from [24]. For 400 ms long pulse, the average electric field for electroporation was 6 times lower than for 100 µs pulse. Therefore, the reversible and irreversible threshold for the LV pulse were set to 100 V/cm and 200 V/cm, respectively. Between both thresholds, electrical conductivity increases due to electroporation. The increase in conductivity with respect to electric field was assumed to follow a sigmoid curve [25, 26].

Temperature is another important variable to be considered in the optimization of gene electrotransfer parameters. Resistive heating leads to substantial temperature increase inside the LTRs, which can damage the surrounding cells. However, thermal damage affects smaller volume of cells than irreversible electroporation [27, 28] and was, therefore, not specifically evaluated. Also, all thermally damaged cells lie within the volume subjected to irreversible electroporation. Nevertheless, resistive heating was included in simulation, since it affects the expansion of LTRs. The resistive heat, generated during the pulses, was used as a source term in the heat transfer equation:

$$\rho c \frac{\partial T}{\partial t} = \nabla \cdot (k \nabla T) + \sigma |\nabla \varphi|^2 \quad (2)$$

ρ, c and k are mass density, specific heat capacity and thermal conductivity of the material, respectively. A stationary study was employed to calculate electric field distribution, since a time-dependent study considering the conductivity changes as a result of LTR expansion during the pulses would be computationally too demanding. The size of LTRs was updated before the calculation of electric field generated by the LV pulse. It turned out that neglecting the effect of LTR expansion during the pulse was justified also for long LV pulses. Namely, only the LV pulse with the highest voltage-to-distance ratio, 180 V/cm, produced sufficient heating for LTR expansion to occur.

GENE ELECTROTRANSFER MODELING

We modeled the distribution of plasmid DNA in the skin tissue as a result of electrophoretic movement of plasmid DNA during the pulse delivery. Namely, negatively charged pDNA molecules migrate toward the anode under the influence of electrophoretic force, generated by local electric field. In addition to the local electric field E, the distance L travelled by DNA molecules depends on their mobility (μ) and the duration of pulses (t) [29]:

$$L = \mu E t \quad (3)$$

In [29], the mobility of 1.5×10^4 μm^2/Vs is estimated for a plasmid with 4700 base pairs. Since electrophoretic mobility is proportional to the length of the plasmid, the following values were used in simulations: $\mu = 2.0 \times 10^4$ μm^2/Vs for pCMV-luc plasmid with 6233 base pairs and $\mu = 2.3 \times 10^4$ μm^2/Vs for INVAC-1 plasmid with 7120 base pairs.

Charged particle tracing module provided by Comsol Multiphysics® (v5.3, Stockholm, Sweden) was employed to simulate the trajectories of DNA molecules. We neglected the contribution of HV pulse to electrophoresis due to its short duration (100 μs). Therefore, the simulation of trajectories was based on the stationary electric field distribution, generated by the LV pulse. In the model, the charged particle originated from the surface of ellipsoid representing the injected volume of plasmid DNA. Particles were released uniformly across the surface of the ellipsoid every 10 ms to simulate the continuous inlet of DNA molecules into the dermis. After determining the distribution of plasmid DNA at the end of the LV pulse, we assessed the number of DNA present inside the volume of reversible electroporation. The number of simulated particles was chosen large enough to achieve reliable results in terms of relative transfection efficiencies.

RESULTS

In the study of Calvet et al [17] it was found that plate electrodes are more suitable for electrotransfer of pCMV-luc and INVAC-1 plasmids than both invasive electrodes (finger and needle).

The difference between invasive and noninvasive electrodes was more pronounced in the case of INVAC-1 plasmid. Interestingly, the numerical model predicts a better gene electrotransfer efficiency of invasive electrodes (Table 2). According to the model, invasive electrodes should be more suitable due to significantly larger volume of reversible electroporation. However, the volume of reversible electroporation in the case of plate electrodes strongly depends on the electrical properties of stratum corneum, which are not completely understood. Particularly important for electroporation of underlying layers are the size and the distribution of LTRs. As we can see from Table 2, increasing the initial size of LTRs from 10 to 20 μm in diameter resulted in more than 30 % larger volume of reversible electroporation. Consequently, similar increase is obtained in amount of plasmid DNA brought in contact with electropermeabilized cells, ranging from 28 % in the case of INVAC plasmid to 37% in the case of PMV-luc plasmid. It is important to emphasize that reversible electroporation volume was evaluated at the end of the HV pulse, taking into account the expansion of LTRs during the pulse. The diameter of LTRs increased, on average, for 10 μm regardless of the initial size of LTRs.

Comparison of different electrodes for gene electrotransfer was followed by a comparison of various HV-LV pulse combinations, delivered by plate electrodes. In experiments, the best pulse combinations in terms of luciferase expression proved to be 1000 V/cm + 180 V/cm, 1400 V/cm + 140 V/cm and 1400 V/cm + 180 V/cm. These three pulse combinations, in addition to 1000 V/cm + 140 V/cm pulse combination, were then tested for vaccination with INVAC-1. Both pulse combinations with the amplitude of HV pulse being 1400 V/cm achieved higher transgene expression than pulse combinations with lower HV pulse amplitude (1000 V/cm).

According to numerical model, the pulse combination 1000 V/cm + 180 V/cm is the only one where LV pulse generates larger volume of reversible electroporation than HV pulse. The same LV pulse (180 V/cm) is also the only one that generates sufficient heating for LTR expansion. Nevertheless, the diameter of LTRs does not increase for more than 10 μm.

The impact of the HV pulse intensity on the predicted amount of DNA inside the volume of reversible electroporation is as expected – higher amplitude of the pulse leads to larger volume of reversible electroporation and, therefore, more DNA molecules come in contact with permeabilized cells (Table 3). However, the importance of HV pulse amplitude was indicated only in terms of INVAC-1 expression. Luciferase expression, on the other hand, shows only moderate dependency on the HV pulse amplitude. By contrast, increasing the amplitude of LV pulses resulted in gradual increase in luciferase expression, therefore indicating higher importance of LV than HV amplitude on gene expression. This is not consistent with results of numerical modeling, which predict more pronounced effect of HV than LV amplitude on gene expression. The inconsistencies between the model and experiments show insufficient accuracy of electroporation model and incomplete knowledge and understanding of the parameters determining gene electrotransfer efficiency.

DISCUSSION

Several parameters affecting gene electrotransfer efficiency have been identified so far [7, 30, 31]: electric field distribution, which is related to the electrode configuration and pulse parameters; electrophoretic movement of the plasmid; the delivery site [32]; pH changes near the electrodes [33]; the design of plasmid and plasmid concentration [34]. The role and importance of these factors need to be established to achieve consistent and high efficiency of gene electrotransfer. In this study, we used numerical modeling as an alternative tool to assess the influence of the first two parameters: electric field distribution and electrophoretic movement of the plasmid.

The first parameter considered was the electric field distribution, which depends on electrode geometry and placement. As expected, both invasive electrodes used (i.e. finger and needle) achieved larger volume of reversible electroporation, since they penetrate through stratum corneum. Therefore, the insulating properties of stratum corneum do not hinder the electroporation of underlaying layers. Based on results of our model, the electroporation of skin layers other than dermis is less significant, since majority of plasmid DNA does not reach the adjacent layers. Interestingly, although needle electrodes generate larger volume of reversible electroporation than finger electrodes, the predicted amount of plasmid DNA contributing to electrotransfer efficiency is smaller. This apperant discrepancy can be explained by stronger electrophoretic force generated by finger electrodes, which pulls more DNA molecules inside the reversible electroporation volume. However, the experiments do not fully confirm these predictions, since finger electrodes proved to be a better choice only in the case of INVAC-1 plasmid. Namely, needle electrodes performed better than finger when using pCMV-luc plasmid to evaluate the transfection efficiency.

Even larger discrepancy is observed when comparing finger and needle electrodes to plate electrodes. Regardless of the plasmid used in experiments, plate electrodes achieved the highest transfection efficiency, contrary to results predicted by numerical modeling. One of the reasons for this discrepancy may lie in incomplete understanding of the conductivity changes of the stratum corneum due to electroporation. The conductivity of the stratum corneum namely strongly depends on the size and the density of structural alterations (LTRs) caused by electric pulses. It is known that the density of LTRs associated with HV pulses is higher, but their size is smaller compared to LTRs associated with LV pulses. However, more precise knowledge about this relationship is required, since the size and the distribution of LTRs after the HV pulse strongly affects the evolution of LTRs during subsequent LV pulse. If their size is too small or their density is too high, there is no sufficient Joule heating for phase transition of lipids (i.e. LTR expansion) [35]. Hence, the conductivity of stratum corneum does not increase and less cells experience reversible electroporation. For our particular geometries with the initial diameters of LTRs being 10 and 20 μm, no thermal expansion of LTRs was obtained during the LV pulse with the amplitude of 140 V/cm. As expected, the geometry with larger size of LTRs (20 μm) and, therefore, with larger volume of tissue being reversibly electroporated, resulted in larger amount of DNA contributing to transfection efficiency. However, the predicted transfection efficiency is still significantly lower than in the case of finger or needle electrodes. This indicates, that the conductivity of stratum corneum is probably higher than currently estimated. A similar observation was recently reported in [36]. It is important to emphasize that numerical model assumes uniform distribution of LTRs, which is probably a simplification, since electric field distribution is not uniform.

Incomplete knowledge of the stratum corneum conductivity is probably the main reason also for inconsistencies regarding the optimization of different HV-LV pulse combinations. According to the model, the amplitude of HV pulse is more important for electrotransfer efficiency than the amplitude of LV pulse, contrary to experimental results of luciferase expression. This inconsistency may arise from a difference in the LTR density, which is associated with the HV pulse amplitude. However, this parameter was not studied more in detail, since introducing additional LTRs to the geometry would prolong the already time consuming simulations. Also, other parameters whose importance remains to be investigated, in addition to the parameters mentioned at the beginning of the discussion (the delivery site, pH changes, plasmid concentration), should not be overlooked. For instance, the amount of conductive gel and precise administration of a plasmid volume, to name additional few experimental variables that need to be controlled or their influence evaluated.

CONCLUSION

A three dimensional numerical model was built describing gene electrotransfer to skin. The model simulates the electrophoretic movement of plasmid DNA through the nonuniform distribution of electric field and thus, enables to assess the volume of transfected cells. However, simulation results failed to explain the differences between different types of electrodes and pulse combinations, observed in experiments previously reported. The increase in electrical conductivity of the stratum corneum due to electroporation was identified as one of the critical parameters of the model. Therefore, a better understanding of stratum corneum electroporation as well as other variables and processes involved in gene electrotransfer is required to obtain more accurate results.

Ethics approval and consent to participate

Not applicable

Consent for publication

Not applicable

Availability of Data and Materials

The datasets used and/or analysed during the current study are available from the corresponding author on a reasonable request.

Competing interests

The authors declare that they have no competing interests.

Funding

This work was funded by the Slovenian Research Agency (ARRS).

Authors' contributions

TF and DM designed the study. TF built the numerical model and wrote the manuscript. DM guided the model development process and reviewed the manuscript. All authors read and approved the final version of the manuscript.

Acknowledgements

This work was supported by the Slovenian Research Agency (ARRS) and conducted within the scope of the Electroporation in Biology and Medicine European Associated Laboratory (LEA EBAM).

Author details

[1]University of Ljubljana, Faculty of Electrical Engineering, Trzaska 25, SI-1000 Ljubljana, Slovenia

REFERENCES

1. Weaver JC: **Electroporation of cells and tissues**. *IEEE Trans Plasma Sci* 2000, **28**:24–33.
2. Kotnik T, Kramar P, Pucihar G, Miklavcic D, Tarek M: **Cell membrane electroporation-Part 1: The phenomenon**. *IEEE Electr Insul Mag* 2012, **28**:14–23.
3. Klenchin VA, Sukharev SI, Serov SM, Chernomordik LV, Chizmadzhev YuA: **Electrically induced DNA uptake by cells is a fast process involving DNA electrophoresis**. *Biophys J* 1991, **60**:804–811.
4. Faurie C, Rebersek M, Golzio M, Kanduser M, Escoffre J-M, Pavlin M, Teissie J, Miklavcic D, Rols M-P: **Electro-mediated gene transfer and expression are controlled by the life-time of DNA/membrane complex formation**. *J Gene Med* 2010, **12**:117–125.
5. Golzio M, Teissie J, Rols M-P: **Direct visualization at the single-cell level of electrically mediated gene delivery**. *Proc Natl Acad Sci* 2002, **99**:1292–1297.
6. Escoffre J-M, Portet T, Favard C, Teissié J, Dean DS, Rols M-P: **Electromediated formation of DNA complexes with cell membranes and its consequences for gene delivery**. *Biochim Biophys Acta - Biomembr* 2011, **1808**:1538–1543.
7. Rosazza C, Meglic SH, Zumbusch A, Rols M-P, Miklavcic D: **Gene Electrotransfer: A Mechanistic Perspective.** *Curr Gene Ther* 2016, **16**:98–129.
8. André F, Gehl J, Sersa G, Préat V, Hojman P, Eriksen J, Golzio M, Cemazar M, Pavselj N, Rols M-P: **Efficiency of high-and low-voltage pulse combinations for gene electrotransfer in muscle, liver, tumor, and skin. Efficiency of high-and low-voltage pulse combinations for gene electrotransfer in muscle, liver, tumor, and skin**. *Hum Gene Ther* 2008, **19**:1261–71.
9. Kanduser M, Miklavcic D, Pavlin M: **Mechanisms involved in gene electrotransfer using high- and low-voltage pulses — An in vitro study**. *Bioelectrochemistry* 2009, **74**:265–271.
10. Pavselj N, Préat V: **DNA electrotransfer into the skin using a combination of one high- and one low-voltage pulse.** *J Control Release* 2005, **106**:407–15.
11. Satkauskas S, André F, Bureau MF, Scherman D, Miklavcic D, Mir LM: **Electrophoretic Component of Electric Pulses Determines the Efficacy of In Vivo DNA Electrotransfer**. *Hum Gene Ther* 2005, **16**:1194–1201.
12. Gothelf A, Gehl J: **Gene Electrotransfer to Skin; Review of Existing Literature and Clinical Perspectives**. *Curr Gene Ther* 2010, **10**:287–299.
13. Miklavcic D, Semrov D, Mekid H, Mir LM: **A validated model of in vivo electric field distribution in tissues for electrochemotherapy and for DNA electrotransfer for gene therapy.** *Biochim Biophys Acta* 2000, **1523**:73–83.
14. Zupanic A, Corovic S, Miklavcic D, Pavlin M: **Numerical optimization of gene electrotransfer into muscle tissue.** *Biomed Eng Online* 2010, **9**:66.
15. Zupanic A, Kos B, Miklavcic D: **Treatment planning of electroporation-based medical interventions: electrochemotherapy, gene electrotransfer and irreversible electroporation**. *Phys Med Biol* 2012, **57**:5425–5440.

16. Lackovic I, Magjarevic R, Miklavcic D: **Three-dimensional finite-element analysis of joule heating in electrochemotherapy and in vivo gene electrotransfer**. *IEEE Trans Dielectr Electr Insul* 2009, **16**:1338–1347.
17. Calvet CY, Thalmensi J, Liard C, Pliquet E, Bestetti T, Huet T, Langlade-Demoyen P, Mir LM: **Optimization of a gene electrotransfer procedure for efficient intradermal immunization with an hTERT-based DNA vaccine in mice**. *Mol Ther — Methods Clin Dev* 2014, **1**:14045.
18. Pliquett U, Langer R, Weaver JC: **Changes in the passive electrical properties of human stratum corneum due to electroporation**. *Biochim Biophys Acta - Biomembr* 1995, **1239**:111–121.
19. Pliquett UF, Vanbever R, Preat V, Weaver JC: **Local transport regions (LTRs) in human stratum corneum due to long and short `high voltage' pulses**. *Bioelectrochemistry Bioenerg* 1998, **47**:151–161.
20. Pavselj N, Miklavcic D: **Resistive heating and electropermeabilization of skin tissue during in vivo electroporation: A coupled nonlinear finite element model**. *Int J Heat Mass Transf* 2011, **54**:2294–2302.
21. Becker S, Zorec B, Miklavcic D, Pavselj N: **Transdermal transport pathway creation: Electroporation pulse order**. *Math Biosci* 2014, **257**:60–68.
22. Saulis G, Saule R, Bitinaite A, Zurauskiene N, Stankevic V, Balevicius S: **Theoretical Analysis and Experimental Determination of the Relationships Between the Parameters of the Electric Field Pulse Required to Electroporate the Cells**. *IEEE Trans Plasma Sci* 2013, **41**:2913–2919.
23. Pavselj N, Préat V, Miklavcic D: **A numerical model of skin electropermeabilization based on in vivo experiments**. *Ann Biomed Eng* 2007, **35**:2138–2144.
24. Pucihar G, Krmelj J, Rebersek M, Napotnik T, Miklavcic D: **Equivalent Pulse Parameters for Electroporation**. *IEEE Trans Biomed Eng* 2011, **58**:3279–3288.
25. Pavselj N, Bregar Z, Cukjati D, Batiuskaite D, Mir LM, Miklavcic D: **The Course of Tissue Permeabilization Studied on a Mathematical Model of a Subcutaneous Tumor in Small Animals**. *IEEE Trans Biomed Eng* 2005, **52**:1373–1381.
26. Sel D, Cukjati D, Batiuskaite D, Slivnik T, Mir LM, Miklavcic D: **Sequential Finite Element Model of Tissue Electropermeabilization**. *IEEE Trans Biomed Eng* 2005, **52**:816–827.
27. Garcia PA, Davalos R V., Miklavcic D: **A Numerical Investigation of the Electric and Thermal Cell Kill Distributions in Electroporation-Based Therapies in Tissue**. *PLoS One* 2014, **9**:e103083.
28. Yarmush ML, Golberg A, Serša G, Kotnik T, Miklavčič D: **Electroporation-Based Technologies for Medicine: Principles, Applications, and Challenges**. *Annu Rev Biomed Eng* 2014, **16**:295–320.
29. Pavlin M, Kanduser M: **New insights into the mechanisms of gene electrotransfer--experimental and theoretical analysis.** *Sci Rep* 2015, **5**:9132.
30. Haberl S, Kanduser M, Flisar K, Hodzic D, Bregar VB, Miklavcic D, Escoffre J-M, Rols M-P, Pavlin M: **Effect of different parameters used for in vitro gene electrotransfer on gene expression efficiency, cell viability and visualization of plasmid DNA at the membrane level**. *J Gene Med* 2013, **15**:169–181.
31. Lambricht L, Lopes A, Kos S, Sersa G, Préat V, Vandermeulen G: **Clinical potential of electroporation for gene therapy and DNA vaccine delivery**. *Expert Opin Drug Deliv* 2016, **13**:295–310.
32. Vandermeulen G, Vanvarenberg K, De Beuckelaer A, De Koker S, Lambricht L, Uyttenhove C, Reschner A, Vanderplasschen A, Grooten J, Préat V: **The site of administration**

influences both the type and the magnitude of the immune response induced by DNA vaccine electroporation. *Vaccine* 2015, **33**:3179–3185.

33. Olaiz N, Signori E, Maglietti F, Soba A, Suárez C, Turjanski P, Michinski S, Marshall G: **Tissue damage modeling in gene electrotransfer: The role of pH**. *Bioelectrochemistry* 2014, **100**:105–111.
34. Kanduser M, Miklavcic D, Pavlin M: **Mechanisms involved in gene electrotransfer using high- and low-voltage pulses — An in vitro study**. *Bioelectrochemistry* 2009, **74**:265–271.
35. Zorec B, Becker S, Rebersek M, Miklavcic D, Pavselj N: **Skin electroporation for transdermal drug delivery: The influence of the order of different square wave electric pulses**. *Int J Pharm* 2013, **457**:214–223.
36. Dermol-Cerne J, Miklavcic D: **From Cell to Tissue Properties—Modeling Skin Electroporation With Pore and Local Transport Region Formation**. *IEEE Trans Biomed Eng* 2018, **65**:458–468.

Table 1: Definition of numerical model: geometry of the skin together with electrical and thermal properties of the skin tissue, plasmid volume and electrodes

	Thickness [µm]	Electrical conductivity [S/m]	Density [kg/m^3]	Thermal conductivity [W/mK]	Heat capacity [J/kgK]
Local Transport Region (LTR)	5	0.1	1400	0.2	3600
Stratum Corneum	5	0.0001	1400	0.2	3600
Epidermis	15	0.2 – 0.8*	1200	0.24	3600
Dermis	200	0.2 – 0.8*	1200	0.45	3300
Adipose tissue	150	0.05 – 0.2*	900	0.19	2400
Muscle tissue	90	0.5	1040	0.5	3350
Subcutaneous tissue	2000	0.05	900	0.19	2400
Plasmid volume	-	1.4	1000	0.6	3600
Electrodes	-	1.35×10^6	7810	16.9	477

**nonpermeabilized - fully permeabilized tissue*

Table 2: Model-based prediction of gene electrotransfer efficiency resulting from the pulse combination 1000 V/cm (100 µs) + 140 V/cm (400 ms). The measure of gene electrotransfer efficiency is the number of charged particles representing plasmid DNA inside the volume of reversible electroporation at the end of the pulse delivery. From all particles released from the surface of the plasmid volume, 5000 were selected randomly for evaluation. Increasing the number of evaluated particles did not affect the relative gene electrotransfer efficiencies.

	Plate (LTR diameter=10 µm)	Plate (LTR diameter=20 µm)	Finger	Needle
Volume of reversible electroporation – dermis (mm^3)	2.61	3.61	6.18	10.19
Volume of reversible electroporation - all layers (mm^3)	16.36	21.63	216.40	330.72
pCMV-luc (6233 bp)				
Number of charged particles inside the volume of reversible electroporation - dermis	307	422	1024	937
Number of charged particles inside the volume of reversible electroporation – all layers	310	422	1205	994
INVAC-1 (7120 bp)				
Number of charged particles inside the volume of reversible electroporation - dermis	305	387	941	870
Number of charged particles inside the volume of reversible electroporation – all layers	305	389	1122	931

Table 3: Gene electrotransfer efficiencies of different HV-LV pulse combination, delivered by plate electrodes. The initial diameter of LTRs was 10 µm. The electrophoretic movement of charged particle during the HV pulse was neglected due to its short duration (100 µs). The values in the table represent the number of charged particles inside the volume of reversible electroporation at the end of the LV pulse out of 5000 randomly selected particles. Reversible electroporation volume was determined from the HV pulse, except for the 1000 V/cm + 180 V/cm pulse combination, where LV pulse generated larger volume of reversible electroporation than HV pulse.

LV pulse amplitude / HV pulse amplitude	60 V/cm	100 V/cm	140 V/cm	180V/cm
1000 V/cm	316	305	310	337
1400 V/cm	441	427	455	552

Figure 1

Click here to download Figure Figure 1.pdf

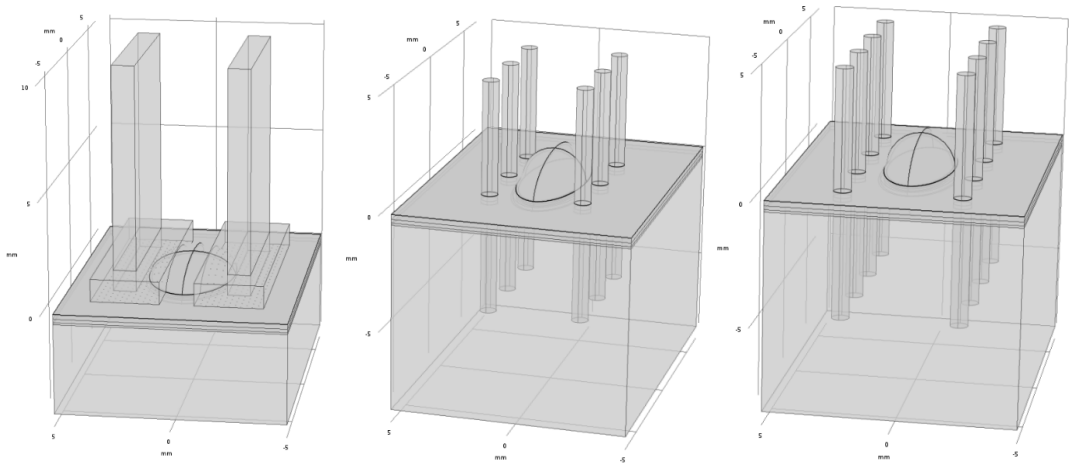

Figure 1: Geometry used in numerical modeling representing the skin tissue, injected plasmid volume and configuration of the following electrodes: a) plate, b) finger and c) needle electrodes.

4. ZAKLJUČEK

V doktorski disertaciji smo predstavili modele različnih odzivov na elektroporacijo in spremljajočih učinkov, ki so posledica dovajanja električnih pulzov. Izboljšana zmogljivost računalnikov in razvoj programske opreme omogočata razvoj vedno kompleksnejših modelov tudi na področju elektroporacije. Numerični modeli, ki smo jih opisali v disertaciji, predstavljajo nadgradnjo obstoječih modelov v smislu večjega števila upoštevanih parametrov in večje kompleksnosti geometrije kože. Plastovita struktura kože predstavlja izziv za numerično modeliranje, predvsem tanke zgornje plasti kože, ki za natančen izračun zahtevajo zelo gosto mrežo točk. Računsko zahtevnost pri modeliranju elektroporacije kože še dodatno povečujejo majhna področja povečane električne prevodnosti v zgornji plasti kože, ki nastanejo ob elektroporaciji z neinvazivnimi elektrodami. Ravno boljše poznavanje prevodnosti zgornje plasti kože pa se je izkazalo kot eden izmed ključnih pogojev za izboljšanje napovedne moči o učinkovitosti genske elektrotransfekcije. Pri uporabi invazivnih elektrod je vpliv zgornje plasti manjši, vendar postanejo pomembnejši drugi vplivi, katerih vloga in pomembnost še ni poznana, kot na primer vpliv pH sprememb v bližini elektrod.

Prednost modeliranja v primerjavi z eksperimenti je predvsem v tem, da lahko poljubno spreminjamo posamezne parametre ali po več parametrov naenkrat in tako opazujemo njihov medsebojni vpliv. Na ta način lahko določimo pogoje za doseganje optimalnih učinkovitosti različnih postopkov in terapij, zato je modeliranje postalo nepogrešljivo orodje v biomedicini. Uporabna vrednost modela pa je odvisna od dobrega poznavanja procesov, ki jih model opisuje. Na področju elektroporacije predstavlja modeliranje že pomembno orodje za načrtovanje elektrokemoterapije, ki temelji na reverzibilni elektroporaciji in atermične ablacije, ki temelji na ireverzibilni elektroporaciji. Kot se je pokazalo v disertaciji, pa lahko modeliranje predstavlja tudi dragoceno orodje za razkrivanje morebitnih pomanjkljivosti v razumevanju procesov, povezanih z elektroporacijo in na elektroporaciji temelječih terapij.

IZVIRNI PRISPEVKI K ZNANOSTI

1. Modeliranje dinamike odziva mišjih tumorjev na zdravljenje z elektrokemoterapijo

Uspešnost elektrokemoterapije je odvisna od več dejavnikov. Poleg visoke znotrajcelične koncentracije in s tem citotoksičnosti kemoterapevtikov, ki jo dosežemo z elektroporacijo, sta bila do sedaj identificirana še vsaj dva učinka, ki prispevata k uspešnosti elektrokemoterapije - spremembe v prekrvitvi tumorja in imunski odziv. Zaradi zmanjšane prekrvitve se tumorske celice znajdejo v hipoksičnem okolju in so dlje časa izpostavljene delovanju kemoterapevtika, imunski odziv pa pripomore k odstranitvi preostalih preživelih tumorskih celic. Nekaj vpogleda k prispevku naštetih učinkov k uspešnosti elektrokemoterapije lahko dobimo z modeliranjem dinamike odziva tumorjev na elektrokemoterapijo. V ta namen sem razvila model na osnovi sistema diferencialnih enačb, ki opisuje spremembe prostornine mišjih tumorjev po elektrokemoterapiji. Z uporabo modela lahko razlikujemo med zgodnjimi in kasnimi učinki elektrokemoterapije, kar med drugim omogoča primerjavo različnih kemoterapevtikov glede na njihovo citotoksičnost in intenzivnost imunskega odziva.

2. Vrednotenje termičnih poškodb tkiva zaradi elektroporacije na podlagi numeričnih modelov in meritev bioluminiscence

Električni pulzi visokih napetosti, ki se uporabljajo za elektroporacijo tkiva, lahko povzročijo termične poškodbe zaradi Joulovega segrevanja. Vpliv različnih pulznih protokolov na termične poškodbe pri elektroporaciji kože sem ocenila z numeričnim modeliranjem na osnovi metode končnih elementov in Arrheniusovega integrala. Izkazalo se je, da testirani pulzni protokoli povzročajo znatne termične poškodbe samo tik pod področji povečane električne prevodnosti zgornje, rožene plasti kože. Rezultati se skladajo z *in vivo* eksperimenti sodelujoče raziskovalne skupine, kjer so bile termične poškodbe ocenjene z meritvami bioluminescence.

3. Primerjava rezultatov izražanja reporterskega gena za luciferazo z numeričnimi izračuni porazdelitve električnega polja

Uspešnost genske elektrotransfekcije, metode, ki omogoča vnos genskega materiala v celice z elektroporacijo, je odvisna od porazdelitve električnega polja. Pri izbiri parametrov električnih pulzov pa je potrebno poznati vpliv več dejavnikov, ki vplivajo na izražanje vnesenih genov. Numerični izračuni porazdelitve električnega polja so pokazali, da sam volumen reverzibilne elektroporacije ne pojasni razlik v učinkovitosti genske elektrotransfekcije glede na vrsto elektrod. Model je bil zato nadgrajen še s simulacijo gibanja DNK molekul v električnem polju. Čeprav se tako nadgrajeni model bolje sklada z eksperimentalnimi rezultati, pa pomanjkljivosti v poznavanju elektroporacije kože predstavljajo glavni razlog za omejeno zanesljivost modela.

VIRI

1. Álvarez, I., Condón, S., Raso J. Microbial Inactivation by Pulsed Electric Fields. Springer, Boston, MA, 97–129, (2006).

2. André, F., Gehl, J., Serša, G., Préat, V., Hojman, P., Eriksen, J., Golzio, M., Čemažar, M., Pavšelj, N. & Rols, M.-P. Efficiency of high-and low-voltage pulse combinations for gene electrotransfer in muscle, liver, tumor, and skin. Efficiency of high-and low-voltage pulse combinations for gene electrotransfer in muscle, liver, tumor, and skin. *Hum Gene Ther* **19,** 1261–71 (2008).

3. Calvet, C. Y., Famin, D., André, F. M. & Mir, L. M. Electrochemotherapy with bleomycin induces hallmarks of immunogenic cell death in murine colon cancer cells. *Oncoimmunology* **3,** e28131 (2014).

4. Calvet, C. Y., Thalmensi, J., Liard, C., Pliquet, E., Bestetti, T., Huet, T., Langlade-Demoyen, P. & Mir, L. M. Optimization of a gene electrotransfer procedure for efficient intradermal immunization with an hTERT-based DNA vaccine in mice. *Mol. Ther. — Methods Clin. Dev.* **1,** 14045 (2014).

5. Čemažar, M., Miklavčič, D. & Serša, G. Intrinsic sensitivity of tumor cells to bleomycin as an indicator of tumor response to electrochemotherapy. *Jpn. J. Cancer Res.* **89,** 328–33 (1998).

6. Davalos, R. V, Mir, I. L. M. & Rubinsky, B. Tissue ablation with irreversible electroporation. *Ann. Biomed. Eng.* **33,** 223–31 (2005).

7. Delemotte, L. & Tarek, M. Molecular Dynamics Simulations of Lipid Membrane Electroporation. *J. Membr. Biol.* **245,** 531–543 (2012).

8. Dermol-Černe, J. & Miklavčič, D. From Cell to Tissue Properties—Modeling Skin Electroporation With Pore and Local Transport Region Formation. *IEEE Trans. Biomed. Eng.* **65,** 458–468 (2018).

9. Edhemović, I., Brecelj, E., Gašljević, G., Marolt Mušič, M., Gorjup, V., Mali, B., Jarm, T., Kos, B., Pavliha, D., Grcar Kuzmanov, B., Čemažar, M., Snoj, M., Miklavčič, D., Gadžijev, E. M. & Serša, G. Intraoperative electrochemotherapy of colorectal liver metastases. *J. Surg. Oncol.* **110,** 320–327 (2014).

10. Escoffre, J.-M., Portet, T., Favard, C., Teissié, J., Dean, D. S. & Rols, M.-P. Electromediated formation of DNA complexes with cell membranes and its consequences for gene delivery. *Biochim. Biophys. Acta - Biomembr.* **1808,** 1538–1543 (2011).

11. Faurie, C., Reberšek, M., Golzio, M., Kandušer, M., Escoffre, J.-M., Pavlin, M., Teissie, J., Miklavčič, D. & Rols, M.-P. Electro-mediated gene transfer and expression are controlled by the life-time of DNA/membrane complex formation. *J. Gene Med.* **12,** 117–125 (2010).

12. Garcia, P. A., Davalos, R. V. & Miklavčič, D. A Numerical Investigation of the Electric and Thermal Cell Kill Distributions in Electroporation-Based Therapies in Tissue. *PLoS One* **9,** e103083 (2014).

13. Golzio, M., Teissie, J. & Rols, M.-P. Direct visualization at the single-cell level of electrically mediated gene delivery. *Proc. Natl. Acad. Sci. U. S. A.* **99,** 1292–7 (2002).

14. Golzio, M., Rols, M. & Teissié, J. In vitro and in vivo electric field-mediated permeabilization, gene transfer, and expression. *Methods* **33,** 126–135 (2004).

15. Gothelf, A. & Gehl, J. What you always needed to know about electroporation based DNA vaccines. *Hum. Vaccin. Immunother.* **8,** 1694–1702 (2012).

16. Grošelj, A., Kos, B., Čemažar, M., Urbančič, J., Kragelj, G., Bošnjak, M., Veberič, B., Strojan, P., Miklavčič, D. & Serša, G. Coupling treatment planning with navigation system: a new technological approach in treatment of head and neck tumors by electrochemotherapy. *Biomed. Eng. Online* **14,** S2 (2015).

17. Haberl, S., Miklavčič, D., Serša, G., Frey, W. & Rubinsky, B. Cell membrane electroporation-Part 2: the applications. *IEEE Electr. Insul. Mag.* **29,** 29–37 (2013).

18. Haberl, S., Kandušer, M., Flisar, K., Hodžić, D., Bregar, V.B., Miklavčič, D., Escoffre, J.-M., Rols, M.-P., Pavlin, M.: Effect of different parameters used for in vitro gene electrotransfer on gene expression efficiency, cell viability and visualization of plasmid DNA at the membrane level. *J. Gene Med.* **15,** 169–181 (2013).

19. Heller, L.C., Jaroszeski, M.J., Coppola, D., McCray, A.N., Hickey, J., Heller, R.: Optimization of cutaneous electrically mediated plasmid DNA delivery using novel electrode. *Gene Ther.* **14,** 275–80 (2007).

20. Jarm, T., Čemažar, M., Miklavčič, D. & Serša, G. Antivascular effects of electrochemotherapy: implications in treatment of bleeding metastases. *Expert Rev. Anticancer Ther.* **10,** 729–46 (2010).

21. Klenchin, V.A., Sukharev, S.I., Serov, S.M., Chernomordik, L.V., Chizmadzhev YuA: Electrically induced DNA uptake by cells is a fast process involving DNA electrophoresis. *Biophys. J.* **60,** 804–811 (1991).

22. Koch, G., Walz, A., Lahu, G. & Schropp, J. Modeling of tumor growth and anticancer effects of combination therapy. *J. Pharmacokinet. Pharmacodyn.* **36,** 179–97 (2009).

23. Kos, B. *et al.* Robustness of Treatment Planning for Electrochemotherapy of Deep-Seated Tumors. *J. Membr. Biol.* **236,** 147–153 (2010).

24. Kotnik, T., Kramar, P., Pucihar, G., Miklavčič, D. & Tarek, M. Cell membrane electroporation- Part 1: The phenomenon. *IEEE Electr. Insul. Mag.* **28,** 14–23 (2012).

25. Kotnik, T., Frey, W., Sack, M., Haberl Meglič, S., Peterka, M. & Miklavčič, D. Electroporation-based applications in biotechnology. *Trends Biotechnol.* **33,** 480–488 (2015).

26. Lacković, I., Magjarevic, R. & Miklavčič, D. Three-dimensional finite-element analysis of joule heating in electrochemotherapy and in vivo gene electrotransfer. *IEEE Trans. Dielectr. Electr. Insul.* **16,** 1338–1347 (2009).

27. Langus, J., Kranjc, M., Kos, B., Šuštar, T. & Miklavčič, D. Dynamic finite-element model for efficient modelling of electric currents in electroporated tissue. *Sci. Rep.* **6,** 26409 (2016).

28. Lee, R. C. & Kolodney, M. S. Electrical injury mechanisms: electrical breakdown of cell membranes. *Plast. Reconstr. Surg.* **80,** 672–9 (1987).

29. Maor, E., Ivorra, A. & Rubinsky, B. Non Thermal Irreversible Electroporation: Novel Technology for Vascular Smooth Muscle Cells Ablation. *PLoS One* **4,** e4757 (2009).

30. Mahnič-Kalamiza, S., Vorobiev, E. & Miklavčič, D. Electroporation in Food Processing and Biorefinery. *J. Membr. Biol.* **247,** 1279–1304 (2014).

31. Marčan, M., Pavliha, D., Kos, B., Forjanič, T. & Miklavčič, D. Web-based tool for visualization of electric field distribution in deep-seated body structures and planning of electroporation-based treatments. *Biomed. Eng. Online* **14,** S4 (2015).

32. Markelc, B., Serša, G. & Čemažar, M. Differential mechanisms associated with vascular disrupting action of electrochemotherapy: intravital microscopy on the level of single normal and tumor blood vessels. *PLoS One* **8,** e59557 (2013).

33. Miklavčič, D., Šemrov, D., Mekid, H. & Mir, L. M. A validated model of in vivo electric field distribution in tissues for electrochemotherapy and for DNA electrotransfer for gene therapy. *Biochim. Biophys. Acta* **1523,** 73–83 (2000).

34. Miklavčič, D., Čorović, S., Pucihar, G. & Pavšelj, N. Importance of tumour coverage by sufficiently high local electric field for effective electrochemotherapy. *Eur. J. Cancer Suppl.* **4,** 45–51 (2006).

35. Miklavčič, D., Snoj, M., Županič, A., Kos, B., Čemažar, M., Kropivnik, M., Bracko, M., Pecnik, T., Gadzijev, E., Serša, G.: Towards treatment planning and treatment of deep-seated solid tumors by electrochemotherapy. *Biomed. Eng. Online* **9,** 10 (2010).

36. Miklavčič, D., Serša, G., Brecelj, E., Gehl, J., Soden, D., Bianchi, G., Ruggieri, P., Rossi, C. R., Campana, L. G. & Jarm, T. Electrochemotherapy: technological advancements for efficient electroporation-based treatment of internal tumors. *Med. Biol. Eng. Comput.* **50,** 1213–1225 (2012).

37. Miklavčič, D., Mali, B., Kos, B., Heller, R. & Serša, G. Electrochemotherapy: from the drawing board into medical practice. *Biomed. Eng. Online* **13,** 29 (2014).

38. Mir, L. M., Orlowski, S., Belehradek, J. & Paoletti, C. Electrochemotherapy potentiation of antitumour effect of bleomycin by local electric pulses. *Eur. J. Cancer* **27,** 68–72 (1991).

39. Mir, L. M., Bureau, M. F., Gehl, J., Rangara, R., Rouy, D., Caillaud, J. M., Delaere, P., Branellec, D., Schwartz, B. & Scherman, D. High-efficiency gene transfer into skeletal muscle mediated by electric pulses. *Proc. Natl. Acad. Sci. U. S. A.* **96,** 4262–7 (1999).

40. Mir, L. M., Gehl, J., Serša, G., Collins, C. G., Garbay, J.-R., Billard, V., Geertsen, P. F., Rudolf, Z., O'Sullivan, G. C. & Marty, M. Standard operating procedures of the electrochemotherapy: Instructions for the use of bleomycin or cisplatin administered either systemically or locally and electric pulses delivered by the CliniporatorTM by means of invasive or non-invasive electrodes. *Eur. J. Cancer Suppl.* **4,** 14–25 (2006).

41. Neumann, E., Schaefer-Ridder, M., Wang, Y. & Hofschneider, P. H. Gene transfer into mouse lyoma cells by electroporation in high electric fields. *EMBO J.* **1,** 841–5 (1982).

42. Olaiz, N., Signori, E., Maglietti, F., Soba, A., Suárez, C., Turjanski, P., Michinski, S., Marshall, G.: Tissue damage modeling in gene electrotransfer: The role of pH. *Bioelectrochemistry* **100,** 105–111 (2014).

43. Pavliha, D., Kos, B., Županič, A., Marčan, M., Serša, G., Miklavčič, D.: Patient-specific treatment planning of electrochemotherapy: Procedure design and possible pitfalls. *Bioelectrochemistry* **87,** 265–273 (2012).

44. Pavliha, D., Mušič, M. M., Serša, G. & Miklavčič, D. Electroporation-Based Treatment Planning for Deep-Seated Tumors Based on Automatic Liver Segmentation of MRI Images. *PLoS One* **8,** e69068 (2013).

45. Pavlin, M. & Kandušer, M. New insights into the mechanisms of gene electrotransfer--experimental and theoretical analysis. *Sci. Rep.* **5,** 9132 (2015).

46. Pavšelj, N., Préat, V.: DNA electrotransfer into the skin using a combination of one high- and one low-voltage pulse. *J. Control. Release* **106,** 407–415 (2005).

47. Pavšelj, N. *et al.* The Course of Tissue Permeabilization Studied on a Mathematical Model of a Subcutaneous Tumor in Small Animals. *IEEE Trans. Biomed. Eng.* **52,** (2005).

48. Pavšelj, N. & Miklavčič, D. Resistive heating and electropermeabilization of skin tissue during in vivo electroporation: A coupled nonlinear finite element model. *Int. J. Heat Mass Transf.* **54,** 2294–2302 (2011).

49. Pliquett, U., Langer, R. & Weaver, J. C. Changes in the passive electrical properties of human stratum corneum due to electroporation. *Biochim. Biophys. Acta - Biomembr.* **1239,** 111–121 (1995).

50. Pliquett, U. F., Vanbever, R., Preat, V. & Weaver, J. C. Local transport regions (LTRs) in human stratum corneum due to long and short `high voltage' pulses. *Bioelectrochemistry Bioenerg.* **47,** 151–161 (1998).

51. Puc, M., Kotnik, T., Mir, L. M. & Miklavčič, D. Quantitative model of small molecules uptake after in vitro cell electropermeabilization. *Bioelectrochemistry* **60,** 1–10 (2003).

52. Pucihar, G., Kotnik, T., Miklavčič, D. & Teissié, J. Kinetics of transmembrane transport of small molecules into electropermeabilized cells. *Biophys. J.* **95,** 2837–48 (2008).

53. Pucihar, G., Miklavčič, D., Kotnik, T.: A Time-Dependent Numerical Model of Transmembrane Voltage Inducement and Electroporation of Irregularly Shaped Cells. *IEEE Trans. Biomed. Eng.* **56,** 1491–1501 (2009).

54. Pucihar G, Krmelj J, Reberšek M, Napotnik T, Miklavčič D. Equivalent Pulse Parameters for Electroporation. *IEEE Trans Biomed Eng*. **58**, 3279–88 (2011).

55. Rems, L., Miklavčič, D. Različni modeli elektroporacije in transporta molekul prek celične membrane. *Elektrotehniški vestnik* **81**, 64-72 (2014).

56. Rems, L., Miklavčič, D. Tutorial: Electroporation of cells in complex materials and tissue. *J. Appl. Phys.* **119,** 201101 (2016).

57. Rols, M.-P., Delteil, C., Golzio, M., Dumond, P., Cros, S. & Teissie, J. In vivo electrically mediated protein and gene transfer in murine melanoma. *Nat. Biotechnol.* **16,** 168–171 (1998).

58. Rosazza, C., Meglič, S.H., Zumbusch, A., Rols, M.-P., Miklavčič, D.: Gene Electrotransfer: A Mechanistic Perspective. *Curr. Gene Ther*. **16**, 98–129 (2016).

59. Sack, M., Sigler, J., Frenzel, S., Eing, C., Arnold, J., Michelberger, T., Frey, W., Attmann, F., Stukenbrock, L. & Müller, G. Research on Industrial-Scale Electroporation Devices Fostering the Extraction of Substances from Biological Tissue. *Food Eng. Rev.* **2,** 147–156 (2010).

60. Scheffer, H. J., Nielsen, K., de Jong, M. C., van Tilborg, A. A. J. M., Vieveen, J. M., Bouwman, A., Meijer, S., van Kuijk, C., van den Tol, P. & Meijerink, M. R. Irreversible Electroporation for Nonthermal Tumor Ablation in the Clinical Setting: A Systematic Review of Safety and Efficacy. *J. Vasc. Interv. Radiol.* **25,** 997–1011 (2014).

61. Sel, D. *et al.* Sequential Finite Element Model of Tissue Electropermeabilization. *IEEE Trans. Biomed. Eng.* **52,** 816–827 (2005).

62. Serša, G., Čemažar, M. & Miklavčič, D. Antitumor effectiveness of electrochemotherapy with cis-diamminedichloroplatinum(II) in mice. *Cancer Res.* **55,** 3450–5 (1995).

63. Serša, G., Miklavčič, D., Čemažar, M., Belehradek, J., Jarm, T., Mir, L.M.: Electrochemotherapy with CDDP on LPB sarcoma: comparison of the anti-tumor effectiveness in immunocompotent and immunodeficient mice. *Bioelectrochemistry Bioenerg*. **43**, 279–283 (1997).

64. Serša, G. *et al.* Vascular disrupting action of electroporation and electrochemotherapy with bleomycin in murine sarcoma. *Br. J. Cancer* **98,** 388–98 (2008).

65. Stepišnik, T., Jarm, T., Grošelj, A., Edhemović, I., Djokić, M., Ivanecz, A., Trotovšek, B., Brecelj, E., Potrč, S., Čemažar, M., Glumac, N., Pečnik, T., Veberič, B., Gadžijev, E., Strojan, P., Snoj, M., Miklavčič, D. & Serša, G. Elektrokemoterapija – učinkovita metoda zdravljenja tumorjev s kombinacijo kemoterapevtika in električnega polja. *Slov. Med. J.* **85,** (2016).

66. Stoll, A. M. & Greene, L. C. Relationship between pain and tissue damage due to thermal radiation. *J. Appl. Physiol.* **14,** 373–82 (1959).

67. Šatkauskas, S., André, F., Bureau, M.F., Scherman, D., Miklavčič, D., Mir, L.M.: Electrophoretic Component of Electric Pulses Determines the Efficacy of In Vivo DNA Electrotransfer. *Hum. Gene Ther*. **16**, 1194–1201 (2005).

68. Tsong, T. Y. Electroporation of cell membranes. *Biophys. J.* **60,** 297–306 (1991).

69. Voyer, D., Silve, A., Mir, L. M., Scorretti, R. & Poignard, C. Dynamical modeling of tissue electroporation. *Bioelectrochemistry* **119,** 98–110 (2018).

70. Weaver, J. C. & Chizmadzhev, Y. A. Theory of electroporation: A review. *Bioelectrochemistry Bioenerg.* **41,** 135–160 (1996).

71. Weaver, J. C. Electroporation of cells and tissues. *IEEE Trans. Plasma Sci.* **28,** 24–33 (2000).

72. Wolf, H., Rols, M.P., Boldt, E., Neumann, E., Teissié, J.: Control by pulse parameters of electric field-mediated gene transfer in mammalian cells. *Biophys. J.* **66**, 524–31 (1994).

73. Wong, T.-K. & Neumann, E. Electric field mediated gene transfer. *Biochem. Biophys. Res. Commun.* **107,** 584–587 (1982).

74. Yarmush, M. L., Golberg, A., Serša, G., Kotnik, T. & Miklavčič, D. Electroporation-Based Technologies for Medicine: Principles, Applications, and Challenges. *Annu. Rev. Biomed. Eng.* **16,** 295–320 (2014).

75. Županic, A., Čorović, S., Miklavčič, D., Pavlin, M.: Numerical optimization of gene electrotransfer into muscle tissue. *Biomed. Eng. Online* **9,** 66 (2010).

76. Županič, A., Kos, B., Miklavčič, D.: Treatment planning of electroporation-based medical interventions: electrochemotherapy, gene electrotransfer and irreversible electroporation. *Phys. Med. Biol*. **57**, 5425–5440 (2012).